This is to certify that the
dissertation entitled

INVESTIGATING DFNA20 MUTATIONS IN γ-ACTIN:
STUDIES IN YEAST, CELL CULTURE, AND MOUSE

presented by

MEGHAN CHAPMAN DRUMMOND

has been accepted towards fulfillment
of the requirements for the

Ph.D. degree in Genetics

Karen Frideria
Major Professor's Signature

8-24-2010
Date

INVESTIGATING DFNA20 MUTATIONS IN γ-ACTIN: STUDIES IN YEAST, CELL CULTURE, AND MOUSE

By

Meghan Chapman Drummond

A DISSERTATION

Submitted to
Michigan State University
in partial fulfillment of the requirements
for the degree of

DOCTOR OF PHILOSOPHY

Genetics

2010

INVESTIGATING DFNA20 MUTATIONS IN γ-ACTIN: STUDIES IN YEAST, CELL CULTURE, AND MOUSE

By

Meghan Chapman Drummond

Ten dominant missense mutations in gamma-actin (ACTG1) have been reported as the cause of hearing loss in DFNA20 families. Although the mutations are located in different functional domains of γ-actin, the end result is a progressive form of non-syndromic sensorineural hearing loss beginning in the high frequencies with an onset in the second to third decade of life. This shared phenotype is indicative of a common functional deficit in mutant gamma-actin protein function. To address questions pertaining to the unique function of γ-actin in the inner ear, I implemented a yeast 2-hybrid screen of an inner ear library. Surprisingly, given then number of proteins in the inner ear known to interact with actin, only identified six proteins were identified more than once in the screens: γ-actin, β-actin, cyclase associated protein 2, cofilin 1, cofilin 2, and a novel actin binding protein, ubiquitin E2i ligase. Furthermore, I used a directed yeast 2-hybrid to show deficits in the interaction of P264L mutant γ-actin with four of the actin binding proteins from the initial library screens.

Next I evaluated the localization of a γ-actin specific binding protein, annexin 5a (ANXA5), in the inner ear of the mouse. My data demonstrate that in the postnatal mouse ear, annexin 5a is differentially localized to the stereocilia, cell body, and nuclear membrane of developing hair cells. *Anxa5* knock-out mice do not show hearing loss by 3 months of age. Furthermore, γ-actin is

appropriately localized to the periphery of the stereocilia and F-actin gaps in these mice. Using a GST-pulldown assay, I confirmed that annexin 5a interacts exclusively with the γ-isoform of cytoplasmic actin. Therefore, the interaction of annexin 5a and γ-actin in the inner ear is not critical for establishing or maintaining proper hearing in mice.

Finally, to address questions regarding the effects of these mutations on the structure and function of the inner ear and the molecular mode of action, we generated a knock-in mouse model for the p.P264L mutation. In the process, I identified a novel *Actg1* transcript, enriched in skeletal muscle-containing tissues. Splicing of this alternative transcript creates a premature termination codon and is concurrent with down-regulation of *Actg1*. A protein product corresponding to the use of this stop codon was not found. I provide evidence that inclusion of exon 3a is means of post-transcriptionally down-regulating *Actg1* via the nonsense mediated decay pathway. The knock-in mouse model recapitulates aspects of the DFNA20 deafness phenotype observed in humans. Mice homozygous for this mutation have early onset hearing loss which progresses rapidly in adolescent mice. My data demonstrate that the mutant P264L protein is stably expressed and localized properly to the stereocilia. Scanning electron micrographs support the hypothesis that hearing loss involves outer hair cell dysfunction, and provides evidence that degeneration of the stereocilia occurs in the two rows of stereocilia uniquely responsible for mechanotransduction.

This dissertation is dedicated to my beloved grandparents:

Mary Sylvia Trout & Robert Manford Chapman

and

Rose Mary Drummond & Richard Leo Puzdrowski

ACKNOWLEDGEMENTS

My graduate education has been rich with interactions, many of which I would like to acknowledge here. First and foremost, I would like to thank my mentor, Karen Friderici, who is a remarkable woman in many ways. Karen is an advocate for others – students, colleagues, and friends alike have benefited from her support, love, kindness, and patience. She is confident in her intelligence and high level of success without being boastful. Likewise, Karen has taught me to be quietly confident in my work and in life, to take big risks for big rewards, to take pride in my accomplishments, the importance of communication, the value of honesty, and to not settle for mediocrity. She has pushed me to explore new techniques, pursue novel ideas, and has cultivated my love of science and research. Karen has guided me in all aspects of life and for that I am eternally grateful. I truly revere and respect her.

Three individuals in particular have played indispensible roles in my graduate career. First, Mei Zhu, my first instructor in the lab, a colleague, and above all, my close friend. Mei trained me in many technical skills that are the foundation of my work, but more importantly, by her own example taught me that there is no substitute for hard work, accuracy, and high quality data. The exceptional standards that she has set for herself and others are evident in all that she does. Second, Mirna Mustapha, a colleague who taught me organ of Corti dissections and in the process became a good friend. Mirna has shown me the importance of self-sufficiency and confidence though her inarguable success. Finally, Inna

Belyantseva, a collaborator, instructor, future co-worker, and friend. Inna demonstrates the value of being the best in the field, as her work is widely recognized by colleagues for its unparalleled quality. Many, including myself, have benefited from the support, guidance, and advice that Inna selflessly provides. She has taught me that dissections and imaging are more than a technical skill; they are an art form, one which requires attention to detail and finesse. I am so fortunate to have these strong and successful women as role-models, colleagues, and friends. I admire them dearly and endeavor to one day achieve the level of success that they continue to experience.

I would also like to acknowledge my labmates, past and present: Kathy Jernigan, Ellen Wilch, Bill Payne, Mei Zhu, Soumya Korrapati, Donna Housley, Eric Schauberger, Ayo Ajibola, Andrew Riedy, Lawrence Lee, Tychele Turner, Jingyun Fang, and Stefanie Sherman. In particular, I would like to thank Ellen Wilch, Kathy Jernigan and Soumya Korrapati – my friends and support system. Thank you for all of the laughs and good times together. I am also grateful to my friends outside of the lab: Tejas, Erin, Gabby, Rachel, Rabeah, Tuddow, Arianna, Walid, and Paula.

I also owe a great deal of gratitude to those who provided support in other aspects of my graduate studies: Sally Camper and Qing Fang, who provided me with a lab away from home; Dave Dolan and Karin Hasley, for helping with the ABR data; Melinda Frame, Stanley and Carol Flegler, and Abby Tirrell, for their

invaluable instruction and assistance with imaging and microscopy; and Tom Friedman, for his insight and suggestions. I am grateful to my committee members, John Fyfe, Steve Heidemann, Ron Patterson, Rich Schwartz, and Vilma Yuzbasiyan-Gurkan. I will remember and apply your advice and constructive criticism. You have taught me to think critically about my data, to pay attention to details, and about how to succeed as a professional in the field of research.

Without the love and support of my family none of this would be possible. My parents nurtured and pushed to be successful in life. They have instilled the values of hard work and education, which continue to be indispensible as I grow as an adult. Finally, my husband, Gabe. You are my rock. You believe in me when I have doubts. You make me laugh. You not-so-quietly accept my long nights at the lab. You help me to pursue my dreams. Thank you.

TABLE OF CONTENTS

List of Tables ..... **xii**

List of Figures ..... **xiii**

List of Abbreviations ..... **xv**

Introduction **1**

Chapter 1
Literature Review **2**
Actin 3
Hearing Loss 9
Structures of inner ear 18
Mouse models of deafness 24

Chapter 2
Identification of actin binding proteins using a yeast 2-hybrid screen **39**
Abstract 40
Introduction 41
Materials and Methods 44
Vectors 44
Prey library 44
Western Blotting 44
Primary antibodies 45
Yeast Transformation 46
Whole colony PCR 47
Isolation and identification of prey vectors 48
Growth Assays 48
Results 50
Identification of actin:protein interactions 50
Deafness associated mutant γ-actin shows deficiency in interactions with prey identified in the Y2H screen 55
Discussion 59
References 64

Chapter 3
Studies of the localization of annexin 5a in the inner ear of mouse and the interaction of annexin 5a with γ-actin **68**
Abstract 69
Introduction 70
Materials and Methods 74
Animals 74
Primary antibodies 74

Immunofluorochemistry 75
Auditory-evoked Brainstem Response (ABR) 76
Vectors 77
Purification of Recombinant GST-ANXA5 77
GST-Pulldown 78
Western Blotting 79
In vitro synthesis of proteins 80
Co-sedimentation Assay 80
Results 82
Annexin 5a localization in the organ of Corti and vestibular end organs 82
Annexin 5a localizes to the stereocilia and cellular membranes in auditory hair cells 82
In vestibular hair cells, annexin 5a is present in hair cell bundles and at the nuclear membrane 87
Annexin 5a is found associated with membranes and within the cytoplasm of supporting cells 90
Annexin 5a is on the internal leaflet of apical hair cell membranes 90
γ-actin localizes properly in Anxa5-null mice 91
Annexin 5a knock-out mice do not have hearing deficits 99
GST-Pulldown shows annexin 5a is specific for γ-actin in whole cell lysates 99
Pure Annexin5a does not interact with monomeric or filamentous γ-actin in vitro. 101
Discussion 106
References 110

Chapter 4
Identification and characterization of a novel γ-actin regulatory transcript 113
Abstract 114
Introduction 115
Materials and Methods 118
Bioinformatics 118
Animals and Tissue Preparation 118
Cell Culture 118
RNA isolation and cDNA synthesis 119
Nuclear and Cytoplasmic RNA Isolation 119
PCR Amplification 120
Cycloheximide 120
Protein Isolation 121
Western Blotting 121
Expression Constructs 122
Transfections and Mass Selection 122
Results 124
Identification of a novel Actg1 transcript 124
Exon 3a containing transcripts are enriched in muscle 124
Exon 3a is highly conserved among mammals 128

Developmental regulation of Actg1 alternative splicing 131
Cytoplasm contains RNA with exon 3a but no corresponding protein product 131
Inhibition of nonsense mediated decay results in an increase of exon 3a-containing transcripts 135
Cells expressing exogenous human ACTG1 regulate splicing to include exon 3a during development 137
References 149

Chapter 5
Characterization of a knock-in mouse model for DFNA20 deafness. 151
Abstract 152
Introduction 154
Materials and Methods 158
Animals 158
Generation of congenic mice 158
Rotarod 159
Protein isolation 159
Western Blotting 160
Immunofluorochemistry 161
Auditory-evoked Brainstem Response (ABR) 162
Scanning Electron Microscopy (SEM) 163
Results 165
The mutant P264L protein is expressed at normal levels, however, the neo cassette reduces expression 165
P264L heterozygotes and homozygotes are physically fit and fertile 165
P264L homozygotes have an early onset, progressive hearing loss 167
Hearing loss in PL/PL mice is due to degeneration of stereocilia 173
Mutant P264L γ-actin is properly localized to the stereocilia in homozygous mice 188
Discussion 194
References 199

Chapter 6
Conclusions and Future Directions 202
Conclusions and Future Directions 203

Appendices
Commonly used methods and reagents 208
A. PCR 209
B. Polyacrylamide Gels (Reducing) 210
C. Continuous Native Gels 211

LIST OF TABLES

Table 1-1: Summary of previous DFNA20 studies in yeast.....17

Table 1-2: Actin binding proteins and deafness.....26

Table 2-1: Actin prey identified in yeast 2-hybrid screens.....54

LIST OF FIGURES

Figure 1-1: Conservation of actin.....5

Figure 1-2: Location of γ-actin missense mutations.....13

Figure 1-3: Audiograms from DFNA20 families.....15

Figure 1-4: Components of the inner ear.....21

Figure 1-5: The organ of Corti.....22

Figure 2-1: Western blot of actin bait.....51

Figure 2-2: Screening strategy for yeast 2-hybrid.....52

Figure 2-3: Yeast growth assays.....58

Figure 3-1: Annexin 5a in the organ of Corti.....84

Figure 3-2: Annexin 5a in auditory hair cell stereocilia.....86

Figure 3-3: Annexin 5a in vestibular hair cell stereocilia.....89

Figure 3-4: Annexin 5a is on the internal face of the cell membrane.....93

Figure 3-5: γ-actin in wild-type and *Anxa5*-null mice.....96

Figure 3-6: Annexin 5a does not localize to vestibular stereocilia gaps.....98

Figure 3-7: GST-pulldown assay with annexin 5a.....100

Figure 3-8: Band-shift assay with *in vitro* synthesized annexin 5a and γ-actin..103

Figure 3-9: Co-sedimentation assay with annexin 5a and F-actin.....105

Figure 4-1: Coding sequence of mouse and human actins.....126

Figure 4-2: PCR assay for alternative transcript in mouse tissues.....127

Figure 4-3: Conservation of γ-actin intron 3.....130

Figure 4-4: Splicing of *Actg1* in C2C12 myoblasts and myotubes.....133

Figure 4-5: Nuclear and cytoplasmic RNA fractions from myotubes.....134

Figure 4-6: Cycloheximide treatment of myotube cultures.....136

Figure 4-7: Human *ACTG1* expression constructs.....140

Figure 4-8: Mutation of 3' acceptor site abolishes splicing.....142

Figure 4-9: Conservation of intron 3a.....148

Figure 5-1: P264L knock-in targeting vector.....157

Figure 5-2: Expression of recombinant P264L γ-actin.....166

Figure 5-3: Rotarod test and body weights in normal and mutant mice.....169

Figure 5-4: Auditory-evoked brainstem response in P264L mice.....172

Figure 5-5: Scanning electron micrograph overview of the cochlear bulla.....175

Figure 5-6: Scanning electron micrograph of the 8 kHz region.....178

Figure 5-7: High magnification of outer hair cells at 8 kHz.....180

Figure 5-8: Scanning electron micrograph of the 16 kHz region.....182

Figure 5-9: High magnification of inner hair cells at 16 kHz.....183

Figure 5-10: High magnification of outer hair cells at 16 kHz.....185

Figure 5-11: Scanning electron micrograph of the 32 kHz region.....187

Figure 5-12: Localization of P264L and wild-type γ-actin in auditory hair cells..191

Figure 5-13: Abnormal actin filaments in outer hair cells of P264L mice.....193

Images in this dissertation are presented in color.

LIST OF ABBREVIATIONS

ABR	Auditory-evoked brainstem response
ACTB	Cytoplasmic β-actin
ACTG1	Cytoplasmic γ-actin
ADF	Actin depolymerizing factor
ADP	Adenosine diphosphate
ANXA5	Annexin 5a
ATP	Adenosine 5'-triphosphate
BSA	Bovine serum albumin
CAP2	Cyclase associated protein 2
CCT	Chaperonin containing TCP1
cDNA	Complimentary DNA
CFL1	Cofilin 1 (non-muscle)
CFL2	Cofilin 2 (muscle)
CHX	Cycloheximide
DAPI	4',6-diamidino-2-phenylindole
DC	Deiter's cells
DNA	Deoxyribonucleic acid
DNase1	Deoxyribonuclease 1
DPOAE	Distortion product otoacoustic emission
EDTA	Ethylenediaminetetraacetic acid
F-actin	Filamentous actin

G-actin	Globular actin
GFP	Green fluorescent protein
GST	Glutathione-s-transferase
HL	Hearing loss
HRP	Horseradish peroxidase
IHC	Inner hair cells
ISC	Inner sulcus cells
MPSS	Massively parallel signature sequence
mRNA	Messenger RNA
neo	Neomycin
NIDCD	National Institute on Deafness and Other Communication Disorders
NIH	National Institutes of Health
NMD	Nonsense mediated decay
OHC	Outer hair cells
PBS	Phosphate buffered saline
IPC	Inner pillar cells
PCR	Polymerase chain reaction
PFA	Paraformaldehyde
PS	Phosphatidylserine
PTC	Premature termination codon
PVDF	Polyvinylidene difluoride
qRT-PCR	quantitative reverse transcription polymerase chain reaction

RNA	Ribonucleic acid
RT-PCR	Reverse transcription polymerase chain reaction
RUST	Regulated unproductive splicing and translation
SC	Supporting cells
SDS-PAGE	Sodium dodecyl sulfate polyacrylamide gel electrophoresis
SEM	Scanning electron microscopy
SSM	Splice site mutation
TE	Tris-EDTA
TEL	Tris-EDTA lithium acetate
TEMED	Tetramethylethylenediamine
UBE2I	Ubiquitin E2i ligase
UTR	Untranslated region

INTRODUCTION

The overall goal of my doctoral research was to gain insight into the pathophysiology of mutations in γ-actin that cause nonsyndromic deafness. I used several approaches to address this goal. First, I implemented two yeast 2-hybrid screens to interrogate an inner ear library to identify potentially novel γ- and β-actin binding proteins or perhaps identify ear specific isoforms of already known proteins. Next, I investigated the localization of a γ-actin specific binding protein, annexin 5a, during development using immunofluorochemistry. Finally, I characterized hearing loss in a knock-in mouse model for one of the γ-actin deafness mutations, p.P264L. In the course of these experiments, I also identified and characterized a novel regulatory mechanism for γ-actin. The purpose of this literature review is to discuss the material that forms the basis for my study of actin and its role in hearing. I will provide a brief overview of actin, actin regulation, and differences between actin isoforms. Next, I discourse on hearing loss, in particular, DFNA20 deafness. Finally, I describe the physical structures of the inner ear and provide examples of mutations related to dysfunction of these structures.

CHAPTER 1

LITERATURE REVIEW

Actin

Actin is a 42 kD protein that is ubiquitously expressed. In humans, six different isoforms exist; four muscle-specific actins (cardiac, skeletal and two smooth muscle) and two cytoskeletal actins, β and γ (Figure 1-1). The two cytoplasmic actins differ by only 4 amino acids in the N-termini of the polypeptides and are perfectly conserved among vertebrates, so the protein sequence in mouse is exactly the same as in humans (Erba *et al.*, 1986). β-actin is the predominant isoform in almost all tissues of the body with the exception of the gut epithelium and hair cells of the inner ear, in which γ-actin is the predominant isoform existing at a 2:1 γ:β ratio (Khaitlina, 2001). Actin filaments in the cell provide structure and a network upon which other proteins and some organelles are trafficked. A number of proteins interact with actin and I will discuss more of these later in the context of hearing loss and deafness associated genes.

Our knowledge of *Actb* and *Actg1* regulation comes from work with mouse cardiomyocyte and myoblast cell culture. The β-actin promoter is constitutively expressed (Quitschke *et al.*, 1989), however in muscle, expression is drastically reduced during differentiation. The details of β-actin down-regulation were first described by DePonte-Zilli *et al* (1988) and Lohse *et al* (1988). In these two studies, a 40 bp region within the 3'UTR was demonstrated as necessary and sufficient to down-regulate β-actin expression in differentiating chick myocardiocyte cultures (DePonti-Zilli *et al.*, 1988; Lohse and Arnold, 1988).

Figure 1-1

Alignment of the protein sequence of the six actin isoforms reveals a high degree of similarity at the amino acid level in humans and are well conserved compared to the single yeast actin. From top to bottom human *ACTB*, *ACTG1*, *ACTC*, *ACTA1*, *ACTA2*, *ACTG2*, yeast actin. Locations of DFNA20 missense mutations are denoted by arrows above the amino acid. All but one of the missense mutations, T89I, involve a amino acid residue that is perfectly conserved between the six mammalian isoforms and yeast. Alignment generated using Clustal X2.

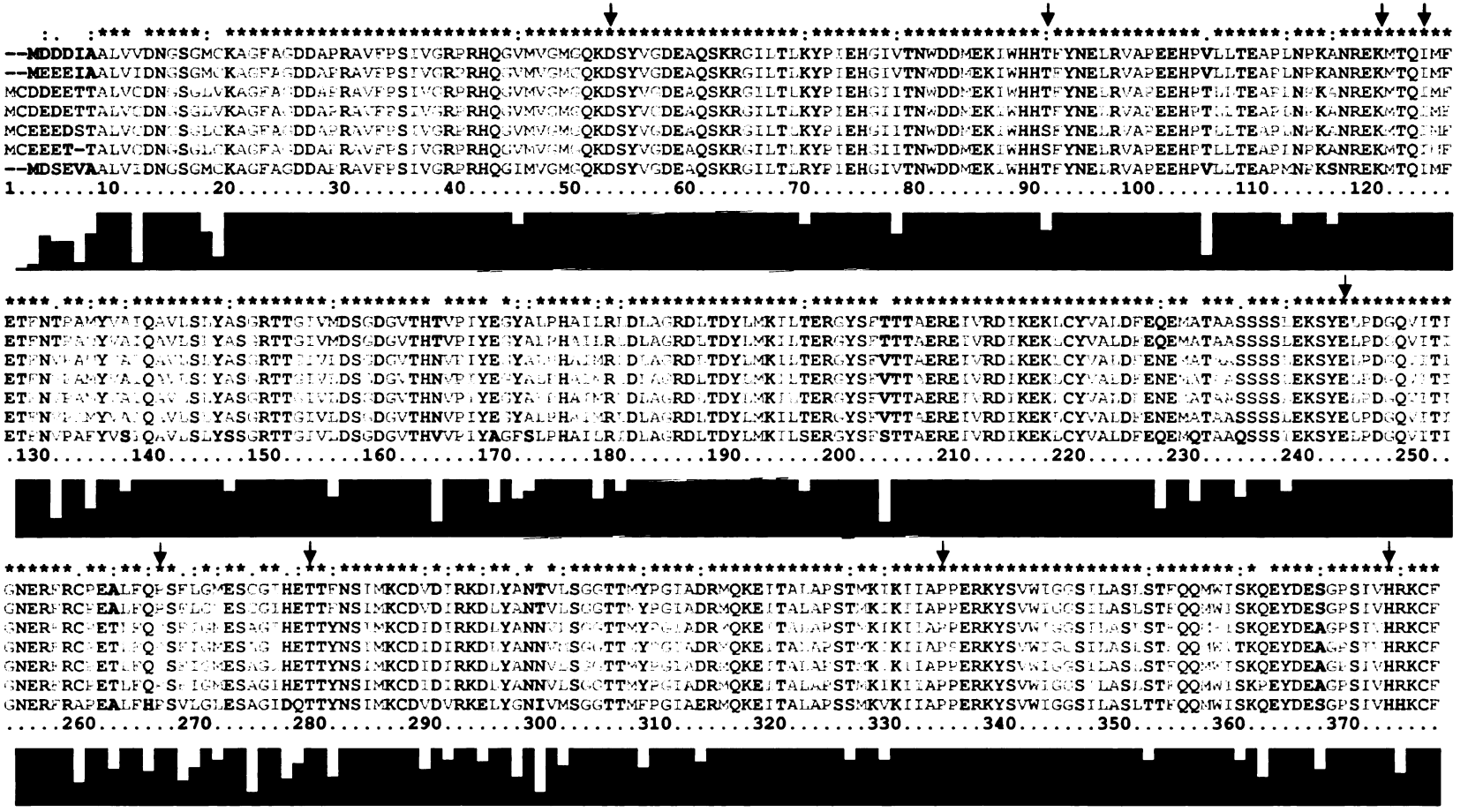

5

Extensive work by Lloyd and Gunning (2002) has examined cytoplasmic actin expression and over-expression in C2C12 myoblast cell culture. In these studies, *ACTG1* mRNA was found to be appropriately down-regulated during myotube differentiation only when intron 3 was present in genomic DNA, though unlike β-actin, the 3'UTR was dispensable for this process (Lloyd and Gunning, 2002).

Actins exist in two functional forms, globular actin (G-actin) and filamentous actin (F-actin). The X-ray crystallographic structure of β-actin has been solved (Schutt *et al.*, 1993). There are two major domains, each with two subdomains. Actin monomers bind either ATP or ADP in the cleft between subdomains 1 and 2 (Sheterline and Sparrow, 1998). ATP-G-actin readily associates to form actin filaments under ideal conditions *in vitro* and with the aid of a number of actin binding proteins. Actin filaments are helical and polar, with ends designated as barbed and pointed end. F-actin "treadmills" by a process in which new ATP-actin monomers are added to the barbed end of the growing actin filament, the ATP is hydrolyzed to confer a conformational change, and ADP-actin monomers are released or severed from the pointed end of the filament (Sheterline and Sparrow, 1998). For proper cell mobility and structural regulation, F-actin must be severed, depolymerized, converted to ATP-actin, and then localized to the site of rapid polymerization. All of these processes are catalyzed by a variety of actin binding proteins. Michelot *et al* has recently shown that F-actin turnover occurs

at a 155-fold higher rate in the presence of formin, profilin, and ADF/cofilin *in vitro* compared to studies using actin alone (Michelot *et al.*, 2007).

The current working model for F-actin turnover involves three steps. First, old actin filaments are severed and depolymerized. This process is aided by ADF/cofilin, a protein that recognizes ADP-F-actin, and then severs and depolymerizes it into G-actin (Fass *et al.*, 2004). The second step is to sequester the ADP-G-actin monomer, exchange ADP for ATP, and prevent spontaneous repolymerization. Studies in yeast have shown that Srv2/CAP, the yeast homolog of CAP1, forms a hexameric complex to catalyze the exchange of ADP for ATP (Balcer *et al.*, 2003). Srv2/CAP has a low affinity for ATP-actin and therefore profilin is able to compete with the Srv2/CAP complex to sequester the ATP-G-actin (Mattila *et al.*, 2004; Bertling *et al.*, 2007; Chaudhry *et al.*, 2010). The final step in the turnover of actin filaments is to localize recharged ATP-actin monomers to sites of rapid F-actin polymerization. Recent work by Bergeron *et al* revealed subtle biochemical differences in nucleotide exchange and polymerization rates of the two cytoplasmic actins. Specifically, in the presence of calcium, γ-actin exchanges nucleotides and polymerizes 50% more slowly than β-actin, however, this difference is less pronounced when magnesium is the available ion (Bergeron *et al.*, 2010). The authors speculate that these differences may have implications for isoform specific functions in subcellular microenvironments, such as hair cell stereocilia, where there are high levels of Ca^{2+}.

Other isoform specific data include a report that arginine tRNA transferase, ATE1, interacts specifically with β-actin to arginylate the N-terminus of the polypeptide (Karakozova *et al.*, 2006). Post-translational arginyation is a unique feature of β-actin, not shared with γ-actin. The only report of a γ-actin specific interacting protein is annexin 5a (ANXA5). Tzima and colleagues showed that during platelet cell activation, the actin cytoskeleton undergoes significant remodeling (Tzima *et al.*, 1999). During this process, γ-actin associates with annexin 5a at the cell membranes (Tzima *et al.*, 2000). Annexin 5a is a member of a family of 12 annexin proteins, all of which bind reversibly to membranes in the presence of high Ca^{2+} (Moss and Morgan, 2004). Many of these proteins have also demonstrated F-actin binding properties, suggesting a role in membrane and cytoskeleton dynamics (Hayes *et al.*, 2004). To date ATE1 and ANXA5 are the only proteins known to distinguish between and interact exclusively with only one of the two cytoplasmic isoforms.

Understanding the specific roles of β- and γ-actin is an area of active research. Differences in subcellular localization of the cytoplasmic actins in tissues and cell culture are well documented (Otey *et al.*, 1987, 1988; Khaitlina, 2001). There are conflicting reports of γ- and β-actin localization in cultured cells. Early studies showed that in myoblasts γ-actin preferentially locates to stress fibers whereas β-actin is found at sites of active remodeling for cell motility (Hill and Gunning, 1993). In contrast, a recent report provides contradictory data from fibroblasts

and endothelial cells that β-actin is associated with the less dynamic stress fibers and γ-actin is localized to the periphery of the cells in the lamellopodia (Dugina *et al.*, 2009). In skeletal muscle, γ-actin is found exclusively in the z-disc, a region which connects adjacent myofibrils (Nakata *et al.*, 2001; Papponen *et al.*, 2009). Though expressed at relatively low levels in differentiated skeletal muscle compared to other tissues, γ-actin is required for proper muscle function, as its absence in a skeletal muscle specific knock-out mouse caused progressive myopathy compared to wild-type littermates (Sonnemann *et al.*, 2006). Additionally, γ-actin was found up-regulated to levels 10-fold above normal in various animal models for muscular dystrophy and the authors proposed that γ-actin may be involved in a compensatory remodeling process (Hanft *et al.*, 2006). A homozygous whole body γ-actin knock-out mouse was less viable, smaller, and had an overt muscular myopathy (Belyantseva *et al.*, 2009). Furthermore, this mouse model had a progressive hearing loss apparent first in the high frequency range at 16 weeks of age. This audiological phenotype shares similarities with human patients who suffer from age related hearing loss due to missense mutations in γ-actin, though in humans this hearing loss is nonsyndromic and dominant.

Hearing Loss

Hearing loss is the most common sensory disorder in humans. Approximately 1 in 300-500 Americans are born deaf or hard of hearing, and an additional 30% will begin to suffer some degree of hearing loss by the age of 65

(http://www.nidcd.nih.gov/health/statistics/quick.htm). Genetic hearing loss accounts for 50% of perinatal deafness and genetic factors contribute to age related hearing loss. Genetic hearing loss is a highly heterogeneous disorder and is typically described in terms of whether or not the hearing loss is accompanied by additional phenotypes in the body: syndromic versus nonsyndromic hearing loss. Both classifications can be further subdivided into categories based on age of onset, progression and whether it is a conductive or sensorineural loss. To date, mutations in over 61 genes have been shown to cause nonsyndromic deafness in humans, and an additional 53 deafness loci are mapped to specific chromosomal regions, though the particular genetic lesions of them are yet unknown (Van Camp G, 2010).

Syndromic deafness accounts for roughly one third of genetic hearing loss. Two prevalent and well studied examples of syndromic deafness are Pendred Syndrome and Usher Syndrome. These syndromes exemplify both genetic and phenotypic heterogeneity. Patients with Pendred syndrome harbor mutations in pendrin, a solute carrier protein, or Fox1, a transcription factor that regulates pendrin expression (Everett *et al.*, 1997; Hulander *et al.*, 1998; Yang *et al.*, 2007). When mutated, these proteins cause hearing loss and also affect the structure of the vestibular aqueduct and cause goiter (Yang *et al.*, 2007; Pera *et al.*, 2008). Usher Syndromes are associated with sensorineural hearing loss accompanied by vestibular dysfunction and retinitis pigmentosa (Smith *et al.*, 1994). There are 11 loci so far implicated in Usher Syndrome, and mutations in

these loci result in varying degrees of deafness and vision loss (Kremer *et al.*, 2006; Ahmed *et al.*, 2009). Not surprisingly, less severe mutations in Usher Syndrome genes, as well as the Pendrin genes mentioned above, also cause nonsyndromic hearing loss.

Much of our understanding of the cell biology of the ear has sprung from identifying genetic causes of nonsyndromic deafness. Genes involved in nonsyndromic deafness range from well characterized genes with high expression in other tissues (Kelsell *et al.*, 1997; Morell *et al.*, 1998), to genes primarily expressed in the cochlea whose only functional clues arise from the deafness phenotype, such as TMC1 – transmembrane cochlea-expressed 1 (Kurima *et al.*, 2002; Friedman and Griffith, 2003; Kurima *et al.*, 2003). When a new locus is mapped for nonsyndromic deafness, it is assigned a DFN type and number. Autosomal dominant deafness is designated DFNA, autosomal recessive is DFNB, and X-linked is DFN. Mutations in the gene encoding connexin 26 (DFNB1) are the most common cause of nonsyndromic deafness (Hilgert *et al.*, 2009).

In some instances, though certainly not all, nonsyndromic deafness is caused by mutations in proteins or isoforms that function specifically in the inner ear. By studying the aberrant phenotype these mutations cause in the cochlea, we can begin to understand the function of the wild-type protein. A number of insights into the structure and function of the inner ear have been made by studying

mutations in both well characterized and novel genes that are expressed in the inner ear and cause hearing loss when mutated. Many of these genes important in hearing have largely been identified by determining deafness causing mutations in families segregating hereditary deafness.

The first mutation in cytoplasmic γ-actin linked to progressive, nonsyndromic sensorineural hearing loss (DFNA20) was identified in our laboratory (Zhu *et al.*, 2003). Since the initial identification of the p.T89I missense mutation in the MSU-DF1 family, an additional 9 missense mutations have been found that segregate with deafness in 9 different families (Figure 1-2) (van Wijk *et al.*, 2003; Zhu *et al.*, 2003; Kemperman *et al.*, 2004; Rendtorff *et al.*, 2006; de Heer *et al.*, 2009; Morin *et al.*, 2009). Though these mutations are private and not a shared ancestral allele, DFNA20 is the 5th most prevalent cause of autosomal dominant nonsyndromic deafness (Hilgert *et al.*, 2009). Phenotypically, these missense mutations have similar clinical consequences. In all families observed, hearing loss begins at high frequencies in the 2nd to 3rd decade of life and progresses to nearly complete deafness across all frequencies by the 5th to 6th decade (Figure 1-3). These audiologic data suggest a deficit in a common functional process in which wild-type γ-actin is indispensible. A sensitive test of hearing, distortion product otoacoustic emission (DPOAE), indicates that loss of the outer hair cells occurs first (JL Elfenbein, personal communication). Given that hearing is properly established in these individuals, it is most likely that these mutations interfere with a repair, rather than developmental, mechanism.

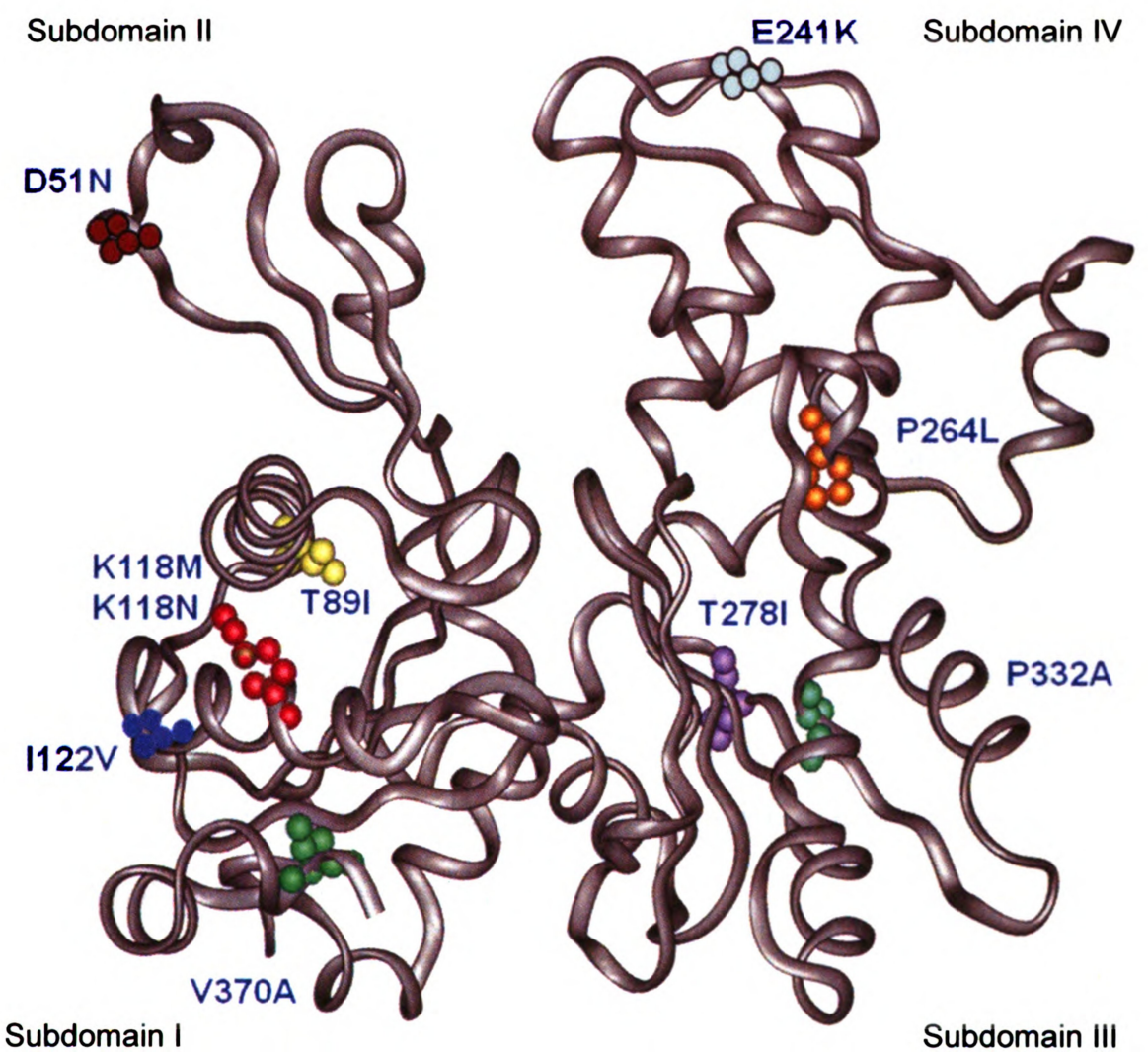

Figure 1-2

Ribbon diagram of a γ-actin monomer with approximate location of 10 missense mutations associated with DFNA20 deafness. The missense mutations are found in all subdomains of the protein and are not clustered within a single functional domain or protein interaction site. A number of actin binding proteins interact at the hinge located between subdomains I and III. Modified from Zhu *et al* 2003.

Figure 1-3

Audiograms from patients in two of the ten DFNA20 families with mutations in γ-actin. The normal range of hearing is from -10 to 20 dB, as indicated by the yellow box. Missense mutations represented are T89I (**A**) and P264L (**B**). In all families hearing loss is postlingual, however there is variability in the age of onset and rate of progression between DFNA20 families with different mutations. For example, individuals with the T89I mutation have a much later onset than those with P264L. Modified from Zhu *et al* 2003.

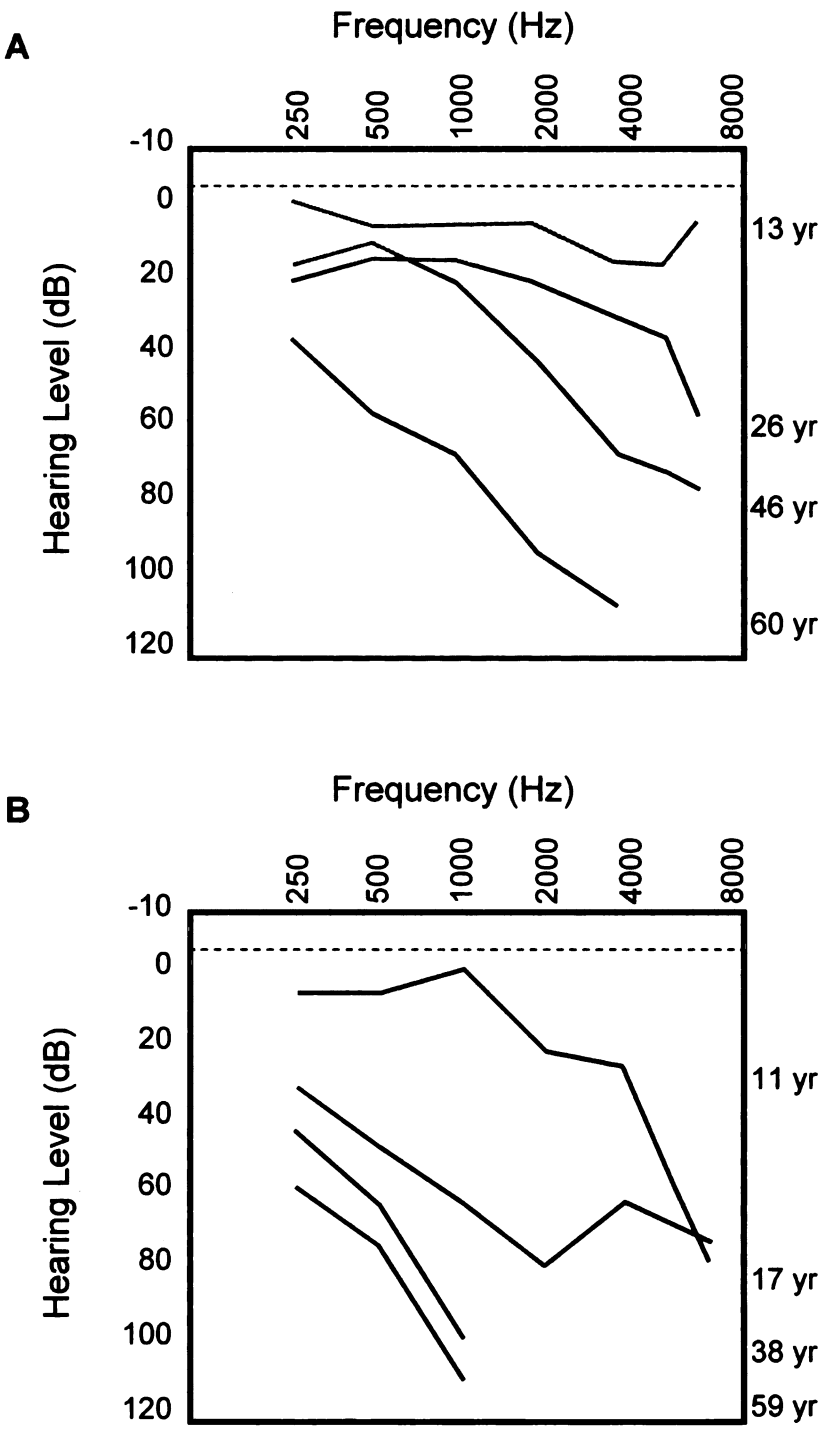
A
Frequency (Hz)
250
500
1000
2000
4000
8000
-10
0
20
40
60
80
100
120
Hearing Level (dB)
13 yr
26 yr
46 yr
60 yr
B
Frequency (Hz)
250
500
1000
2000
4000
8000
-10
0
20
40
60
80
100
120
Hearing Level (dB)
11 yr
17 yr
38 yr
59 yr

The majority of our knowledge pertaining to the molecular effect of DFNA20 mutations on actin comes from *in vitro*, yeast, and cell culture based assays. In our laboratory, Mei Zhu synthesized 7 mutant γ-actins (p.D51N, p. T89I, p.K118M, p.P264L, p.T278I, p.P332A, and p.V370A) *in vitro* to examine folding and stability compared to wild-type γ-actin using native gel electrophoresis (Zhu PhD dissertation, 2008). In the presence of ATP, all six mutant actins folded properly, were released from the CCT-chaperone complex, and migrated as a distinct band on a native polyacrylamide gel. Without ATP present in the native gel during electrophoresis, two mutants P264L and P332A were unable to fold properly and migrated as a diffuse smear. The *in vitro* synthesized proteins were also utilized to examine the functionality of the four subdomains of actins with missense mutations. Using a gel-shift assay, all of the missense mutations showed association with the actin binding proteins tested.

Studies done in yeast engineered to express DFNA20 mutations in the yeast actin gene have differences in growth rates. For example, in complete growth medium, only yeast with the p.K118N mutation grew normally. Similarly, when grown on medium with glycerol as the sole carbon source, only the p.T89I, p.K118N, and p.P264L thrived. In addition to growth rate, other physical and biochemical properties were examined in the mutant yeast. These experiments and results are summarized in Table 1-1. Cell culture based models have also provided insight into the pathogenesis of 6 of the DFNA20 mutations: p.T89I, p.K118M, p.P264L, p.T278I, p.P332A, and p.V307A. In this model, a kidney

	Rate of Growth in YPD liquid culture	Growth on YPG	Altered mitochondrial morphology?	Normal actin filaments in yeast cytoskeleton	Vacuole morphology: number and size of lobes	Thermal Stability, temp of 50% denaturation	ATP-exchange, time in seconds	Polymerization kinetics	Cofilin decoration of F-actin	Susceptibility to cofilin severing
WT		Yes			<5, small	60	52.9	normal	normal	normal
T89I	slight	Yes	Yes	No	<5, small	61	75.6	normal	none	increased
K118M	impaired	No	Yes	No	>5 large & small	57	50	normal	less	normal
K118N	normal	Yes	No	Yes	similar to wt	54	44*	normal	normal	normal
E241K	impaired	No	Yes	No	>5, large & small	58	35	faster, bundled filaments	none	increased
P264L	slight	Yes	Yes	No	<5, one large	54	10.1	normal	less	normal
T278I	impaired	No	Yes	No	>5, large & small	59	49	normal	less	normal
P332A	impaired	No	Yes	No	>5, large & small	55	14.7	normal	normal	decreased
V370A	impaired	No	Yes	No	>5, small	60	x	faster, shorter filaments	none	increased

*This was not statistically different compared to wild-type sample within same experiment.

Table 1-1

Results are compiled from Bryan *et al 2006,* Bryan and Rubenstein 2009, and Morin *et al 2009.*

epithelial cell line was transfected to stably expressing espin, an actin bundling protein. When confluent, these transfected cells will generate F-actin based microvilli reminiscent to stereocilia. Cells that were co-transfected with the mutant γ-actins produced significantly shorter microvilli. However, assembly of F-actin was not impaired as was evident by the ability of microvilli to recover post-treatment actin destabilizing drugs (Korrapati PhD dissertation, 2009). In organ of Corti explant cultures, mutant γ-actin localizes properly to the tips of stereocilia within four hours after biolistic transfection of plasmids with GFP tagged actin constructs (IA Belyantseva, unpublished personal communication). In both the explant and cell culture systems, the overwhelming level of endogenous wild type γ-actin may mask any effect within the observable timeframe of these experimental models.

Structures of inner ear

Cytoplasmic actins are an important component of the hearing process and play a central role in producing the unique structures found in the cells of the inner ear. In mammals, the inner ear has two primary components, the cochlea and the vestibular system. The cochlea is a snail shell shaped structure and contains three fluid-filled compartments: scala tympani and scala vestibule comprised of filled with perilymph, and the scala media filled with endolymph (Friedman and Griffith, 2003). Physical separation of these compartments is necessary to maintain the proper endocochlear potential. Similar to the cochlea, the vestibular system is also characterized by semi-circular canals filled with fluid similar in

composition to the cochlear endolymph. Together, the cochlea and vestibular system are encased within a bony labyrinth and embedded in the temporal bone of the skull. The primary organs of hearing and balance are the organ of Corti and vestibular end organs, respectively. These sensory organs are composed of polarized epithelia which contain hair cells responsible for converting mechanical displacements into neural transmissions for sound and balance processing by the brain, a process termed mechanotransduction (Figure 1-4) (Gillespie and Muller, 2009).

In the mouse, inner ear development begins *in utereo* and is completed by postnatal day 12-14 (P12-14) (Frolenkov *et al.*, 2004). Development of the organ of Corti occurs from base to apex. Likewise, innervation the organ of Corti is also tonotopically mapped from base to apex, encoding low to high frequencies, respectively. The hair cells of the organ of Corti can be likened to the keyboard of a piano, with each hair cell being the equivalent of ~1/60th of a piano key (Musiek and Baran, 2007). In the organ of Corti hair cells are arranged in a single row of inner hair cells and three rows of outer hair cells (Figure 1-5A). The initial processing of the sound is achieved by deflection of inner hair cell stereocilia. Outer hair cells amplify sound by prestin-mediated vertical motility which in turn generates the DPOAE, a measure of sound waves exiting the outer ear which serves as a clinical indication of outer hair cell function (Dallos, 2008). Directly adjacent to and beneath the hair cells are populations of supporting cells. In birds and reptiles, these cells are capable of re-entering the cell cycle to generate

Figure 1-4

Components of the mouse inner ear. Sound waves are channeled through the ear canal and create vibrations of the ear drum (**A**). These vibrations are transferred through the bones of the inner ear to the cochlea. The tallest row of stereocilia of hair cells is embedded in the gelatinous tectorial membrane (**C**). Pressure by the tectorial membrane deflects the hair bundle and opens mechanotransduction channels on the tips of the two shortest rows of stereocilia. The rapid influx of K+ and Ca^{2+} into the cell through the stereocilia cause depolarization and neurotransmitters are released at the basal end of the hair cell. Hair cell containing sensory epithelia (yellow) of the vestibular end organs transduce changes in gravitational forces using a similar mechanism (**D**). Panels A-C are from Frolenkov *et al* 2005.

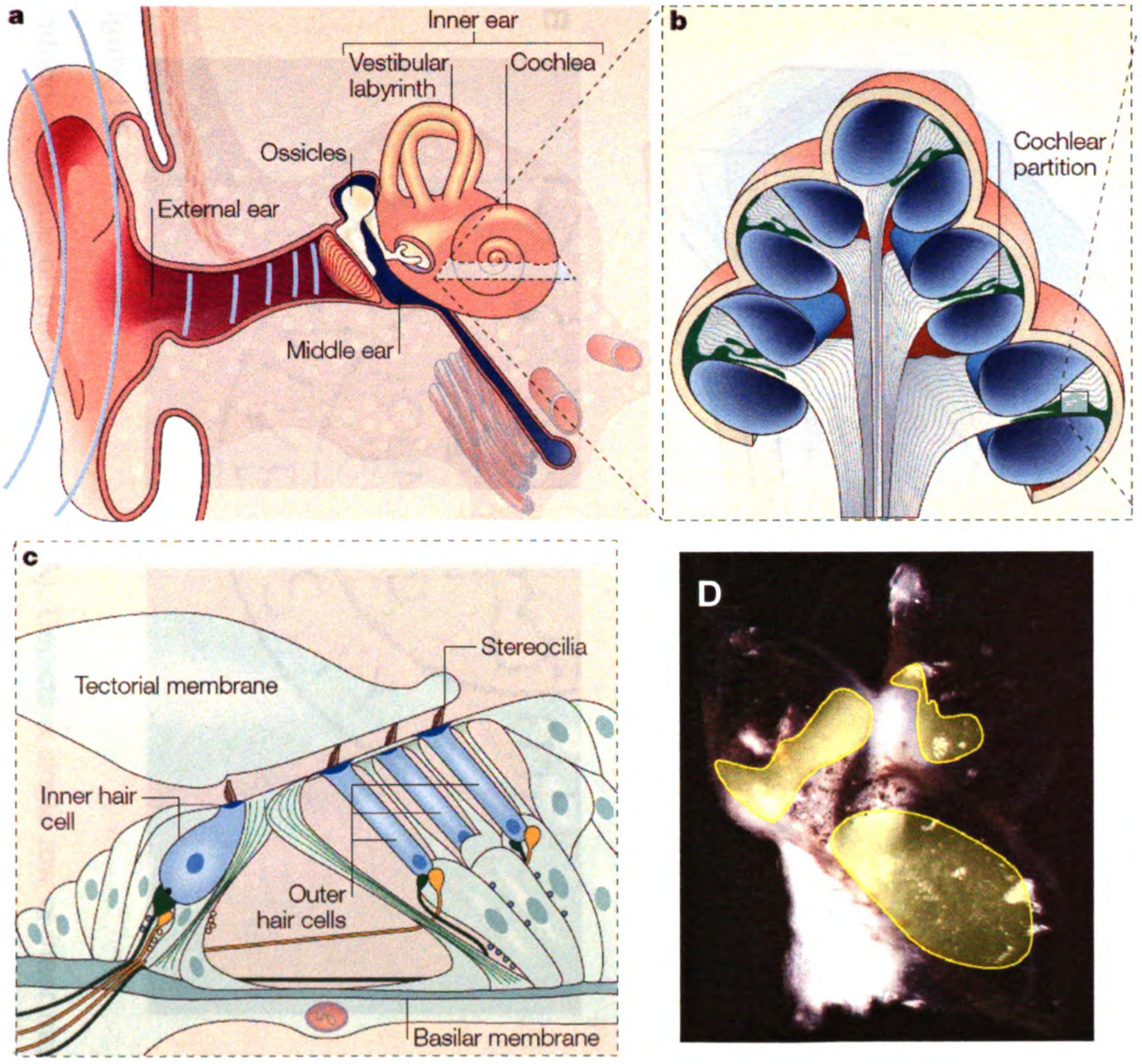
a
Inner ear
Vestibular labyrinth
Cochlea
Ossicles
External ear
Middle ear
b
Cochlear partition
c
Stereocilia
Tectorial membrane
Inner hair cell
Outer hair cells
Basilar membrane
D

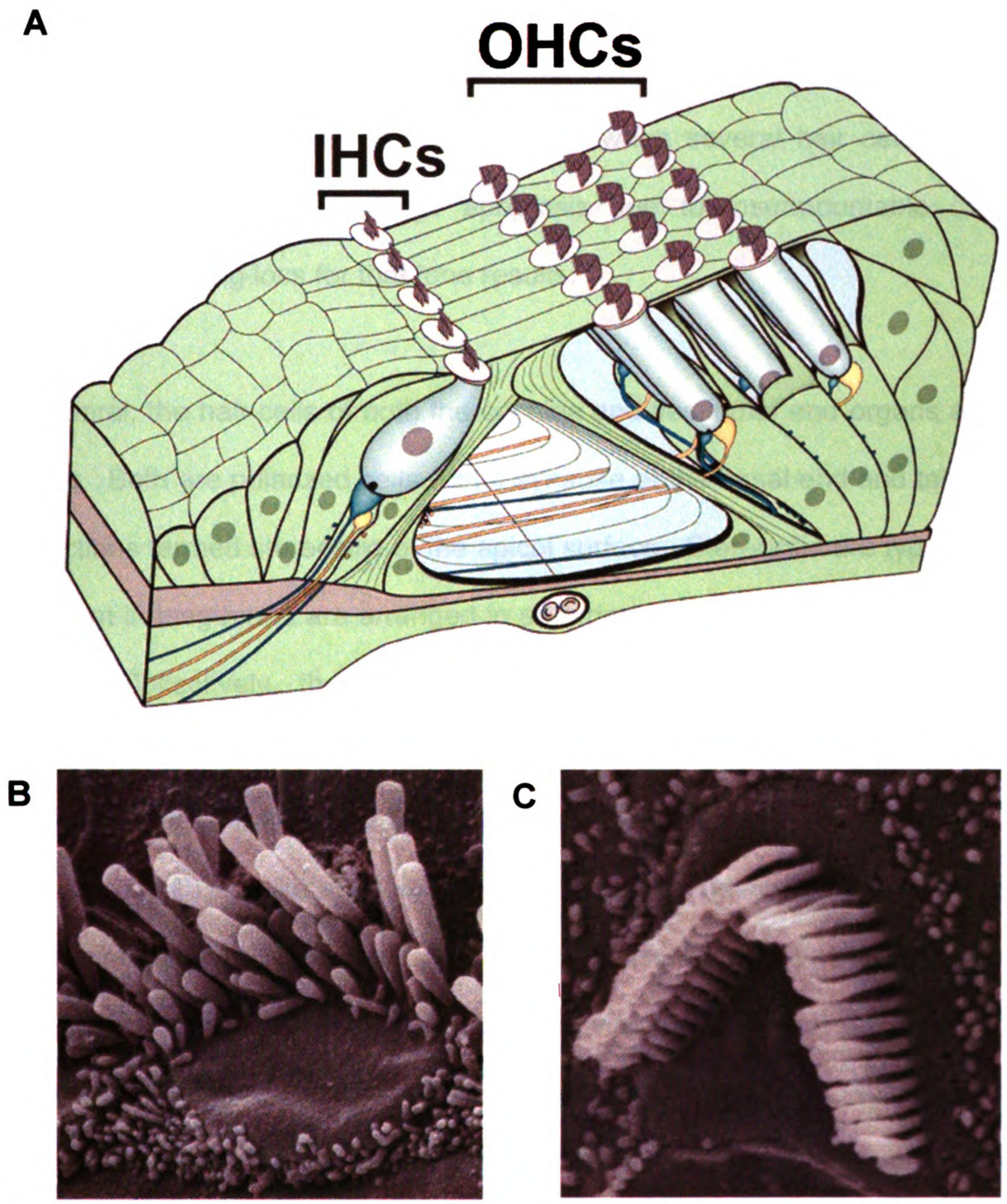

Figure 1-5

Cartoon schematic of the organ of Corti (**A**). Depicts a single row of inner hair cells (IHCs) and three rows of outer hair cells (OHCs) and supporting cells. Belyantseva *et al* 2009. Scanning electron micrograph of the hair bundle of a mouse inner hair cell (**B**) and outer hair cell (**C**).

new auditory hair cells (Groves, 2010). In mammals, auditory hair cells of the cochlea are terminally differentiated and vestibular hair cells have limited capacity for renewal (Groves, 2010). Thus, when several hair cells within the same tonotopic region undergo apoptosis due to insurmountable damage, permanent hearing loss for that tone results.

In general, the hair cells of both the cochlea and vestibular end organs are quite similar. Both are polarized cells with a synapse at the basal end and tall hair-like projections termed stereocilia at the apical surface. Stereocilia are typically 2 μm to 15 μm in length and are arranged in an orderly staircase structure (Shin *et al.*, 2007). Collectively, these projections are known as the hair cell bundle. Mammalian organ of Corti hair cells have three rows of stereocilia within each hair cell bundle. In the outer hair cells, the bundle has a characteristic "v" shape (Figure1- 5B,C). Unlike auditory hair cells, vestibular hair cells have several rows of stereocilia (Frolenkov *et al.*, 2004). Evidence from hair bundle purification experiments suggest that there are ~60 proteins that contribute to the structure, function, and maintenance of the stereocilia (Shin *et al.*, 2007). By far, the most abundant proteins are the two cytoplasmic actins, γ and β, which are present at roughly a 5:1 ratio (Hofer *et al.*, 1997; Furness *et al.*, 2005), and together account for up to 50% of the total protein content in hair cell bundles (Shin *et al.*, 2007). Mutations in a number of actin binding proteins found in the stereocilia are the cause of syndromic and nonsyndromic deafness (Table 1-2). The pathology of these mutations in mouse models usually demonstrate a change in stereocilia

morphology, however, the type of change depends on the protein being mutated. Many of these proteins are myosins and/or their protein cargo. For the remainder of the introduction, I will focus primarily on these proteins, as they demonstrate a great deal about the cell biology of the hair cell, and in particular stereocilia.

Mouse models of deafness

The core of a stereocilium is composed largely of parallel crosslinked and bundled actin filaments (Tilney *et al.*, 1980). Proteins responsible for crosslinking and bundling in stereocilia include fimbrin, espin, and triobp. Mutations in espin and triobp are associated with autosomal recessive nonsyndromic deafness, DFNB36 and DFNB28, respectively (Naz *et al.*, 2004; Riazuddin *et al.*, 2006; Shahin *et al.*, 2006). Though both proteins bundle actin filaments, the subcellular localization and phenotypes associated with loss of function are different. Espin is found along the length of stereocilia in wild-type mice. In the spontaneous espin mouse mutant, *jerker*, stereocilia are abnormally short and thin (Sekerkova *et al.*, 2006). Studies using GFP-β-actin and GFP-espin biolistically transferred into organ of Corti explants cultures demonstrated that espin-actin bundles in the stereocilia treadmill toward the cell body (Rzadzinska *et al.*, 2004). In contrast to espin, triobp is confined to the rootlet of stereocilia and loss of function in an engineered knock-out mouse results in floppy stereocilia and eventual fusion and degradation, reinforcing the importance of a properly formed rootlet upon which stereocilia can deflect (Kitajiri *et al.*, 2010). Functional assays indicate that while

espin bundles filaments by cross-linking, triobp wraps around the periphery of multiple filaments to create a bundle (Kitajiri *et al.*, 2010).

To build actin filaments, there must first be a nucleation event. *In vitro,* this can be achieved by incubating actin above the critical concentration at which spontaneous filament formation occurs after a brief lag phase. In the hair cell, actin dymanics must be tightly regulated so as to control when and where filaments form. For instance, one of the hallmarks of a dying hair cell is uncontrolled filament formation, as is observed in the *shaker-2* mouse which produces long actin-rich projections termed cytocauds that protrude from the basal surface of the hair cell (Kanzaki *et al.*, 2002). However, this phenomenon is not exclusive to the pathology observed in the presence of mutations in actin or actin binding proteins, since aberrant filament formation is also observed in aged organ of Corti cultures (IA Belyantseva personal correspondence). Some proteins serve dual functions in regulating actin dynamics, such as members of the formin family of actin cappers. *In vitro* evidence demonstrates that formins function to nucleate filaments as well as cap existing filaments (Zigmond, 2004). These caps, however, are considered "leaky" because they are also capable of adding monomers to the barbed end of a treadmilling filament (Goode and Eck, 2007). Mutations of diaphanous 1, a formin, is the cause of DFNA1 deafness in humans (Lynch *et al.*, 1997).

Protein	Hearing Loss Loci in Humans	Function	Hair Cell Phenotype	References
γ-actin	DFNA20	cytoskeleton	See Chapter 5	Zhu et al., 2003, van Wjik et al., 2003
Myosin 7a	DFNB2, DFNA11, Usher Type 1b	motor protein	Long stereocilia	Weil et al., 1997 , Holme et al. 2002
Myosin 15a	DFNB3	motor protein	Short stereocilia	Wang et al., 1998 , Mustapha et al., 2007
Harmonin b	DFNB18, Usher Type Ic	scaffold protein	Disorganized stereocilia	Ouyang et al., 2002 ; Ahmed et al., 2002
Radixin	DFNB24	membrane:cytoskeleton		Khan et al., 2007
GRXCR1	DFNB25	cytoskeletal colocalization		Schraders et al., 2010
TrioBP	DFNB28	actin bundling	Floppy sterocilia, no rootlet	Riazuddin et al., 2006, Kitajiri et al. 2010
Myosin 3a	DFNB30	motor protein		Walsh et al., 2002
Whirlin	DFNB31, Usher Type 2d	cytoskeletal elongation	Short stereocilia	Mburu et al., 2003 , Holme et al., 2002
Espin	DFNB36	actin bundling	Thin stereocilia	Naz et al., 2004 , Sekerkova et al., 2006
Myosin 6a	DFNB37, DFNA22	motor protein	Giant, fused stereocilia	Ahmed et al., 2003 , Sakagushi et al., 2008
Taperin	DFNB79	cytoskeletal colocalization	n/a	Rehman et al., 2010; Li et al., 2010
Diaphanous 1	DFNA1	actin capping, nucleation	n/a	Lynch et al., 1997
Myosin 1a	DFNA48	motor protein, scaffold		Donaudy et al., 2003
PTPRQ	DFNB84	scaffold protein	Giant, fused stereocilia	Sakaguchi et al 2008, Schraders et al., 2010

Table 1-2

Actin binding proteins implicated in deafness. These models are described in further detail in the body of the literature review. Pictured to the left are images of stereocilia from the whirlin mutant (**A**), the myosin 7a mutant (**B**), and the myosin 6a mutant (**C**).

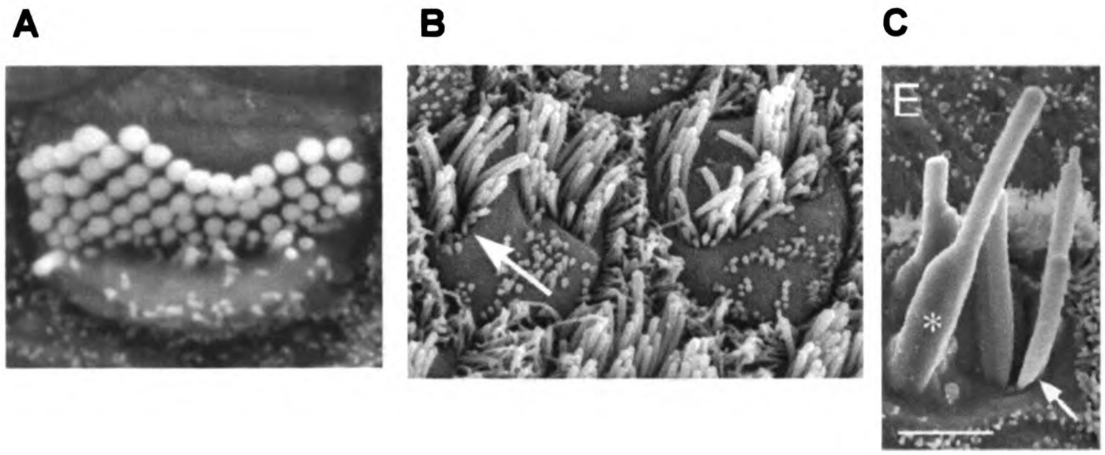

Individual stereocilia within a single hair cell bundle are adjoined to one another from the shorter to the taller via extracellular links composed a heteromeric complex of protocadherin 15 and cadherin 23 (Siemens *et al.*, 2004; Ahmed *et al.*, 2006; Kazmierczak *et al.*, 2007). Recent studies using calcium imaging revealed that in mammals, the mechanotransduction channels are located in the tip of the shorter stereocilia (Beurg *et al.*, 2009), though the composition of this channel remains elusive. Mutations in either tip-link protein cause deafness, and there exist a number of spontaneous cadherin 23 mouse and dog mutants (Schwander *et al.*, 2009). The well characterized C57Bl/6J strain has progressive, age-related hearing loss beginning around 2 months of age due to a cadherin 23 donor splice-site mutation (Johnson *et al.*, 2006).

Height regulation of stereocilia is controlled by a number of actin binding proteins and their cargo. Insights into which proteins are involved in height regulation have been made by studying mouse mutants. Most notably, three spontaneous mutants, *shaker-1*, *shaker-2,* and *Snell's waltzer* are deficient in myosin 7a, myosin 15a, and myosin 6a, respectively, and each display a distinct phenotype (Table 1-2). Not surprisingly, mutations in these three myosins cause autosomal dominant and/or autosomal recessive hearing loss.

Myosin 7a is found along the length of stereocilia and missense mutations cause abnormally long and disorganized stereocilia in *shaker-1* mice (Self *et al.*, 1998).

This phenotype may be due to improper localization of twinfilin 2, an actin capping protein that co-localizes with myosin 7a in stereocilia (Rzadzinska *et al.*, 2009). Using a CL4 cell culture model, Peng *et al* demonstrated that twinfilin 2 is required for length regulation of the shorter rows of stereocilia (Peng *et al.*, 2009).

In contrast to myosin 7a mutants, missense and partial deletion mutations in myosin 15a cause abnormally short stereocilia in *shaker-2* mice (Anderson *et al.*, 2000). Myosin 15a delivers whirlin, a protein aptly named for its phenotype in whirling mice, to the tips of stereocilia where it is proposed to mediate elongation (Belyantseva *et al.*, 2005). Interestingly, *whirler* mice also have abnormally short stereocilia reminiscent of *shaker-2*, and *whirler/shaker-2* double homozygotes have a slightly exacerbated phenotype (Mogensen *et al.*, 2007; Mustapha *et al.*, 2007). *Snell's waltzer* is a spontaneous mouse mutant with a myosin 6a deficiency (Avraham *et al.*, 1995). However, the hair cell phenotype is different from either of the two myosin mutants discussed above. In *Snell's waltzer,* PTPRQ, a protein important within the taper of stereocilia, is improperly localized (Sakaguchi *et al.*, 2008). Not surprisingly, Myosin 6a and PTPRQ deficient mice have the same phenotype of enlarged stereocilia, which do not taper at the point of insertion into the cuticular plate.

Another class of proteins in the stereocilia are those which associate with membranes. DFNB24 deafness is caused by mutations in radixin, a protein

found near the base of the stereocilia that functions to link the cytoskeleton to the membrane (Khan *et al.*, 2007). Annexin 5a is also a membrane protein highly enriched in the organ of Corti, in particular the stereocilia (Peters *et al.*, 2007; Shin *et al.*, 2007). Studies from other cell lines indicate a possible function in linking membrane and cytoskeletal dynamics, though a precise function in the stereocilia remains elusive.

Due to the dynamic function of the hair cell and the repeated mechanical stress placed on the stereocilia, mechanisms must be in place to repair these terminally differentiated cells. Recent evidence suggests a role for γ-actin in the repair of stereocilia. At the cellular level, loss of stiffness and gaps within the actin core are observed after repeated noise damage and in correlation with aged vestibular hair cells (Belyantseva *et al.*, 2009). Proteins that are particularly abundant in these gaps are likely candidates for repair of stereocilia. Not surprisingly, proteins identified in these gaps are largely actin and actin binding proteins, including, but not limited to, γ-actin, cofilin, DNaseI, and espin (Belyantseva *et al.*, 2009). These data are consistent with a model where the filamentous actin core is rebuilt and possibly "filled in" by rejoining existing actin filaments, perhaps similarly to what has been observed in the bristles of *Drosophila* (Guild *et al.*, 2005).

References

Ahmed, Z. M., Goodyear, R., Riazuddin, S., Lagziel, A., Legan, P. K., Behra, M., Burgess, S. M., Lilley, K. S., Wilcox, E. R., Riazuddin, S., *et al.*, 2006. The tip-link antigen, a protein associated with the transduction complex of sensory hair cells, is protocadherin-15. Journal of Neuroscience. 26, 7022-7034.

Ahmed, Z. M., Riazuddin, S., Khan, S. N., Friedman, P. L., Riazuddin, S., Friedman, T. B., 2009. USH1H, a novel locus for type I Usher syndrome, maps to chromosome 15q22-23. Clin Genet. 75, 86-91.

Anderson, D. W., Probst, F. J., Belyantseva, I. A., Fridell, R. A., Beyer, L., Martin, D. M., Wu, D., Kachar, B., Friedman, T. B., Raphael, Y., *et al.*, 2000. The motor and tail regions of myosin XV are critical for normal structure and function of auditory and vestibular hair cells. Hum Mol Genet. 9, 1729-38.

Avraham, K. B., Hasson, T., Steel, K. P., Kingsley, D. M., Russell, L. B., Mooseker, M. S., Copeland, N. G., Jenkins, N. A., 1995. The mouse Snell's waltzer deafness gene encodes an unconventional myosin required for structural integrity of inner ear hair cells. Nat Genet. 11, 369-75.

Balcer, H. I., Goodman, A. L., Rodal, A. A., Smith, E., Kugler, J., Heuser, J. E., Goode, B. L., 2003. Coordinated regulation of actin filament turnover by a high-molecular-weight Srv2/CAP complex, cofilin, profilin, and Aip1. Curr Biol. 13, 2159-69.

Belyantseva, I. A., Boger, E. T., Naz, S., Frolenkov, G. I., Sellers, J. R., Ahmed, Z. M., Griffith, A. J., Friedman, T. B., 2005. Myosin-XVa is required for tip localization of whirlin and differential elongation of hair-cell stereocilia. Nat Cell Biol. 7, 148-56.

Belyantseva, I. A., Perrin, B. J., Sonnemann, K. J., Zhu, M., Stepanyan, R., McGee, J., Frolenkov, G. I., Walsh, E. J., Friderici, K. H., Friedman, T. B., *et al.*, 2009. Gamma-actin is required for cytoskeletal maintenance but not development. Proc Natl Acad Sci U S A. 106, 9703-8.

Bergeron, S. E., Zhu, M., Thiem, S. M., Friderici, K. H., Rubenstein, P. A., 2010. Ion-dependent polymerization differences between mammalian beta- and gamma-nonmuscle actin isoforms. J Biol Chem. 285, 16087-95.

Bertling, E., Quintero-Monzon, O., Mattila, P. K., Goode, B. L., Lappalainen, P., 2007. Mechanism and biological role of profilin-Srv2/CAP interaction. J Cell Sci. 120, 1225-34.

Beurg, M., Fettiplace, R., Nam, J. H., Ricci, A. J., 2009. Localization of inner hair cell mechanotransducer channels using high-speed calcium imaging. Nat Neurosci. 12, 553-8.

Chaudhry, F., Little, K., Talarico, L., Quintero-Monzon, O., Goode, B. L., 2010. A central role for the WH2 domain of Srv2/CAP in recharging actin monomers to drive actin turnover in vitro and in vivo. Cytoskeleton (Hoboken). 67, 120-33.

Dallos, P., 2008. Cochlear amplification, outer hair cells and prestin. Curr Opin Neurobiol. 18, 370-6.

de Heer, A. M., Huygen, P. L., Collin, R. W., Oostrik, J., Kremer, H., Cremers, C. W., 2009. Audiometric and vestibular features in a second Dutch DFNA20/26 family with a novel mutation in ACTG1. Ann Otol Rhinol Laryngol. 118, 382-90.

DePonti-Zilli, L., Seiler-Tuyns, A., Paterson, B. M., 1988. A 40-base-pair sequence in the 3' end of the beta-actin gene regulates beta-actin mRNA transcription during myogenesis. Proc Natl Acad Sci U S A. 85, 1389-93.

National Institute on Deafness and other Communication Disorders. Quick Statistics. http://www.nidcd.nih.gov/health/statistics/quick.htm Bethesda, MD.

Dugina, V., Zwaenepoel, I., Gabbiani, G., Clement, S., Chaponnier, C., 2009. Beta and gamma-cytoplasmic actins display distinct distribution and functional diversity. J Cell Sci. 122, 2980-8.

Erba, H. P., Gunning, P., Kedes, L., 1986. Nucleotide sequence of the human gamma cytoskeletal actin mRNA: anomalous evolution of vertebrate non-muscle actin genes. Nucleic Acids Res. 14, 5275-94.

Everett, L. A., Glaser, B., Beck, J. C., Idol, J. R., Buchs, A., Heyman, M., Adawi, F., Hazani, E., Nassir, E., Baxevanis, A. D., *et al.*, 1997. Pendred syndrome is caused by mutations in a putative sulphate transporter gene (PDS). Nature Genetics. 17, 411-422.

Fass, J., Gehler, S., Sarmiere, P., Letourneau, P., Bamburg, J. R., 2004. Regulating filopodial dynamics through actin-depolymerizing factor/cofilin. Anat Sci Int. 79, 173-83.

Friedman, T. B., Griffith, A. J., 2003. Human nonsyndromic sensorineural deafness. Annu Rev Genomics Hum Genet. 4, 341-402.

Frolenkov, G. I., Belyantseva, I. A., Friedman, T. B., Griffith, A. J., 2004. Genetic insights into the morphogenesis of inner ear hair cells. Nat Rev Genet. 5, 489-98.

Furness, D. N., Katori, Y., Mahendrasingam, S., Hackney, C. M., 2005. Differential distribution of beta- and gamma-actin in guinea-pig cochlear sensory and supporting cells. Hear Res. 207, 22-34.

Gillespie, P. G., Muller, U., 2009. Mechanotransduction by hair cells: models, molecules, and mechanisms. Cell. 139, 33-44.

Goode, B. L., Eck, M. J., 2007. Mechanism and function of formins in the control of actin assembly. Annu Rev Biochem. 76, 593-627.

Groves, A. K., 2010. The challenge of hair cell regeneration. Exp Biol Med (Maywood). 235, 434-46.

Guild, G. M., Connelly, P. S., Ruggiero, L., Vranich, K. A., Tilney, L. G., 2005. Actin filament bundles in Drosophila wing hairs: hairs and bristles use different strategies for assembly. Mol Biol Cell. 16, 3620-31.

Hanft, L. M., Rybakova, I. N., Patel, J. R., Rafael-Fortney, J. A., Ervasti, J. M., 2006. Cytoplasmic gamma-actin contributes to a compensatory remodeling response in dystrophin-deficient muscle. Proc Natl Acad Sci U S A. 103, 5385-90.

Hayes, M. J., Rescher, U., Gerke, V., Moss, S. E., 2004. Annexin-actin interactions. Traffic. 5, 571-6.

Hilgert, N., Smith, R. J., Van Camp, G., 2009. Forty-six genes causing nonsyndromic hearing impairment: which ones should be analyzed in DNA diagnostics? Mutat Res. 681, 189-96.

Hill, M. A., Gunning, P., 1993. Beta and gamma actin mRNAs are differentially located within myoblasts. J Cell Biol. 122, 825-32.

Hofer, D., Ness, W., Drenckhahn, D., 1997. Sorting of actin isoforms in chicken auditory hair cells. J Cell Sci. 110 (Pt 6), 765-70.

Hulander, M., Wurst, W., Carlsson, P., Enerback, S., 1998. The winged helix transcription factor Fkh10 is required for normal development of the inner ear. Nat Genet. 20, 374-6.

Johnson, K. R., Zheng, Q. Y., Noben-Trauth, K., 2006. Strain background effects and genetic modifiers of hearing in mice. Brain Res. 1091, 79-88.

Kanzaki, S., Beyer, L. A., Canlon, B., Meixner, W. M., Raphael, Y., 2002. The cytocaud: a hair cell pathology in the waltzing Guinea pig. Audiol Neurootol. 7, 289-97.

Karakozova, M., Kozak, M., Wong, C. C., Bailey, A. O., Yates, J. R., 3rd, Mogilner, A., Zebroski, H., Kashina, A., 2006. Arginylation of beta-actin regulates actin cytoskeleton and cell motility. Science. 313, 192-6.

Kazmierczak, P., Sakaguchi, H., Tokita, J., Wilson-Kubalek, E. M., Milligan, R. A., Muller, U., Kachar, B., 2007. Cadherin 23 and protocadherin 15 interact to form tip-link filaments in sensory hair cells. Nature. 449, 87-U59.

Kelsell, D. P., Dunlop, J., Stevens, H. P., Lench, N. J., Liang, J. N., Parry, G., Mueller, R. F., Leigh, I. M., 1997. Connexin 26 mutations in hereditary non-syndromic sensorineural deafness. Nature. 387, 80-3.

Kemperman, M. H., De Leenheer, E. M., Huygen, P. L., van Wijk, E., van Duijnhoven, G., Cremers, F. P., Kremer, H., Cremers, C. W., 2004. A Dutch family with hearing loss linked to the DFNA20/26 locus: longitudinal analysis of hearing impairment. Arch Otolaryngol Head Neck Surg. 130, 281-8.

Khaitlina, S. Y., 2001. Functional specificity of actin isoforms. Int Rev Cytol. 202, 35-98.

Khan, S. Y., Ahmed, Z. M., Shabbir, M. I., Kitajiri, S., Kalsoom, S., Tasneem, S., Shayiq, S., Ramesh, A., Srisailpathy, S., Khan, S. N., *et al.*, 2007. Mutations of the RDX gene cause nonsyndromic hearing loss at the DFNB24 locus. Hum Mutat. 28, 417-23.

Kitajiri, S., Sakamoto, T., Belyantseva, I. A., Goodyear, R. J., Stepanyan, R., Fujiwara, I., Bird, J. E., Riazuddin, S., Riazuddin, S., Ahmed, Z. M., *et al.*, 2010. Actin-bundling protein TRIOBP forms resilient rootlets of hair cell stereocilia essential for hearing. Cell. 141, 786-98.

Korrapati, S., Functional analysis of cytoplasmic gamma-actin mutations causing non-syndromic, progressive autosomal dominant hearing loss. Genetics Program. PhD. Dissertation, 2009.

Kremer, H., van Wijk, E., Marker, T., Wolfrum, U., Roepman, R., 2006. Usher syndrome: molecular links of pathogenesis, proteins and pathways. Hum Mol Genet. 15 Spec No 2, R262-70.

Kurima, K., Peters, L. M., Yang, Y., Riazuddin, S., Ahmed, Z. M., Naz, S., Arnaud, D., Drury, S., Mo, J., Makishima, T., *et al.*, 2002. Dominant and recessive deafness caused by mutations of a novel gene, TMC1, required for cochlear hair-cell function. Nat Genet. 30, 277-84.

Kurima, K., Yang, Y., Sorber, K., Griffith, A. J., 2003. Characterization of the transmembrane channel-like (TMC) gene family: functional clues from hearing loss and epidermodysplasia verruciformis. Genomics. 82, 300-8.

Lloyd, C., Gunning, P., 2002. beta- and gamma-actin genes differ in their mechanisms of down-regulation during myogenesis. J Cell Biochem. 84, 335-42.

Lohse, P., Arnold, H. H., 1988. The down-regulation of the chicken cytoplasmic beta actin during myogenic differentiation does not require the gene promoter but involves the 3' end of the gene. Nucleic Acids Res. 16, 2787-803.

Lynch, E. D., Lee, M. K., Morrow, J. E., Welcsh, P. L., Leon, P. E., King, M. C., 1997. Nonsyndromic deafness DFNA1 associated with mutation of a human homolog of the Drosophila gene diaphanous. Science. 278, 1315-8.

Mattila, P. K., Quintero-Monzon, O., Kugler, J., Moseley, J. B., Almo, S. C., Lappalainen, P., Goode, B. L., 2004. A high-affinity interaction with ADP-actin monomers underlies the mechanism and in vivo function of Srv2/cyclase-associated protein. Mol Biol Cell. 15, 5158-71.

Michelot, A., Berro, J., Guerin, C., Boujemaa-Paterski, R., Staiger, C. J., Martiel, J. L., Blanchoin, L., 2007. Actin-filament stochastic dynamics mediated by ADF/cofilin. Curr Biol. 17, 825-33.

Mogensen, M. M., Rzadzinska, A., Steel, K. P., 2007. The deaf mouse mutant whirler suggests a role for whirlin in actin filament dynamics and stereocilia development. Cell Motil Cytoskeleton. 64, 496-508.

Morell, R. J., Kim, H. J., Hood, L. J., Goforth, L., Friderici, K., Fisher, R., Van Camp, G., Berlin, C. I., Oddoux, C., Ostrer, H., *et al.*, 1998. Mutations in the connexin 26 gene (GJB2) among Ashkenazi Jews with nonsyndromic recessive deafness. N Engl J Med. 339, 1500-5.

Morin, M., Bryan, K. E., Mayo-Merino, F., Goodyear, R., Mencia, A., Modamio-Hoybjor, S., del Castillo, I., Cabalka, J. M., Richardson, G., Moreno, F., *et al.*, 2009. In vivo and in vitro effects of two novel gamma-actin (ACTG1) mutations that cause DFNA20/26 hearing impairment. Hum Mol Genet. 18, 3075-89.

Moss, S. E., Morgan, R. O., 2004. The annexins. Genome Biol. 5, 219.

Musiek, F. E., Baran, J. A., 2007. The auditory system : anatomy, physiology and clinical correlates. Pearson, Boston.

Mustapha, M., Beyer, L. A., Izumikawa, M., Swiderski, D. L., Dolan, D. F., Raphael, Y., Camper, S. A., 2007. Whirler mutant hair cells have less severe pathology than shaker 2 or double mutants. J Assoc Res Otolaryngol. 8, 329-37.

Nakata, T., Nishina, Y., Yorifuji, H., 2001. Cytoplasmic gamma actin as a Z-disc protein. Biochem Biophys Res Commun. 286, 156-63.

Naz, S., Griffith, A. J., Riazuddin, S., Hampton, L. L., Battey, J. F., Jr., Khan, S. N., Riazuddin, S., Wilcox, E. R., Friedman, T. B., 2004. Mutations of ESPN cause autosomal recessive deafness and vestibular dysfunction. J Med Genet. 41, 591-5.

Otey, C. A., Kalnoski, M. H., Bulinski, J. C., 1987. Identification and quantification of actin isoforms in vertebrate cells and tissues. J Cell Biochem. 34, 113-24.

Otey, C. A., Kalnoski, M. H., Bulinski, J. C., 1988. Immunolocalization of muscle and nonmuscle isoforms of actin in myogenic cells and adult skeletal muscle. Cell Motil Cytoskeleton. 9, 337-48.

Papponen, H., Kaisto, T., Leinonen, S., Kaakinen, M., Metsikko, K., 2009. Evidence for gamma-actin as a Z disc component in skeletal myofibers. Exp Cell Res. 315, 218-25.

Peng, A. W., Belyantseva, I. A., Hsu, P. D., Friedman, T. B., Heller, S., 2009. Twinfilin 2 regulates actin filament lengths in cochlear stereocilia. J Neurosci. 29, 15083-8.

Pera, A., Dossena, S., Rodighiero, S., Gandia, M., Botta, G., Meyer, G., Moreno, F., Nofziger, C., Hernandez-Chico, C., Paulmichl, M., 2008. Functional assessment of allelic variants in the SLC26A4 gene involved in Pendred syndrome and nonsyndromic EVA. Proc Natl Acad Sci U S A. 105, 18608-13.

Peters, L. M., Belyantseva, I. A., Lagziel, A., Battey, J. F., Friedman, T. B., Morell, R. J., 2007. Signatures from tissue-specific MPSS libraries identify transcripts preferentially expressed in the mouse inner ear. Genomics. 89, 197-206.

Quitschke, W. W., Lin, Z. Y., DePonti-Zilli, L., Paterson, B. M., 1989. The beta actin promoter. High levels of transcription depend upon a CCAAT binding factor. J Biol Chem. 264, 9539-46.

Rendtorff, N. D., Zhu, M., Fagerheim, T., Antal, T. L., Jones, M., Teslovich, T. M., Gillanders, E. M., Barmada, M., Teig, E., Trent, J. M., *et al.*, 2006. A novel missense mutation in ACTG1 causes dominant deafness in a Norwegian DFNA20/26 family, but ACTG1 mutations are not frequent among families with hereditary hearing impairment. Eur J Hum Genet. 14, 1097-105.

Riazuddin, S., Khan, S. N., Ahmed, Z. M., Ghosh, M., Caution, K., Nazli, S., Kabra, M., Zafar, A. U., Chen, K., Naz, S., *et al.*, 2006. Mutations in TRIOBP, which encodes a putative cytoskeletal-organizing protein, are associated with nonsyndromic recessive deafness. Am J Hum Genet. 78, 137-43.

Rzadzinska, A. K., Nevalainen, E. M., Prosser, H. M., Lappalainen, P., Steel, K. P., 2009. MyosinVIIa interacts with Twinfilin-2 at the tips of mechanosensory stereocilia in the inner ear. PLoS One. 4, e7097.

Rzadzinska, A. K., Schneider, M. E., Davies, C., Riordan, G. P., Kachar, B., 2004. An actin molecular treadmill and myosins maintain stereocilia functional architecture and self-renewal. J Cell Biol. 164, 887-97.

Sakaguchi, H., Tokita, J., Naoz, M., Bowen-Pope, D., Gov, N. S., Kachar, B., 2008. Dynamic compartmentalization of protein tyrosine phosphatase receptor Q at the proximal end of stereocilia: implication of myosin VI-based transport. Cell Motil Cytoskeleton. 65, 528-38.

Schutt, C. E., Myslik, J. C., Rozycki, M. D., Goonesekere, N. C., Lindberg, U., 1993. The structure of crystalline profilin-beta-actin. Nature. 365, 810-6.

Schwander, M., Xiong, W., Tokita, J., Lelli, A., Elledge, H. M., Kazmierczak, P., Sczaniecka, A., Kolatkar, A., Wiltshire, T., Kuhn, P., *et al.*, 2009. A mouse model for nonsyndromic deafness (DFNB12) links hearing loss to defects in tip links of mechanosensory hair cells. Proc Natl Acad Sci U S A. 106, 5252-7.

Sekerkova, G., Zheng, L., Loomis, P. A., Mugnaini, E., Bartles, J. R., 2006. Espins and the actin cytoskeleton of hair cell stereocilia and sensory cell microvilli. Cell Mol Life Sci. 63, 2329-41.

Self, T., Mahony, M., Fleming, J., Walsh, J., Brown, S. D., Steel, K. P., 1998. Shaker-1 mutations reveal roles for myosin VIIA in both development and function of cochlear hair cells. Development. 125, 557-66.

Shahin, H., Walsh, T., Sobe, T., Abu Sa'ed, J., Abu Rayan, A., Lynch, E. D., Lee, M. K., Avraham, K. B., King, M. C., Kanaan, M., 2006. Mutations in a novel isoform of TRIOBP that encodes a filamentous-actin binding protein are responsible for DFNB28 recessive nonsyndromic hearing loss. Am J Hum Genet. 78, 144-52.

Sheterline, P., Sparrow, J. C. J. C., 1998. Actin. Oxford University Press, New York.

Shin, J. B., Streijger, F., Beynon, A., Peters, T., Gadzala, L., McMillen, D., Bystrom, C., Van der Zee, C. E., Wallimann, T., Gillespie, P. G., 2007. Hair bundles are specialized for ATP delivery via creatine kinase. Neuron. 53, 371-86.

Siemens, J., Lillo, C., Dumont, R. A., Reynolds, A., Williams, D. S., Gillespie, P. G., Muller, U., 2004. Cadherin 23 is a component of the tip link in hair-cell stereocilia. Nature. 428, 950-5.

Smith, R. J., Berlin, C. I., Hejtmancik, J. F., Keats, B. J., Kimberling, W. J., Lewis, R. A., Moller, C. G., Pelias, M. Z., Tranebjaerg, L., 1994. Clinical diagnosis of the Usher syndromes. Usher Syndrome Consortium. Am J Med Genet. 50, 32-8.

Sonnemann, K. J., Fitzsimons, D. P., Patel, J. R., Liu, Y., Schneider, M. F., Moss, R. L., Ervasti, J. M., 2006. Cytoplasmic gamma-actin is not required for skeletal muscle development but its absence leads to a progressive myopathy. Dev Cell. 11, 387-97.

Tilney, L. G., Derosier, D. J., Mulroy, M. J., 1980. The organization of actin filaments in the stereocilia of cochlear hair cells. J Cell Biol. 86, 244-59.

Tzima, E., Trotter, P. J., Orchard, M. A., Walker, J. H., 1999. Annexin V binds to the actin-based cytoskeleton at the plasma membrane of activated platelets. Exp Cell Res. 251, 185-93.

Tzima, E., Trotter, P. J., Orchard, M. A., Walker, J. H., 2000. Annexin V relocates to the platelet cytoskeleton upon activation and binds to a specific isoform of actin. Eur J Biochem. 267, 4720-30.

Van Camp G, S. R., Hereditary Hearing Loss Homepage. 2010.

van Wijk, E., Krieger, E., Kemperman, M. H., De Leenheer, E. M., Huygen, P. L., Cremers, C. W., Cremers, F. P., Kremer, H., 2003. A mutation in the gamma actin 1 (ACTG1) gene causes autosomal dominant hearing loss (DFNA20/26). J Med Genet. 40, 879-84.

Yang, T., Vidarsson, H., Rodrigo-Blomqvist, S., Rosengren, S. S., Enerback, S., Smith, R. J., 2007. Transcriptional control of SLC26A4 is involved in Pendred syndrome and nonsyndromic enlargement of vestibular aqueduct (DFNB4). Am J Hum Genet. 80, 1055-63.

Zhu, M., Examining the folding and stability of in vitro synthesized gamma-actin mutations. Cell and Molecular Biology. Ph.D. Dissertation, 2009.

Zhu, M., Yang, T., Wei, S., DeWan, A. T., Morell, R. J., Elfenbein, J. L., Fisher, R. A., Leal, S. M., Smith, R. J., Friderici, K. H., 2003. Mutations in the gamma-actin gene (ACTG1) are associated with dominant progressive deafness (DFNA20/26). Am J Hum Genet. 73, 1082-91.

Zigmond, S. H., 2004. Formin-induced nucleation of actin filaments. Curr Opin Cell Biol. 16, 99-105.

CHAPTER 2

IDENTIFICATION OF ACTIN BINDING PROTEINS USING A YEAST 2-HYBRID SCREEN

Abstract

Mutations in γ-actin cause non-syndromic sensorineural hearing loss. To identify known and novel actin:protein interactions specific to γ-actin in the inner ear, two independent yeast 2-hybrid experiments were performed. In the first experiment, human γ-actin was used as the bait protein to query a prey library constructed from postnatal mouse inner ear cDNA. More than million clones were screened and 395 positive interactions identified. In the second experiment, β-actin was used as the bait protein to probe the same inner ear prey library. Greater than one million clones were screened and 582 positive interactions identified. In both experiments, the majority of interacting preys were γ- or β-actin. Other actin binding proteins were identified, although with much lower frequency compared to the actin prey. Prey proteins found multiple times in both screens included ubiquitin e2i (UBE2I), cyclase associated protein 2 (CAP2), cofilin 2 (CFL2), and cofilin 1 (CFL1). None of the proteins identified in the library screens were specific to β or γ-actin.

To determine if γ-actin bearing a mutation known to cause hearing loss is able to interact with the prey identified in the initial two experiments, P264L γ-actin served as the bait for a directed yeast 2-hybrid experiment. Unlike wild-type γ-actin, P264L γ-actin showed deficiencies in interactions with all actin binding prey tested.

Introduction

Mutations in γ-actin (*ACTG1*) are the cause of autosomal dominant non-syndromic sensorineural hearing loss in DFNA20 families (van Wijk *et al.*, 2003; Zhu *et al.*, 2003; Rendtorff *et al.*, 2006; Liu *et al.*, 2008; de Heer *et al.*, 2009; Morin *et al.*, 2009). Noting the conserved and ubiquitous nature of cytoplasmic actins (Erba *et al.*, 1986), it is remarkable that hearing loss is the only pathology observed. Vertebrates express six isoforms of actin: α-cardiac (*ACTC*), α-skeletal (*ACTA1*), α-aortic (*ACTA2*), γ-enteric (*ACTG2*), β-cytoplasmic (*ACTB*), and γ-cytoplasmic (*ACTG1*). The cytoplasmic β- and γ-actins are expressed at roughly a 2:1 ratio in most tissues of the body (Otey *et al.*, 1987). However, in the inner ear, γ-actin is the predominant isoform expressed at an overall β-:γ-actin ratio of 1:2, with subcellular microdomains reaching ratios as high as 1:5, in the case in the auditory hair cell stereocilia (Hofer *et al.*, 1997; Furness *et al.*, 2005). The two cytoplasmic actins have nearly identical amino acid sequences with the exception of four amino acids in the N-terminal portion of the 375 amino acid polypeptide. Though expression levels of the cytoplasmic actins are well characterized in various tissues, functional differences between β- and γ-actin remain elusive. Some clues have arisen from the distinct subcelluar localization of the two isoforms. β-actin transcripts and proteins are found in dynamic regions of cells which undergo constant remodeling of the actin-based cytoskeleton, such as lamellipodia. In contrast, γ-actin co-localizes with stress fibers, relatively stable actin-based structures (Hill and Gunning, 1993; Korrapati Ph.D Dissertation, 2009). However, a recent report provides conflicting data which

demonstrate that γ-actin is concentrated to the lamellipodia and β-actin to the stress fibers (Dugina *et al.*, 2009). Consistent with the report by Dugina and colleagues, γ-actin is primarily localized to the periphery of and sites of damage to the F-actin core of hair cell stereocilia (Belyantseva *et al.*, 2009).

Given the high levels of expression in almost all cells and tissues of the body, β-actin-null mice are predictably embryonic lethal (Shawlot *et al.*, 1998). In contrast, γ-actin knockout mice are not embryonic lethal, but have reduced viability, muscular myopathy, and progressive deafness (Belyantseva *et al.*, 2009). It is unclear whether actin isoforms are able to substitute for the function of each other, though recent work in mice provides insight; both γ-cytoplasmic and α-cardiac actins rescue muscle function in α-skeletal actin knockout mice (Jaeger *et al.*, 2009; Nowak *et al.*, 2009).

We hypothesized that the cause of DFNA20 deafness is due to the ablation of a specific and indispensable γ-actin:actin binding protein interaction in the inner ear, for which β-actin cannot substitute. To date, only two proteins have been reported to interact exclusively with only one of the cytoplasmic actin isoforms: ATE1 (Arg-tRNA protein transferase 1) and ANXA5 (annexin 5a). ATE1 arginylates β-actin polypeptides, a post-translational modification thought to hinder the association of β-actin filaments into bundles (Karakozova *et al.*, 2006). Annexin 5a interacts exclusively with γ-actin at the membrane of activated

platelet cells (Tzima *et al.*, 2000). At present, the functional details of the association of annexin 5a and γ-actin are unclear.

To identify novel isoform-specific interactions, I implemented yeast 2-hybrid assays. Unlike many protein:protein interaction assays, yeast 2-hybrid experiments can be utilized to detect novel interactions without *a priori* knowledge by screening a tissue-specific library. Yeast 2-hybrid technology can also be used to validate known interactions using a directed approach with single bait and prey proteins of interest. Both of these techniques were previously employed to interrogate postnatal mouse inner ear libraries and validate a protein interaction network. In particular, Adato *et al* performed library-based and directed yeast 2-hybrid screens to identify and validate proteins involved in Usher 1c deafness, a syndrome caused by mutations in harmonin b (Adato *et al.*, 2005).

In this chapter, I describe two yeast 2-hybrid assays in which I used γ-actin and β-actin as bait proteins to identify novel actin isoform-specific protein interactions potentially relevant to γ-actin related deafness. To enrich for γ-actin specific proteins, as well as inner ear specific isoforms, a postnatal mouse inner ear library was used as the prey. Furthermore, I followed the library based-screen with a directed yeast 2-hybrid experiment to determine if a mutant γ-actin, P264L, is able to interact with the prey identified.

Materials and Methods

Vectors

Human γ-actin (*ACTG1*) and β-actin (*ACTB*) coding sequences were obtained from previously cloned pcDNA3.1+ACTG1 and pcDNA3.1+ACTB vectors (Zhu PhD Dissertation, 2008). NdeI and EcoR1 restriction sites were attached to the coding sequence via PCR with Taq polymerase (Invitrogen, Carlsbad, CA) and cloned into a pTOPO-PCR (Invitrogen, Carlsbad, CA) intermediate vector, prior to ligation into the bait (pGBKT7-BD) and prey (pGADT7-AD) vectors (Clontech, Mountain View, CA). The p.P264L mutation was introduced into the intermediate pTOPO-PCR vector containing *ACTG1* coding sequence via QuickChange Site-Directed Mutagenesis (Agilent Technologies, Santa Clara, CA) PCR using primers $^{5'}$CGCTGTTCCAGCTTTCCTTCCT$^{3'}$ and $^{5'}$AGGAAGGAAAGCTGGAACAGCG$^{3'}$, prior to ligation into the bait and prey vectors. All plasmids were sequence verified.

Prey library

The P3 mouse inner ear prey library was a gift from Dr. Erich Boger at the National Institute for Deafness and other Communication Disorders, NIH.

Western Blotting

Proteins were separated via SDS-PAGE on discontinuous 10% Laemmli gels (see appendix). Proteins were transferred in 10 mM Tris base, 100 mM glycine,

15% methanol (transfer buffer) at 4°C either overnight at a constant current of 5 mAmp or for 1.5 hours at a constant voltage of 110V onto polyvinylidene difluoride (PVDF) membranes (BioRad, Hercules, CA). Membranes were incubated in 5% non-fat milk in 0.025% Tween-20 in PBS pH 7.4 (blocking buffer) for either one hour at room temperature or overnight at 4°C. Rabbit polyclonal anti-γ-actin antiserum (Belyantseva *et al*, 2009) was diluted 1:10,000 in blocking buffer and rabbit polyclonal anti-β-actin antiserum (Abcam, Cambridge, MA; ab8227) was diluted 1:1000 in blocking buffer. Membranes were incubated with primary antisera for either 2 hours at room temperature or overnight at 4°C. Goat polyclonal anti-rabbit IgG-HRP conjugated secondary antibody (Sigma, St. Louis, MO) was used at 1:3,000 in blocking buffer for one hour at room temperature. Proteins were detected using an ECL Detection Kit (GE Healthcare, Waukesha, WI) with Amersham Hyperfilm™ MP autoradiography film (GE healthcare, Waukesha, WI). The length of exposure was determined by signal intensity observed.

Primary antibodies

Rabbit polyclonal anti-γ-actin antiserum generated by our lab was raised against the first 15 amino acids of the mammalian γ-actin polypeptide (NH_2-MEEEIAALVIDNGSG), and the exsanguination bleed was affinity purified. Antibody specificity for immunofluorochemistry was demonstrated using *ACTG1*-null mice (Belyantseva *et al.*, 2009). To verify that this antiserum is specific for γ-actin in immunoblotting applications, HeLa cells expressing either GFP-γ-actin or

GFP-β-actin were evaluated by western blot (Dr. Mei Zhu, unpublished data). In addition to endogenous γ-actin at 42 kDa, a single band of ~70 kDa corresponding to GFP-γ-actin was observed in lysate from cells transfected with GFP-γ-actin, but not in lysate from cells transfected with GFP-β-actin. Similarly, a commercially available rabbit polyclonal anti-β-actin antiserum (Abcam, Cambridge, MA; ab8227) raised against a synthetic peptide containing the first 100 amino acids of mammalian β-actin, was determined to be specific for β-actin in immunoblotting applications because in addition to endogenous β-actin, a single band at ~70 kDa was detected in lysate from cells transfected with GFP-β-actin and not in lysate from cells transfected with GFP-γ-actin.

Yeast Transformation

The bait vectors were independently transformed into the AH109 (Clontech, Mountain View, CA) strain of *S. cerevisiae* using a modified lithium acetate mediated transformation (Schiestl and Gietz, 1989). Overnight cultures were diluted 1:10 and grown to an OD_{600}=0.6-1. Cells were centrifuged at 2,000xg for 5 minutes and washed twice with 10 mL TEL buffer (10mM Tris-HCl, pH 7.5, 1 mM EDTA, 0.1M lithium acetate). Cells were resuspended in a final volume of 100 µL TEL with 50 µg of denatured herring testis carrier DNA and 50 ng of plasmid DNA and incubated at room temperature without shaking. After 30 minutes, 700 µL of 40% PEG-4,000 (w/v) in TEL was added and samples were incubated at room temperature for an additional 45 minutes. Cells were

centrifuged at 1,000 xg and washed twice in TE pH 8.0 to remove lithium acetate prior to plating.

Once established, bait strains were transformed with 150 µg of inner ear prey library using lithium acetate and herring testis carrier DNA (Promega, Madison, WI) and the previously described method. The transformations were plated on SD/-Ade/-His/–Leu/-Trp quadruple drop out medium containing 20µg/mL X-α-galactose (Glycosynth, Cheshire, UK), a substrate for the protein product of the MEL1 reporter gene. Incubation at 30°C was carried out for 21 days. Over 1.2 million clones were screened for both the γ-actin and β-actin bait through three separate transformations per bait.

Whole colony PCR

Approximately 1/2 of each colony was resuspended in 100 µL of ddH_20 and used for whole colony PCR to identify γ-actin and β-actin prey. PCR reactions and cycling conditions are described in detail in the appendix. Two minor modifications were made: the entire volume of water and template DNA in each reaction was substituted with cell resuspension, and the initial 95°C denaturation step was extended to 10 minutes. The forward primers were situated within the prey vector and reverse primers were located in the 5' coding sequence of the actin insert. Gamma-actin primers $^{5'}$TTGGAATCACTACAGGGATGTTT$^{3'}$ and $^{5'}$CGGCGATTTCTTCTTCCAT$^{3'}$, and beta-actin primers

$^{5'}$TGAAGATACCCCACCAAACC$^{3'}$ and $^{5'}$GCAGCGATATCGTCATCCAT$^{3'}$ demonstrated specificity for γ-actin and β-actin prey, respectively.

Isolation and identification of prey vectors

Overnight cultures were lysed using 425-600 μm acid-washed glass beads (Sigma, St. Louis, MO) in a 1.5 mL microfuge tube with approximately a 1:1 (v:v) culture to bead ratio. Samples were vortexed at maximum speed for 2-3 minutes to insure complete lysis of cells. Extraction of plasmid DNA from yeast was done according to the Qiagen (Valencia, CA) QIAprep Spin Miniprep Kit instructions. The prey inserts were amplified using pGADT7-AD specific primers situated within vector sequence that flanked the prey insertion site $^{5'}$ATGATGAAGATACCCCACCAAA$^{3'}$ and $^{5'}$ACGATGCACAGTTGAAGTGAA$^{3'}$. Each PCR product was digested with AluI restriction endonuclease to identify duplicate clones. Novel inserts were sequenced and genome wide identification analysis was performed by blastx (http://www.ncbi.nlm.nih.gov) and confirmed with a BLAT search (http://genome.ucsc.edu) using mouse genome reference sequences.

Growth Assays

Single colonies were selected for serial dilution growth assays. Colonies were propagated in synthetic drop-out medium lacking leucine and tryptophan. Overnight cultures were diluted 1:2 and the OD_{600} was measured. Cultures were further diluted to an OD_{600}=0.1 and grown at 30°C with shaking at 250 rpm for 6

hours. Each culture was serially diluted 1:10, 1:100, and 1:1,000 in TE pH8.0 and spotted onto quadruple drop-out plates (-Leu/-Trp/-His/-Ade) using a multichannel pipettor. Plates were left upright until the 5 µL spot of liquid culture was no longer visible (approximately 10 minutes) and then incubated upside-down for 3 days at 30°C.

Results

Identification of actin:protein interactions

The particular yeast 2-hybrid system (Matchmaker 3) that I used identifies positive interactions using auxotrophic and colorometeric criteria. When the bait and prey interact, transcriptional activation of HIS3 and ADE2 allow for growth on double drop-out medium lacking histidine and arginine. TRP1 and LEU2 serve as additional nutritional selection for the presence of the bait and prey vectors. Activation of the MEL1 reporter gene is used for color-based screening of colonies. Expression of the γ- and β-actin baits in AH109 yeast was evaluated by western blot (Figure 2-1). Though these antibodies distinguish between the two vertebrate cytoplasmic actins, I did observe cross-reactivity with yeast actin for both antibodies. The γ-actin and β-actin clones were tested for auto-activation on synthetic triple dropout –Trp/-His/-Ade media. Growth of the bait clones was not observed after several days in culture at 30°C, confirming lack of auto-activation (data not shown).

Using γ-actin as the bait, I screened ~1.2 million clones through three transfections with the P3 inner ear prey library. Given the strong affinity of actin for itself, as well as the abundance of actin transcripts present in the library, I anticipated that the majority of prey identified would be actin. To easily identify these clones, I devised a whole-colony PCR-based method to detect γ- and β-actin prey (Figure 2-2A,B). For the remainder of interactions not identified as

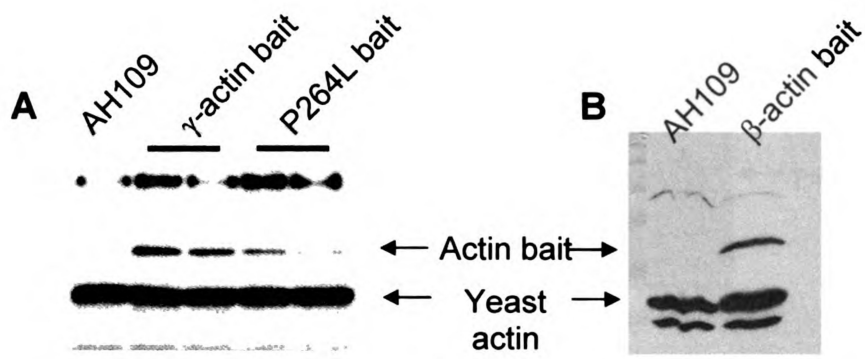

Figure 2-1

Western blot showing expression of bait proteins in transformed AH109 yeast. Transformed γ-actin and P264L γ-actin bait (**A**), and β-actin bait (**B**). Though the γ-actin and β-actin antisera do not cross-react with each other, both recognize endogenous yeast actin.

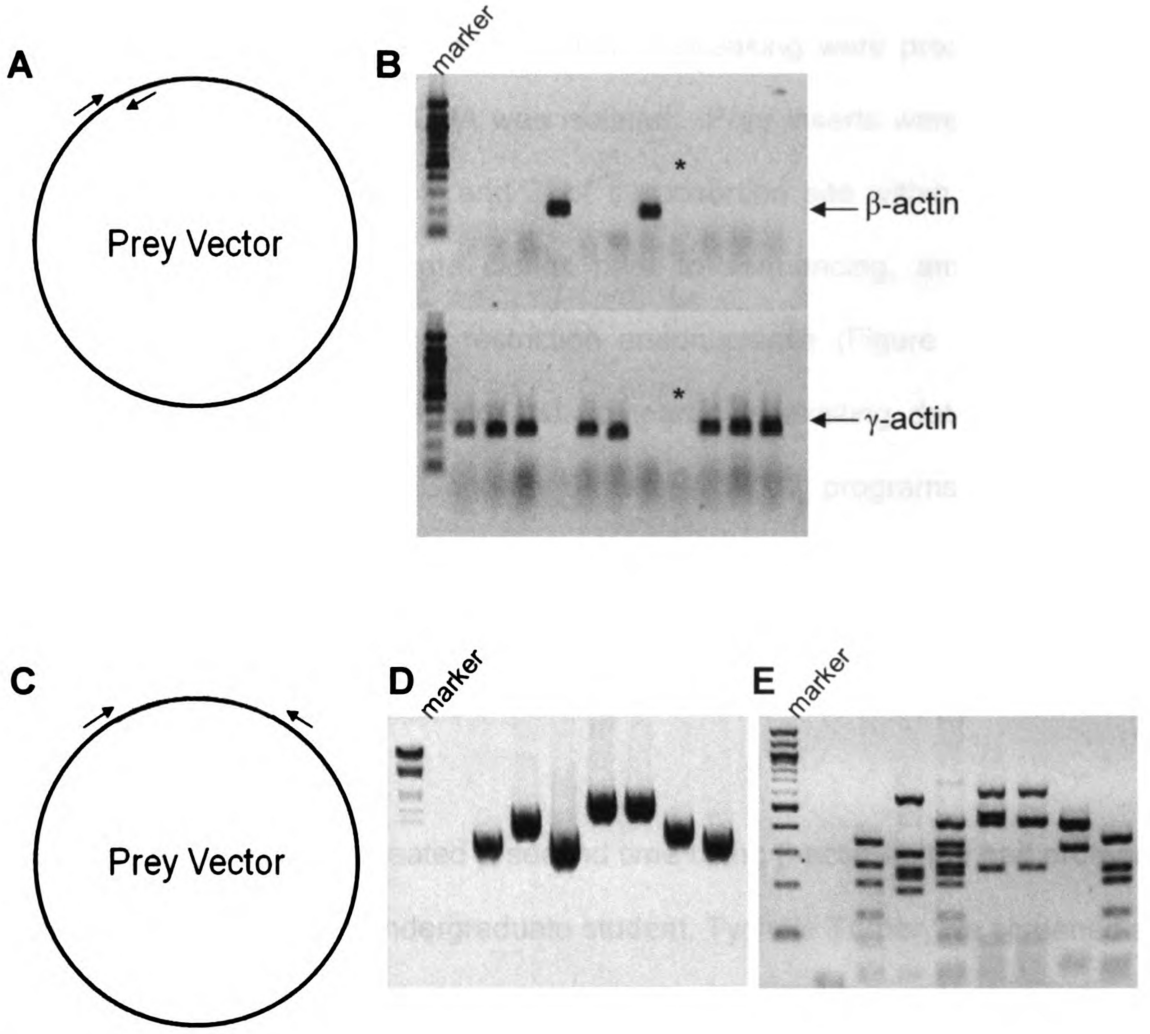

Figure 2-2

Screening strategy for the yeast 2-hybrid library screen experiments. Location of isoform specific primers to amplify γ-actin and β-actin prey (**A**). A representative gel showing specificity of primers for each isoform (**B**). Clones, such as the one indicated by an asterisk, which did not amplify using either of the actin primers were identified by PCR amplification across the entire cDNA insert (**C, D**). Duplicate clones were identified using an AluI restriction digest prior to sequencing (**E**).

either γ- or β-actin, I re-streaked these clones to verify a positive interaction. Clones that tested positive for growth after re-streaking were propagated in an overnight liquid culture, and DNA was isolated. Prey inserts were amplified by PCR using primers situated 5' and 3' of the insertion site within the pGADT7 vector. To eliminate duplicate clones prior to sequencing, amplicons were analyzed via RFLP using AluI restriction endonuclease (Figure 2C-E). Non-duplicate clones were sequenced and compared to existing databases using NCBI's BLAST and UCSC Genome Browser's BLAT programs. In total, I identified 395 positive γ-actin interactions. Of the clones identified more than one time, 276 were γ-actin, 87 β-actin, 12 ubiquitin E2i ligase, 3 cofilin-1, and 3 cofilin-2.

The entire process was repeated a second time using β-actin as the bait protein. With the assistance of an undergraduate student, Tychele Turner, we screened a total of 582 positive β-actin interactions. Of the 582 positive prey clones identified more than once, 388 were γ-actin, 143 β-actin, 9 ubiquitin E2i ligase, 3 cofilin-2, and 2 cyclase associated protein 2. As expected, the majority of the clones isolated in both screens were γ- and β-actin (Table 2-1). In the organ of Corti, γ-actin is the predominant cytoplasmic actin (Hofer *et al.*, 1997; Furness *et al.*, 2005) and my results were consistent with this observation in that the ration of γ:β actin clones is 2.5-3.5:1.

Prey:		total screened	positive	γ-actin	β-actin	γ:β
γ-actin Bait	1	225,000	143	104	30	3.5:1
	2	320,500	57	43	13	3.3:1
	3	609,000	195	129	44	2.9:1
	total	**1,154,500**	**395**	**276**	**87**	**3.2:1**
β-actin Bait	1	324,000	239	158	62	2.5:1
	2	574,000	229	158	57	2.8:1
	3	308,000	114	72	24	3.0:1
	total	**1,206,000**	**582**	**388**	**143**	**2.7:1**

Table 3-1

Actin prey identified in yeast 2-hybrid experiments. Clones not identified as γ- or β-actin were re-streaked for verification and sequenced.

Deafness associated mutant γ-actin shows deficiency in interactions with prey identified in the Y2H screen

Our lab developed a P264L knock-in mouse model that recapitulates the deafness phenotype, however, the molecular mechanism by which this mutation causes deafness is still unclear. Therefore, *in vitro* data using a directed yeast 2-hybrid screen may provide valuable clues pertaining to the molecular pathogenesis of P264L γ-actin. Mutations were introduced into the pTOPO-PCR cloning vectors via site-directed mutatgenesis and cloned into the pGBKT7 bait vector as described in material and methods. As described earlier for wild-type γ- and β-actin prey, expression of the P264L mutant bait was demonstrated using western blot (Figure 2-1A).

I chose four of the prey proteins identified in the screen to test their interaction with P264L γ-actin: γ-actin, β-actin, ubiquitin E2i, and cofilin 2. Human γ-, β-, and P264L γ-actin were cloned into the pGADT7 prey vector by transferring the cDNA inserts from the corresponding bait vectors via NdeI and EcoRI restriction sites described in materials and methods. Ubiquitin E2i ligase and cofilin 2 prey were isolated from positive yeast colonies identified in the original yeast 2-hybrid screens. All prey were co-transformed into AH109 yeast expressing β-actin bait, γ-actin bait, or P264L γ-actin bait. Three colonies from each bait:prey combination were selected at random for serial dilution growth assays (Figure 2-3). When P264L actin was used as the bait, there was no interaction with wild-type β-, γ-actin or P264L actin; however, a weak interaction was observed with

the wild-type actins when P264L actin was the prey instead of the bait. Cofilin 2 and ubiquitin E2i ligase both demonstrated a weak interaction with P264L actin bait, as indicated by the low level of growth in the undiluted spots.

Figure 2-3

Serial dilution growth assays with β-actin, γ-actin, and the DFNA20 hearing loss mutant, p.P264L (PL) γ-actin as the bait protein. Overnight cultures were diluted to an OD_{600} = 0.1 and grown for an additional 6 hours to achieve the exponential growth phase. Cultures were serially diluted to 1:1, 1:10, 1:100, and 1:1,000. Five microliters of each dilution were spotted onto –Trp/-Leu/-His/-Ade plates and grown at 30°C for three days. Each experiment was repeated with three clones, two of which are represented here.

Figure 3

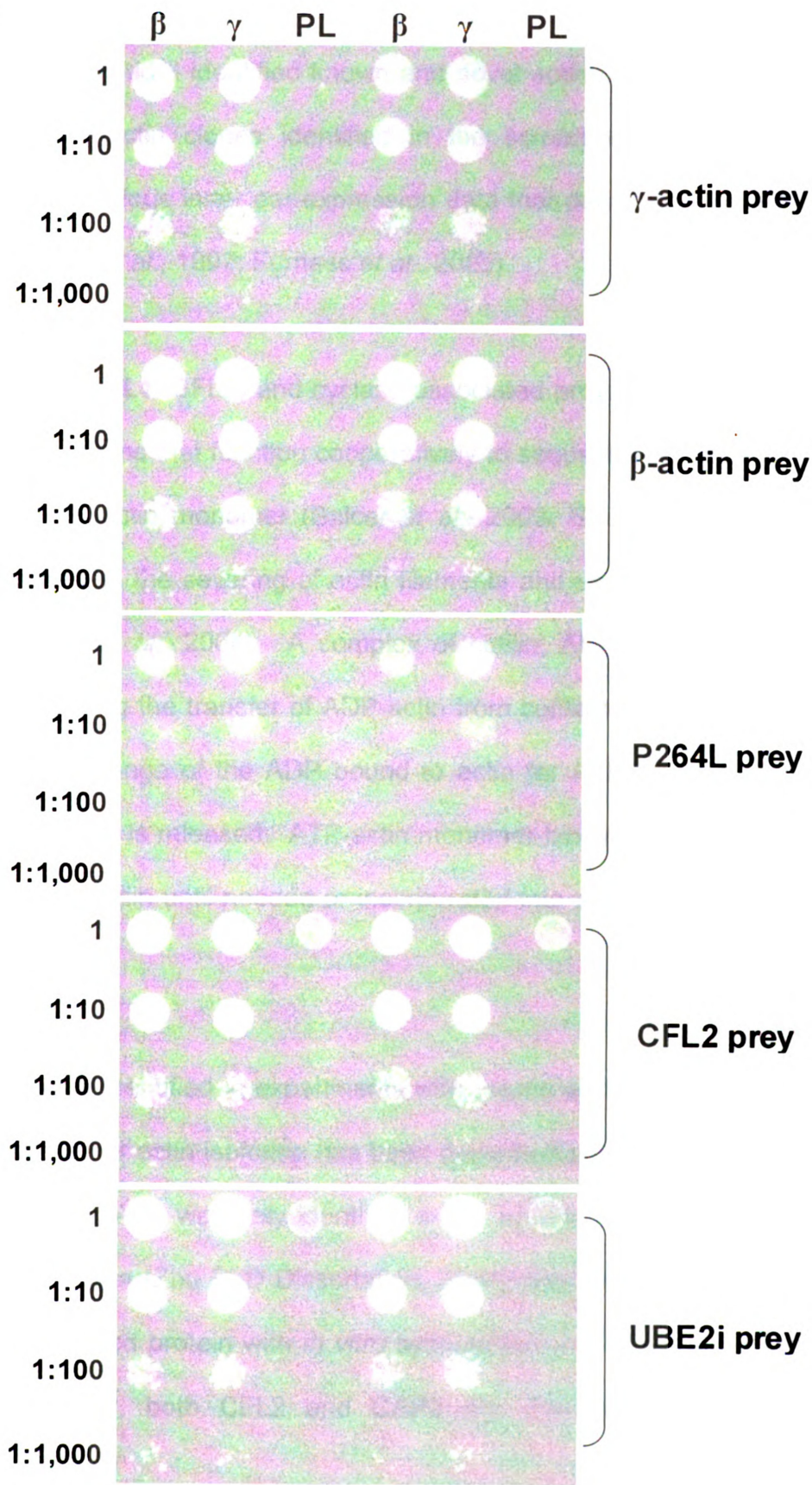
β
γ
PL
β
γ
PL
1
1:10
1:100
1:1,000
γ-actin prey
β-actin prey
P264L prey
CFL2 prey
UBE2i prey

Discussion

Using a yeast 2-hybrid, I identified known and novel actin binding proteins. The large number of actin clones identified in the screen was anticipated and consistent with previous inner ear expression data that demonstrate a 2:1 ration of γ:β-actin (Hofer *et al.*, 1997; Furness *et al.*, 2005).

The two cofilins (CFL1, CFL2) and cyclase associated protein 2 (CAP2) are well characterized proteins that function cooperatively to sequester and exchange the nucleotide on an actin monomer (Balcer *et al.*, 2003; Goode and Eck, 2007). Cofilin is involved in the severing of actin filaments and sequestering ADP-actin monomers (Fass *et al.*, 2004). A complex of cofilin, ADP-actin, and CAP2 is formed briefly during the transfer of ADP-actin from cofilin to CAP2. CAP2 then facilitates the exchange of the ADP bound to actin for ATP and the recharged ATP-actin monomer is released. ATP-actin monomer binding proteins are either sequestered by profilin until needed or incorporated into a new filament (Bertling *et al.*, 2007).

Cofilin 1 was only identified in experiments with γ-actin as the bait, however, an interaction with other actin isoforms has been described previously (Kamal *et al.*, 2007). Similarly, CAP2 was only identified in the experiments with β-actin bait, however *in vitro* data (Zhu PhD Dissertation, 2008) demonstrates an interaction of cyclase associated protein with *in vitro* synthesized γ-actin using a band-shift assay. Interestingly, both CFL2 and CAP2 are considered muscle-specific

isoforms yet were present in the inner ear library, a tissue which does not contain skeletal muscle. Contamination from muscle in the preparation of the cDNA library is unlikely as the organ of Corti is almost completely encapsulated in bone. This finding suggests that CFL2 and CAP2 may perform an as of yet undiscovered function in tissues other than muscle.

The association with ubiquitin E2i ligase (UBE2I) was unexpected. Ubiquitin E2i ligase is an ubiquitin conjugating enzyme that targets proteins for modification or differential localization within the cell (Anckar and Sistonen, 2007). UBE2I is the only E2 ligase for the sumolyation pathway and it facilitates the addition of a SUMO moiety to specific lysine residues. Unlike ubiquitination, addition of SUMO does not target a protein for degradation by the proteosome, rather, it facilitates post-translational modification, such as phosphorylation or acetylation, or changes in localization of the targeted protein (Anckar and Sistonen, 2007). Actins are post-translationally modified (Sheterline and Sparrow, 1998), and recently it was demonstrated that SUMOlyation of actin is essential for retention in the nucleus (Hofmann *et al.*, 2009).

I expected to identify many more actin binding proteins in these screens than I actually did, given the abundance of known actin binding proteins expressed in the inner ear. Though actin is a primarily a cytoskeletal protein, it is also found in the nucleus of most cells and is proposed to aid in the regulation of transcript via association with the PolI, II and III initiation complexes (Miralles and Visa,

2006). Therefore, it is unlikely that expression of actin bait proteins in the nucleus is incompatible with a yeast 2-hybrid experiment. One possible explanation may have to do with the form of actin in the nucleus. In the cytoplasm actins exist as monomers and filaments; however, the form of actin in the nucleus is less clear. A number of actin binding proteins involved in filament dynamics are found in nuclei (Dingova *et al.*, 2009), however, phalloidin staining has not revealed the presence of actin filaments in the nucleus. Typical filamentous actin is visualized using fluorescently labeled phalloidin, leading many to postulate that either unconventional actin filaments are present in the nucleus, or nuclear actin exists only as monomers (Pederson and Aebi, 2002; Bettinger *et al.*, 2004; Castano *et al.*, 2010). If the latter is true, the monomers are likely ADP-actin, not ATP-actin, so as to prevent spontaneous polymerization. Consistent with that notion, all of the actin binding proteins identified in the yeast 2-hybrid screens reported here are ADP-actin binding proteins. A final explanation may be that the SUMOlyation of actin restricts the interaction of many actin binding proteins that typically function in the cytoplasm. As mentioned earlier, Hoffman *et al* (2009) determined that actin lacking a SUMO moiety is readily exported from the nucleus. I would therefore expect the actin bait proteins to be SUMOlyated, as the yeast 2-hybrid assay is dependent on bait and prey proteins remaining in the nucleus. Further insight into the form and function of nuclear actin will aid in the interpretation of the results of this study.

A directed yeast 2-hybrid approach was recently used to characterize the interaction of five of the mutations in γ-actin associated with deafness (Zhong *et al.*, 2009). In this study, the authors constructed mutant γ-actin bait and used γ-actin, β-actin, and three actin depolymerizing factors: cofilin 1, cofilin 2, and destrin as the prey. Activation of the three reporter genes, LACZ, HIS3, and URA3 were tested individually. Yeast expressing the p.P264L γ-actin mutant bait did not interact with any of the prey to activate the LACZ reporter gene, though a weak interaction was observed with wild-type γ- and β-actin prey for the HIS3 and URA3 reporter genes. In my study, I also observed conflicting data with the p.P264L γ-actin bait. When it was used as the bait, no interaction was observed with the wild-type actin prey. However, the converse was not true; γ-actin and β-actin bait did have a weak association p.P264L γ-actin prey. These data may be explained by the inability of p.P264L γ-actin to be SUMOlyated and therefore not retained in the nucleus. Alternatively, differences in expression levels of p.P264L γ-actin as the bait versus the prey may explain the differences in activation. A third scenario may combine the first two explanations in that the mutant γ-actin is not SUMOlyated, though high expression of the prey may allow for low, albeit transient, levels of p.P264L γ-actin in the nucleus prior to exportation.

In closing, this method of analysis provides new, albeit limited data pertaining to possible deficiencies in the function of DFNA20 γ-actin mutations. A directed yeast 2-hybrid experiment may also be useful to investigate other mutant γ-actin:actin binding protein interactions. For example, a former graduate student

found differences in the association of *in vitro* synthesized γ-actin mutants with CAP2 using a band-shift assay (Zhu PhD Dissertation, 2008). However, details of this association, or lack thereof, were limited due to difficulties in expressing recombinant CAP2 in bacteria. In this instance, the directed yeast 2-hybrid approach is well suited to provide additional information regarding a mutant γ-actin:CAP2 interaction, as a strain of yeast expressing CAP2 has already been isolated and described in this study.

References

Adato, A., Michel, V., Kikkawa, Y., Reiners, J., Alagramam, K. N., Weil, D., Yonekawa, H., Wolfrum, U., El-Amraoui, A., Petit, C., 2005. Interactions in the network of Usher syndrome type 1 proteins. Hum Mol Genet. 14, 347-56.

Anckar, J., Sistonen, L., 2007. SUMO: getting it on. Biochem Soc Trans. 35, 1409-13.

Balcer, H. I., Goodman, A. L., Rodal, A. A., Smith, E., Kugler, J., Heuser, J. E., Goode, B. L., 2003. Coordinated regulation of actin filament turnover by a high-molecular-weight Srv2/CAP complex, cofilin, profilin, and Aip1. Curr Biol. 13, 2159-69.

Belyantseva, I. A., Perrin, B. J., Sonnemann, K. J., Zhu, M., Stepanyan, R., McGee, J., Frolenkov, G. I., Walsh, E. J., Friderici, K. H., Friedman, T. B., *et al.*, 2009. Gamma-actin is required for cytoskeletal maintenance but not development. Proc Natl Acad Sci U S A. 106, 9703-8.

Bertling, E., Quintero-Monzon, O., Mattila, P. K., Goode, B. L., Lappalainen, P., 2007. Mechanism and biological role of profilin-Srv2/CAP interaction. J Cell Sci. 120, 1225-34.

Bettinger, B. T., Gilbert, D. M., Amberg, D. C., 2004. Actin up in the nucleus. Nat Rev Mol Cell Biol. 5, 410-5.

Castano, E., Philimonenko, V. V., Kahle, M., Fukalova, J., Kalendova, A., Yildirim, S., Dzijak, R., Dingova-Krasna, H., Hozak, P., 2010. Actin complexes in the cell nucleus: new stones in an old field. Histochem Cell Biol. 133, 607-26.

de Heer, A. M., Huygen, P. L., Collin, R. W., Oostrik, J., Kremer, H., Cremers, C. W., 2009. Audiometric and vestibular features in a second Dutch DFNA20/26 family with a novel mutation in ACTG1. Ann Otol Rhinol Laryngol. 118, 382-90.

Dingova, H., Fukalova, J., Maninova, M., Philimonenko, V. V., Hozak, P., 2009. Ultrastructural localization of actin and actin-binding proteins in the nucleus. Histochem Cell Biol. 131, 425-34.

Dugina, V., Zwaenepoel, I., Gabbiani, G., Clement, S., Chaponnier, C., 2009. Beta and gamma-cytoplasmic actins display distinct distribution and functional diversity. J Cell Sci. 122, 2980-8.

Erba, H. P., Gunning, P., Kedes, L., 1986. Nucleotide sequence of the human gamma cytoskeletal actin mRNA: anomalous evolution of vertebrate non-muscle actin genes. Nucleic Acids Res. 14, 5275-94.

Fass, J., Gehler, S., Sarmiere, P., Letourneau, P., Bamburg, J. R., 2004. Regulating filopodial dynamics through actin-depolymerizing factor/cofilin. Anat Sci Int. 79, 173-83.

Furness, D. N., Katori, Y., Mahendrasingam, S., Hackney, C. M., 2005. Differential distribution of beta- and gamma-actin in guinea-pig cochlear sensory and supporting cells. Hear Res. 207, 22-34.

Goode, B. L., Eck, M. J., 2007. Mechanism and function of formins in the control of actin assembly. Annu Rev Biochem. 76, 593-627.

Hill, M. A., Gunning, P., 1993. Beta and gamma actin mRNAs are differentially located within myoblasts. J Cell Biol. 122, 825-32.

Hofer, D., Ness, W., Drenckhahn, D., 1997. Sorting of actin isoforms in chicken auditory hair cells. J Cell Sci. 110 (Pt 6), 765-70.

Hofmann, W. A., Arduini, A., Nicol, S. M., Camacho, C. J., Lessard, J. L., Fuller-Pace, F. V., de Lanerolle, P., 2009. SUMOylation of nuclear actin. J Cell Biol. 186, 193-200.

Jaeger, M. A., Sonnemann, K. J., Fitzsimons, D. P., Prins, K. W., Ervasti, J. M., 2009. Context-dependent functional substitution of alpha-skeletal actin by gamma-cytoplasmic actin. Faseb J. 23, 2205-14.

Kamal, J. K., Benchaar, S. A., Takamoto, K., Reisler, E., Chance, M. R., 2007. Three-dimensional structure of cofilin bound to monomeric actin derived by structural mass spectrometry data. Proc Natl Acad Sci U S A. 104, 7910-5.

Karakozova, M., Kozak, M., Wong, C. C., Bailey, A. O., Yates, J. R., 3rd, Mogilner, A., Zebroski, H., Kashina, A., 2006. Arginylation of beta-actin regulates actin cytoskeleton and cell motility. Science. 313, 192-6.

Korrapati, S., 2009. Functional analysis of cytoplasmic gamma-actin mutations causing non-syndromic, progressive autosomal dominant hearing loss. Genetics Program. PhD. Dissertation

Liu, P., Li, H., Ren, X., Mao, H., Zhu, Q., Zhu, Z., Yang, R., Yuan, W., Liu, J., Wang, Q., *et al.*, 2008. Novel ACTG1 mutation causing autosomal

dominant non-syndromic hearing impairment in a Chinese family. J Genet Genomics. 35, 553-8.

Miralles, F., Visa, N., 2006. Actin in transcription and transcription regulation. Curr Opin Cell Biol. 18, 261-6.

Morin, M., Bryan, K. E., Mayo-Merino, F., Goodyear, R., Mencia, A., Modamio-Hoybjor, S., del Castillo, I., Cabalka, J. M., Richardson, G., Moreno, F., *et al.*, 2009. In vivo and in vitro effects of two novel gamma-actin (ACTG1) mutations that cause DFNA20/26 hearing impairment. Hum Mol Genet. 18, 3075-89.

Nowak, K. J., Ravenscroft, G., Jackaman, C., Filipovska, A., Davies, S. M., Lim, E. M., Squire, S. E., Potter, A. C., Baker, E., Clement, S., *et al.*, 2009. Rescue of skeletal muscle alpha-actin-null mice by cardiac (fetal) alpha-actin. J Cell Biol. 185, 903-15.

Otey, C. A., Kalnoski, M. H., Bulinski, J. C., 1987. Identification and quantification of actin isoforms in vertebrate cells and tissues. J Cell Biochem. 34, 113-24.

Pederson, T., Aebi, U., 2002. Actin in the nucleus: what form and what for? J Struct Biol. 140, 3-9.

Rendtorff, N. D., Zhu, M., Fagerheim, T., Antal, T. L., Jones, M., Teslovich, T. M., Gillanders, E. M., Barmada, M., Teig, E., Trent, J. M., *et al.*, 2006. A novel missense mutation in ACTG1 causes dominant deafness in a Norwegian DFNA20/26 family, but ACTG1 mutations are not frequent among families with hereditary hearing impairment. Eur J Hum Genet. 14, 1097-105.

Schiestl, R. H., Gietz, R. D., 1989. High efficiency transformation of intact yeast cells using single stranded nucleic acids as a carrier. Curr Genet. 16, 339-46.

Shawlot, W., Deng, J. M., Fohn, L. E., Behringer, R. R., 1998. Restricted beta-galactosidase expression of a hygromycin-lacZ gene targeted to the beta-actin locus and embryonic lethality of beta-actin mutant mice. Transgenic Res. 7, 95-103.

Sheterline, P., Sparrow, J. C. J. C., 1998. Actin. Oxford University Press, New York.

van Wijk, E., Krieger, E., Kemperman, M. H., De Leenheer, E. M., Huygen, P. L., Cremers, C. W., Cremers, F. P., Kremer, H., 2003. A mutation in the gamma actin 1 (ACTG1) gene causes autosomal dominant hearing loss (DFNA20/26). J Med Genet. 40, 879-84.

Zhong, Q., Simonis, N., Li, Q. R., Charloteaux, B., Heuze, F., Klitgord, N., Tam, S., Yu, H., Venkatesan, K., Mou, D., *et al.*, 2009. Edgetic perturbation models of human inherited disorders. Mol Syst Biol. 5, 321.

Zhu, M., 2008. Examining the folding and stability of in vitro synthesized gamma-actin mutations. Cell and Molecular Biology. Ph.D. Dissertation.

Zhu, M., Yang, T., Wei, S., DeWan, A. T., Morell, R. J., Elfenbein, J. L., Fisher, R. A., Leal, S. M., Smith, R. J., Friderici, K. H., 2003. Mutations in the gamma-actin gene (ACTG1) are associated with dominant progressive deafness (DFNA20/26). Am J Hum Genet. 73, 1082-91.

CHAPTER 3

STUDIES OF THE LOCALIZATION OF ANNEXIN 5A IN THE INNER EAR OF MOUSE AND THE INTERACTION OF ANNEXIN 5A WITH GAMMA-ACTIN

Abstract

Annexin 5a is the only protein reported to interact preferentially with γ-actin and not β-actin. This interaction is of interest because missense mutations in the γ-actin gene (*ACTG1*) result in progressive sensorineural hearing loss. Massively Parallel Signature Sequencing data and hair bundle purification experiments indicate that *Anxa5* (annexin 5a) is abundant in the inner ear relative to its expression levels in other organs and tissues in mice. Annexin 5a has been implicated in the reorganization of the actin cytoskeleton, leading us to postulate that the interaction of annexin 5a with γ-actin may be important in maintenance of the cytoskeleton in the organ of Corti.

First, I confirmed the interaction between annexin 5a and γ-actin using a GST-pulldown. Next, to determine if annexin 5a function is potentially relevant to cytoskeletal dynamics in the inner ear I examined the localization pattern of annexin 5a in post-natal mice. Our data show that annexin 5a is present in the stereocilia, cell body, and nuclear membrane of developing auditory and vestibular hair cells. In mature hair cells, annexin 5a is observed primarily in the tips and periphery of the stereocilia, similar to the localization of γ-actin. *Anxa5* knock-out mice do not have hearing loss, and γ-actin is appropriately localized to the periphery of the stereocilia and F-actin gaps in these mice. In conclusion, though annexin 5a is expressed at high levels in the inner ear, it is dispensable for normal hearing or proper γ-actin localization.

Introduction

In mammals, there are two cytoplasmic actin isoforms: β and γ (*Actb* and *Actg1*). In most tissues of the body, β-actin and γ-actin are expressed at roughly a 2:1 ratio (Khaitlina, 2001). However, in the inner ear, γ-actin is the predominant isoform and is reported to be expressed at a β-actin:γ-actin ratio of ~1:2 (Hofer *et al.*, 1997; Furness *et al.*, 2005). The two cytoplasmic actins have identical amino acid sequences with the exception of four amino acids in the N-terminal portion of the 42 kDa protein. To date, only one protein is reported to interact specifically with γ-actin: annexin 5a (Tzima et al., 2000).

Annexin 5a is a member of the larger annexin family of 12 proteins, annexins 1-11 and 13. The physical structure of annexins is characterized by a concave core of relatively conserved, 80 amino acid tandem repeats that bind to both negatively charged membranes and Ca^{2+} (Huber *et al.*, 1990a; Huber *et al.*, 1990b; Brisson *et al.*, 1991; Huber *et al.*, 1992). Annexins typically have 4 repeats in the core domain with the exception of A6, which has eight (Gerke and Moss, 2002). Most annexins reversibly associate with negatively charged membranes composed of phosphatidylserines, via the core domain; an interaction that is typically enhanced by the presence of calcium ions (Gerke et al., 2005). Upon binding to Ca^{2+} and a phosphatidylserines, conformational changes occur in the tertiary structure of the protein (Concha et al., 1993). The nature and specific function of the conformational change is not fully understood for most annexins. However, in the instance of annexin 1a, the conformational

change exposes the N-terminus of the protein which interacts with profilin:actin (Rosengarth and Luecke, 2003). In fact, the specificity of an annexin for other proteins is determined by the unique composition of the N-terminus of the polypeptide (Gerke and Moss, 2002).

In addition to Ca^{2+}-induced changes in protein conformation, annexins also respond to calcium-mediated signaling events. In this response, annexins bring about morphological changes within the cell via coordinating changes in membrane structure with reorganization of the actin cytoskeleton. Indeed, a number of annexins are reported to interact with actin, in particular annexins 1a, 2a, 4a, 5a, and 6a (Gerke and Moss, 2002; Hayes et al., 2004). The nature of the interaction of an annexin with actin is variable. Annexins 2a and 6a bundle filamentous actin (F-actin) in the presence of high Ca^{2+}. Annexin 1a binds F-actin, however it also associates with profilin, a protein which sequesters actin monomers. In activated platelet cells, annexin 5a localizes to the cell membrane where it interacts with the actin-based cytoskeleton (Tzima *et al.*, 1999). It is the only annexin to demonstrate specificity for a particular actin isoform, γ-actin (Tzima et al., 2000).

Annexin 5a has also been implicated in pinocytosis via a nanomechanic mechanism in which polymerized patches bend the plasma membrane to form vesicles internalized by the cell (Kenis et al., 2004). Others reported membrane channel functions of annexin 5a which are supported by both modeling and

experimental data (Jin et al., 2004; Trouve et al., 2007). Further underscoring the dynamic nature of annexin 5a function, in response to Ca^{2+} its subcellular localization changes from diffuse expression within the cytoplasm to association with cellular membranes, the nucleus, and stress fibers in kidney epithelial cells (Markoff and Gerke, 2005). Taken together, annexin 5a clearly plays a role in cytoskeletal and membrane dynamics, however the functional details are yet to be determined (Gerke et al., 2005). The *Anxa5* knock-out mouse model is viable and lacks a discernable phenotype (Brachvogel et al., 2003), suggesting functional redundancy between annexin proteins.

Annexin 5a is abundant in the organ of Corti and is a prominent protein in the stereocilia of hair cells in the inner ear (Peters et al., 2007; Shin et al., 2007). In fact, when compared to the mouse reference transcriptome database, annexin 5a expression is higher in the organ of Corti than in any other tissue. While the subcellular localization of annexin 5a has been well studied in other organs and cell types (Giambanco *et al.*, 1991; Luckcuck *et al.*, 1995; Wang *et al.*, 1995; Gotow *et al.*, 1996; Luckcuck *et al.*, 1997; Kawaminami *et al.*, 1998; Matsuda *et al.*, 2001), the distribution and developmental expression in the inner ear is unknown.

Here I provide the first report describing annexin 5a localization during postnatal development in the mouse organ of Corti and vestibular end organs. I show that annexin 5a is expressed in developing and mature hair cells and supporting cells.

Additionally, I probed the *Anxa5* knock-out model to look for a possible defect in localization of γ-actin to the periphery of the stereocilia in the hair cells of the organ of Corti, or gaps in the stereocilia of vestibular hair cells. Finally, I investigated hearing in *Anxa5* knock-out mice to determine if there is a deafness phenotype associated with a loss of annexin 5a function. Taken together, my data suggest that, in spite of its high expression in the inner ear and overlapping subcellular localization with γ-actin in the stereocilia of auditory hair cells, annexin 5a function is either redundant or dispensable for hearing.

Materials and Methods

Animals

All animals used in this study were housed and euthanized using CO_2 according to NIH guidelines and IACUC approval. Wild-type C57Bl/6J females used for breeding were purchased from Jackson Labs (Bar Harbor, ME). *Anxa5* knock-out mice were a kind gift from Dr. E. Pöschl (Brachvogel et al., 2003).

Primary antibodies

Rabbit polyclonal anti-γ-actin antiserum generated by our laboratory was raised against the first 15 amino acids of the mammalian γ-actin polypeptide (NH_2-MEEEIAALVIDNGSG), and the exsanguination bleed was affinity purified. Antibody specificity for immunofluorochemistry was demonstrated using *ACTG1*-null mice (Belyantseva *et al.*, 2009). To verify that this antiserum is specific for γ-actin in immunoblotting applications, HeLa cells expressing either GFP-γ-actin or GFP-β-actin were evaluated by western blot (Dr. Mei Zhu, unpublished data). A second anti-γ-actin antiserum used in this study was a gift from Dr. J.C. Bulinski, Columbia University, NY (Otey *et al.*, 1986). Similar to the antiserum raised in our laboratory, this rabbit polyclonal anti-γ-actin antiserum was raised against the first 15 amino acids of the mammalian γ-actin polypeptide (NH_2-MEEEIAALVIDNGSG). Antibody specificity for immunofluorochemistry was demonstrated using *ACTG1*-null mice (Belyantseva *et al.*, 2009). The antibody from Dr. Bulinski was only used for immunofluorochemistry.

A commercially available rabbit polyclonal anti-β-actin antiserum (Abcam, Cambridge, MA; ab8227) raised against a synthetic peptide containing the first 100 amino acids of mammalian β-actin, was determined to be specific for β-actin in immunoblotting applications because in addition to endogenous β-actin, a single band at ~70 kDa was detected in lysate from cells transfected with GFP-β-actin and not in lysate from cells transfected with GFP-γ-actin.

Rabbit polyclonal anti-annexin 5a was purchased from AbCam (Cambridge, MA; ab14196). Validation of this antibody for immunoflourochemistry and immunoblotting is provided in this study.

Immunofluorochemistry

Immunofluorochemisty was done as previously described (Belyantseva et al., 2009) with modifications. Cochleae were harvested and immediately perfused with 4% paraformaldehyde (Electron Microscopy Sciences, Hatfield, PA). The organ of Corti and vestibular end organs were microdissected in PBS pH 7.4. Samples were permeabilized with 0.5% Triton X-100 in PBS pH 7.4 and non-specific immunoreactivity was blocked in 5% BSA and 2% goat serum (Invitrogen, Carlsbad, CA) in PBS pH 7.4 (blocking buffer) for either one hour at room temperature or overnight at 4˚C. Rabbit polyclonal anti-annexin 5a was diluted 1:200 in blocking solution and rabbit polyclonal anti-γ-actin was diluted 1:300 in blocking solution. Tissues were incubated with primary antiserum for either 2 hours at room temperature or overnight at 4˚C. Polyclonal anti-rabbit

IgG secondary antiserum conjugated to either Cy3 (Sigma, St. Louis, MO; C2306) or AlexaFluor 488 (Invitrogen, Carlsbad, CA; A11008) was used to label primary antibodies. Secondary antiserum was used at either 1:200 (Cy3) or 1:500 (AlexaFluor 488) in blocking buffer and incubated for 30 minutes at room temperature. Samples were counterstained with either FITC-phalloidin or rhodamine-phalloidin at 1:200 in blocking buffer and DAPI (Invitrogen, Carlsbad, CA) at 1:10,000 in PBS pH7.4. Samples were imaged using Olympus Fluoview LMS (Center Valley, PA) and either a 60x or 100x objective lens. Aside from adjustments to brightness and contrast, no image manipulation was used.

Auditory-evoked Brainstem Response (ABR)

Animals were anesthetized (ketamine 65 mg/kg, xylazine 3.5 mg/kg, and acepromazine 2mg/kg). Body temperature was maintained through the use of water circulating heating pads and heat lamps. Additional anesthetic (ketamine and xylazine) was administered if needed to maintain anesthesia depth sufficient to ensure immobilization and relaxation. ABRs were recorded in an electrically and acoustically shielded chamber (Acoustic Systems, Austin, TX). Needle electrodes were placed at vertex (active), the test ear (reference), and contralateral ear (ground) pinnae. Tucker Davis Technologies (TDT) System III hardware and SigGen/BioSig software (TDT, Alachua, FL) were used to present the stimulus and record responses. Tones were delivered through an EC1 driver (TDT, aluminum enclosure made in-house), with the speculum placed just inside the tragus. Stimulus presentation was 15 ms tone bursts, with 1 ms rise/fall

times, presented 10 times per second. Up to 1024 responses were averaged for each stimulus level. Responses were collected for stimulus levels in 10 dB steps at higher stimulus levels, with additional 5 dB steps near threshold. Thresholds were interpolated between the lowest stimulus level where a response was observed, and 5 dB lower, where no response was observed.

Vectors

Mouse *Anxa5* coding sequence was obtained from IMAGE clone #3488901 (ATCC, Manassas, VA) and subsequently cloned into Invitrogen's Gateway® system. *AttB1/B2* were attached using primers $^{5'}$GGGGACAAGTTTGTACAAAAAAGCAGGCTCCATGGCTACGAGAGGCACTG TGACT$^{3'}$ and $^{5'}$GGGGACCACTTTGTACAAGAAGCTGGGTCTCAGTCATCCTC-GCCCCCGCAG$^{3'}$. BP recombinase enzyme was used to transfer *Anxa5-attb1/2* products into pDONR-221 and clones were sequence verified. LR recombinase enzyme was then used to transfer the *Anxa5* insert into an N-terminal GFP fusion vector, pcDNA-DEST53, and an N-terminal GST fusion vector, pDEST15. pcDNA3.1+Human *ACTG1* was cloned previously in our laboratory by Dr. Mei Zhu (Zhu PhD Dissertation, 2008).

Purification of Recombinant GST-ANXA5

Bl21.AI cells (Invitrogen, Carlsbad, CA) were transformed with 10 ng of pDEST15-*Anxa5* or pDEST15 alone as a GST only control. Single colonies were selected and grown to an OD_{600}=0.4 before induction of protein production with

0.2% L-(+)-arabinose (Sigma, St. Louis, MO) per manufacturer's instructions. Cultures were grown for an additional 4 hours before being centrifuged and snap frozen in liquid nitrogen. Pellets were resuspended in 1% Triton X-100 (Sigma, St. Louis, MO) with a protease inhibitor cocktail (Roche, Basel, Switzerland) in PBS pH 7.4 and sonicated three times in 20 second bursts on ice. Lysates were centrifuged at 14,000 x g at 4°C for 15 minutes. Both the pellet and supernatant were analyzed by SDS-PAGE. Recombinant GST-annexin 5a or GST-only containing supernatant was bound to glutathione sepharose beads (GE Healthcare, Waukesha, WI) at 4°C for one hour with end-over-end tumbling per manufacturer instruction. The beads were washed four times with ice cold PBS supplemented with Complete protease inhibitor cocktail (Roche, Basel, Switzerland). Proteins were eluted using 50 mM reduced glutathione (Sigma, St. Louis, MO) and analyzed by SDS-PAGE.

GST-Pulldown

Recombinant GST-annexin 5a was bound to glutathione sepharose beads as described above. Mammalian cell lystates were prepared from pellets of $1x10^7$ COS-1 cells (ATCC, Manassas, VA). Cell pellets were resuspended in mammalian lysis/binding buffer composed of 100 mM KCl, 10 mM PIPES, 5 mM EGTA, 1% Triton X-100, pH7.4 with Complete protease inhibitor cocktail (Roche, Basel, Switzerland) as described in (Tzima et al., 2000). Cells were sonicated three times in 20 second bursts on ice and then centrifuged at 14,000 x g. GST-ANXA5 or GST-only columns were incubated with COS-1 cell supernatant for

two hours at 4°C with end-over-end tumbling. The lysates were supplemented with 0, 4.8 mM, 4.98 mM, or 6 mM $CaCl_2$, to achieve 0, 0.8μM, 6μM, or 1mM free Ca^{2+}, respectively, as described previously (Tzima et al., 2000). Beads were washed four times with binding buffer and protein complexes were eluted with 50 mM reduced glutathione. Eluted fractions were analyzed by western blotting.

Western Blotting

Proteins were separated via SDS-PAGE on discontinuous 10% Laemmli gels (see appendix). Proteins were transferred in 10 mM Tris base, 100 mM glycine, 15% methanol (transfer buffer) at 4°C either overnight at a constant current of 5 mAmp or for 1.5 hours at a constant voltage of 110V onto polyvinylidene difluoride (PVDF) membranes (BioRad, Hercules, CA). Membranes were incubated in 5% non-fat milk in 0.025% Tween-20 in PBS pH 7.4 (blocking buffer) for either one hour at room temperature or overnight at 4°C. Rabbit polyclonal anti-γ-actin antiserum (Belyantseva *et al*, 2009) was diluted 1:10,000 in blocking buffer, rabbit polyclonal anti-β-actin antiserum was diluted 1:1000 in blocking buffer, and rabbit polyclonal anti-annexin 5a antiserum was diluted 1:1,000 in blocking buffer. Membranes were incubated with primary antiserum for either 2 hours at room temperature or overnight at 4°C. Goat polyclonal anti-rabbit IgG-HRP conjugated secondary antibody (Sigma, St. Louis, MO) was used at 1:3,000 in blocking buffer for one hour at room temperature. Proteins were detected using an ECL Detection Kit (GE Healthcare, Waukesha, WI) with

Amersham Hyperfilm™ MP autoradiography film (GE healthcare, Waukesha, WI). The length of exposure was determined by signal intensity observed.

In vitro synthesis of proteins

Proteins were transcribed and translated *in vitro* using Promega's TnT Rabbit Reticulolysate (Madison, WI) system per manufacturer's instructions and as previously described with minor modifications (Zhu PhD Dissertation, 2008). Five hundred nanograms of either pcDNA3.1+Human ACTG1 or pcDNA-DEST53+ANXA5 plasmid were incubated with T7 RNA polymerase, amino acids (-Met), and 10 μCi/μL ^{35}S-methionine for 60 minutes at 30°C. Equal amounts of synthesized γ-actin and annexin 5a were co-incubated at room temperature for 1 minute. Samples were analyzed on either standard reducing Laemmeli gels (3% stacking, 10% separating) or native gels (10%) supplemented with 1 mM ATP, 1mM ADP and/or 1mM Ca^{2+}. Post-electorphoresis, gels were fixed in 50% methanol, 10% glacial acetic acid for 30 minutes and dried onto Whatman filter paper. Proteins were visualized using a Typhoon phosphoimager and ImageQuant software (GE Healthcare, Waukesha, WI).

Co-sedimentation Assay

These experiments were done by Sarah Bergeron, a graduate student at the University of Iowa; a collaboration I established while attending a national conference. Samples containing 4.8 μM β, γ, or insect actin with or without annexin V, in a 1:1.5 actin:annexin 5a ratio, were polymerized by the addition of

F-salts and incubation at room temperature for about 2.5 hrs. Samples were made with and without 1mM free $CaCl_2$. Aliquots of 60 µl were removed and centrifuged at 80,000 rpm in a Beckman TLA100 rotor for 20 min at 25 °C. The supernatant fraction of each sample was removed, and the pellets were re-suspended in an equivalent amount of F-buffer (Bergeron *et al.*, 2010). Then, equal proportions of the supernatant and the pellet fractions were electrophoresed on a 12% SDS-polyacrylamide gel. The Coomassie-stained gels were optically scanned using a Hewlett Packard 2750 scanner, and the intensities of the actin bands were quantified by Image J (NIH, Bethesda, MD).

Results

Annexin 5a localization in the organ of Corti and vestibular end organs

Bioinformatics suggest that *Anxa5* is more highly expressed in the mouse organ of Corti than in any other tissue (Peters et al., 2007; Shin et al., 2007), but no studies have examined its localization during postnatal development. Therefore, I completed a postnatal developmental expression profile for annexin 5a using wild-type C57Bl/6J mice ages P0 – P28.

Annexin 5a localizes to the stereocilia and cellular membranes in auditory hair cells

Auditory hair cells in the organ of Corti are key to mechanotransduction; the process by which a sound wave is converted into a neural impulse. In the inner hair cells (IHC) of the organ of Corti, annexin 5a was detected prominently in the cell body, nuclear membrane, and stereocilia. At all ages, punctate staining was observed in the region immediately below the actin rich cuticular plate and throughout the cytoplasm of the cell body (Figure 3-1A,B). Immunofluorochemistry shows prominent localization of annexin 5a to the nuclear membrane in IHCs from P0 to P7 (Figure 3-1C, D) which becomes barely detectable by postnatal days 14-28. Annexin 5a was also found in stereocilia of the inner hair cells at P0 and persisted throughout development. Prior to differentiation into distinct stereocilia, annexin 5a appeared to occupy the entire bundle, whereas in mature IHC stereocilia, localization to the periphery of the filamentous actin core was observed (Figure 3-2).

Figure 3-1

Representative images of annexin 5a (red) localization in hair cells (**A-D**) and supporting cells (**E, F**) of the organ of Corti in a P7 wild-type mouse. Immunolocalization using confocal microscopy shows that anti-annexin 5a is present immediately below the actin-rich cuticular plate of inner and outer hair cells (IHC, OHC) and in the cytoplasm of supporting cells, including Deiters cells (DC) and inner pillar cells (IPC) (**A**). A single slice through the center of IHC nuclei (**C**) and maximum intensity projection through the nuclei at P0 (**D**) demonstrate that annexin 5a is associated with nuclear membranes. In other supporting cells, staining was observed on the surface of inner sulcus cells (**E**) and at the plasma membrane of Hensen's cells (**F**). Samples were counterstained with FITC-phalloidin (green) counter-stain (**B, E, F**) and DAPI (blue) to label nuclei (**C,D**). Scale bars = 5 μm.

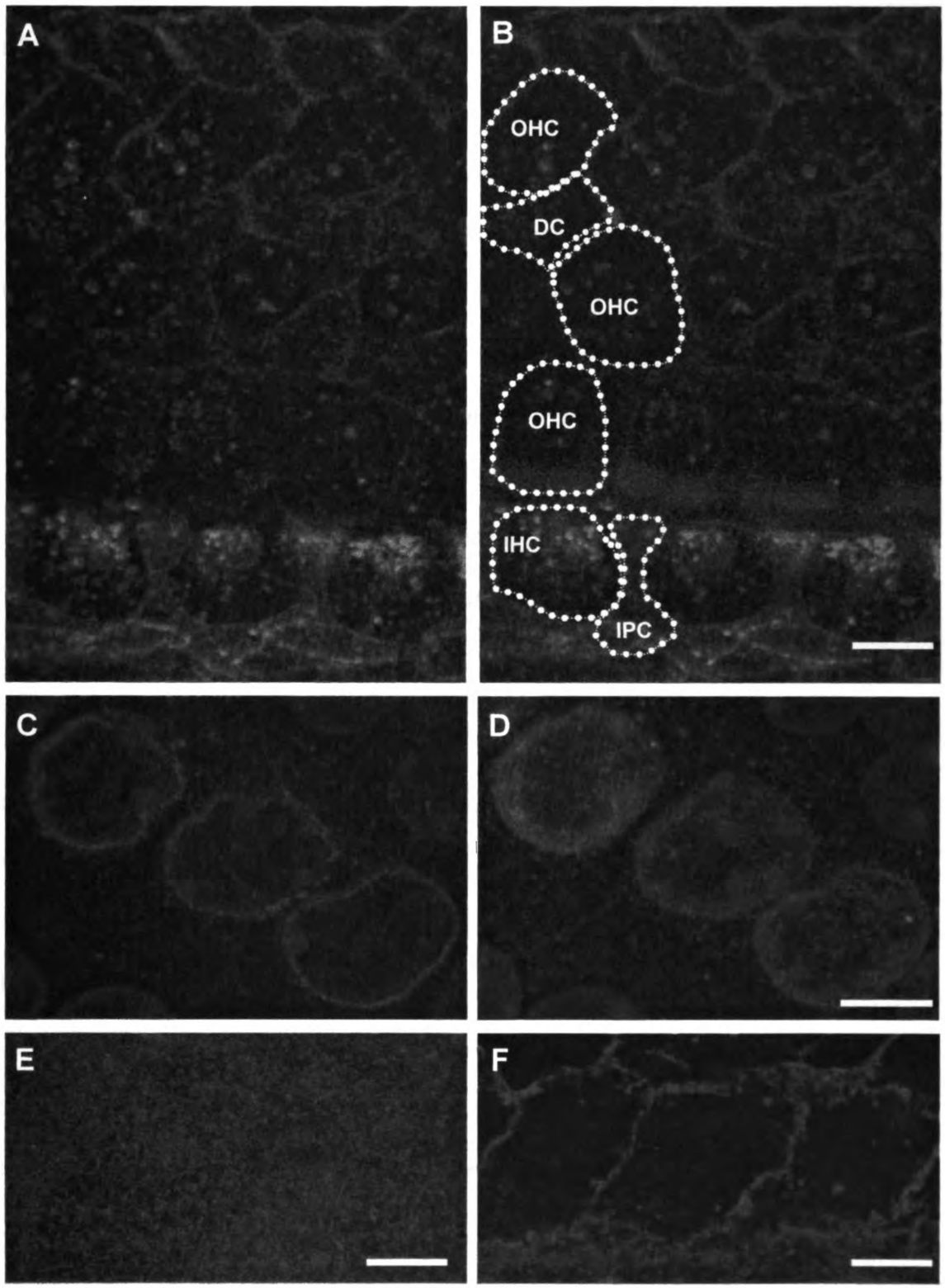
A
B
OHC
DC
OHC
OHC
IHC
IPC
C
D
E
F

Figure 3-2

Confocal microscopy to show the localization of annexin 5a in the stereocilia of organ of Corti hair cells during postnatal development. Samples were labeled with anti-annexin 5a (green) (**A-J**) and counterstained with rhodamine-phalloidin (red) as shown in the merged images (**B, D, F, H, J**). P0 IHC stereocilia have annexin 5a labeling throughout the bundle, whereas it is absent in OHC (**A, B**). At P7 annexin 5a is apparent in OHC stereocilia and displays distinct localization to the tips and periphery of the stereocilia of IHC (**C, D**). At P28, annexin 5a is clearly observed at the tips and along the entire length of the stereocilia in OHC (**E, F**), and at the tips and periphery of the F-actin core of IHC stereocilia (**G, H**). Scale bars = 5 μm

Anti-annexin 5a antibody does not bind non-specifically in *Anxa5*-null organ of Corti samples. P0 organ of Corti samples from *Anxa5*-null mice were immunolabeled with anti-annexin 5a primary and anti-rabbit IgG AlexaFluor 488 secondary antibody (green) (**I**) and counterstained with rhoadamine-phalloidin (red) (**J**). Lack of staining in the null sample validates specificity of the anti-annexin 5a antibody used in this study. Scale bar = 5 μm. Western blot of P0 cochlear lysate (**K**) shows that the anti-annexin 5a antibody recognizes a single protein with a molecular weight ~32 kDa.

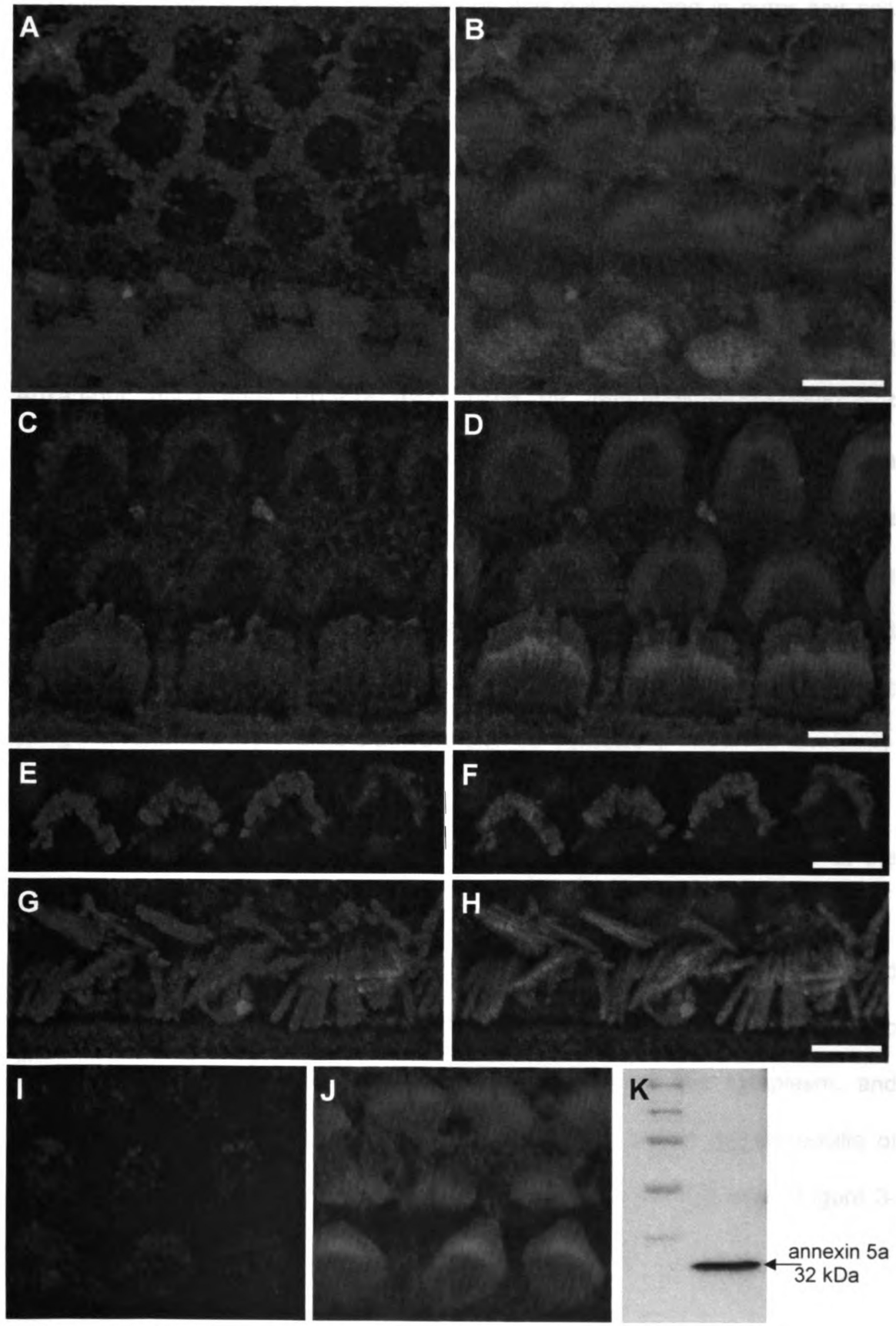
A
B
C
D
E
F
G
H
I
J
K
annexin 5a
32 kDa

In contrast to IHCs, annexin 5a expression was not detected in outer hair cells (OHCs) until P5, however, once present, it also localized to the stereocilia and cell body where it remained present through development (Figure 3-2A-D). Unlike the IHCs, annexin 5a was not detected at the nuclear membrane of OHCs at any stage of development examined (data not shown).

I validated the specificity of anti-annexin 5a antibody using two methods. First, *Anxa5*-null mice ages P0-P28 were used for immunofluorochemistry. A representative image from a P0 knockout mouse shows that there is no signal from the anti-annexin 5a antibody when imaged with the same settings as the wild-type mice (Figure 3-2A, B, I, and J). As further validation, a cochlear lysate from control mice was probed via western blotting. Figure 3-2K demonstrates a single band at 32 kDa corresponding to endogenous annexin 5a was detected using the commercially available anti-annexin 5a antibody.

In vestibular hair cells, annexin 5a is present in hair cell bundles and at the nuclear membrane

Similar to the inner hair cells of the organ of Corti, vestibular hair cells expressed annexin 5a at P0. In early postnatal pups (P0-P7), annexin 5a was found to occupy the entire hair cell bundles, was present within the cytoplasm, and associated with the nuclear membrane. Localization within the stereocilia of vestibular hair cells (VHCs) was not uniform in adolescent P28 mice (Figure 3-3).

Figure 3-3

Changes in the distribution of annexin 5a (green) in the bundle of vestibular hair cells. P7 saccula (**A, B**) and P28 saccula (**C-F**). Filamentous actin is labeled with rhodamine-phalloidin (red) in the merged images (**B, D, F**). At P7, uniform labeling of the hair bundle is noted (**A,B**) whereas difference in neighboring hair cell bundles are apparent at P28 (**C,D**). Distinct localization of annexin 5a to the tips of stereocilia is observed in mature vestibular hair cell bundles (**E, F**). Scale bars = 5 μm.

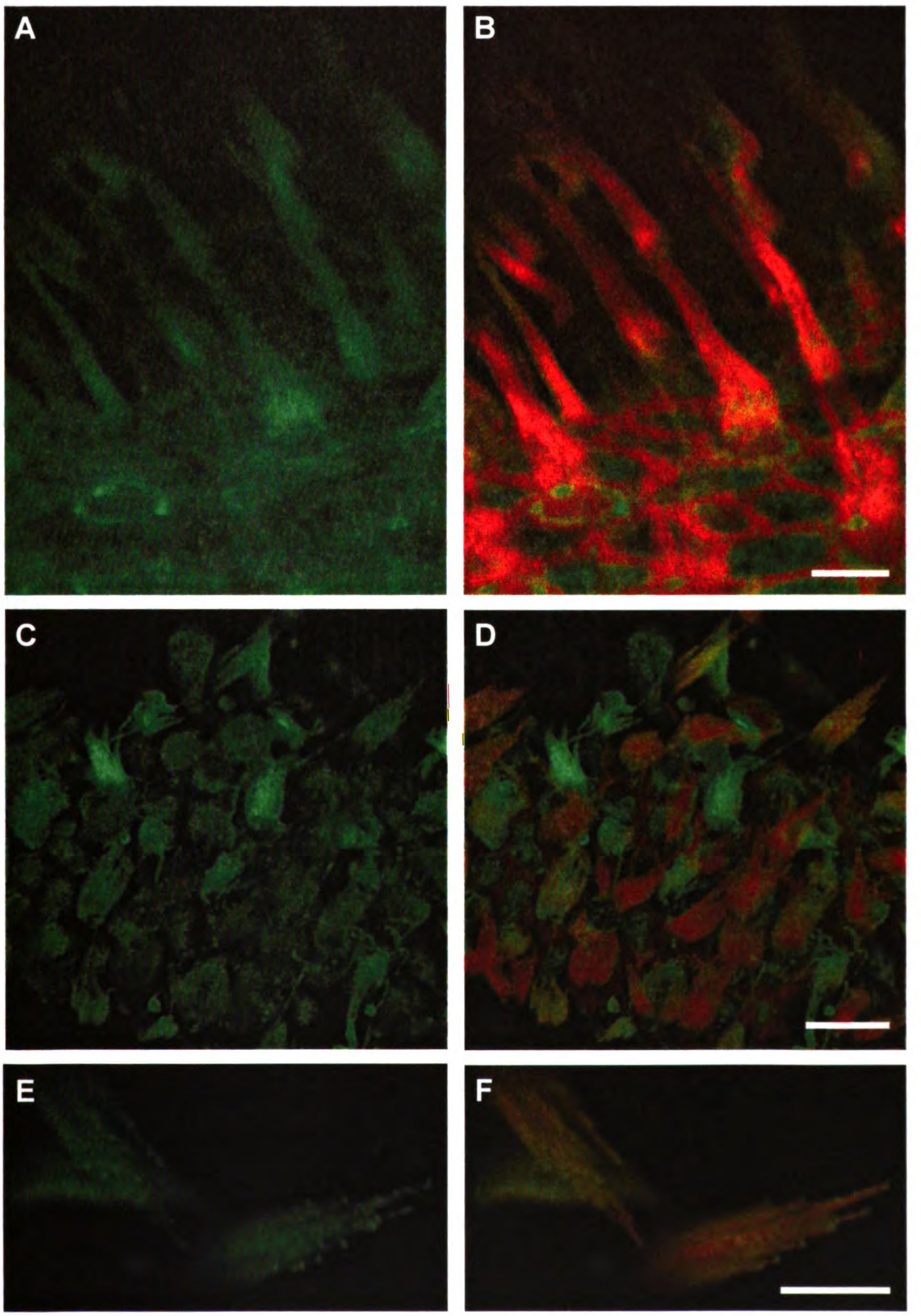
A
B
C
D
E
F

By one month of age, annexin 5a was observed to cover the entire bundle in hair cells that appeared to be either developing or degenerating. This observation is in contrast to mature, healthy hair bundles where less annexin 5a staining was observed overall and was primarily at the tips of the stereocilia. There was an apparent correlation with annexin 5a localization in the entire hair cell bundle and at the nuclear membrane; in those cells displaying annexin 5a only at the tips, nuclear membrane localization was not apparent.

Annexin 5a is found associated with membranes and within the cytoplasm of supporting cells

An abundance of annexin 5a was also observed in the supporting cells of the organ of Corti and vestibular end organs, though localization was more consistent throughout development. In inner sulcus cells (Figure 3-1E), pillar cells and Deiter's cells, annexin 5a was found within the cytoplasm and associated with the plasma and nuclear membranes. Similarly, Hensen's cells also displayed punctate staining on the plasma and nuclear membranes, though they lacked cytoplasmic annexin 5a (Figure 3-1F). Unlike inner hair cells, localization to the nuclear membrane persisted though development in all supporting cell populations.

Annexin 5a is on the internal leaflet of apical hair cell membranes

Shin *et al* (2007) reported the rapid and frequent externalization of phosphotidylserine (PS) to the outer surface of the apical hair cell membrane.

PS externalization was visualized using an exogenous, fluorescently labeled annexin 5a protein (Shin et al., 2007). Exogenous fluorescent-conjugated annexin 5a is frequently used as a marker for apoptosis and membrane externalization because of its high affinity for PS in the presence of calcium. To determine if exogenous circulating annexin 5a is bound to the external surface of the hair cells or is translocated to the outer surface during PS externalization, I incubated organ of Corti samples with anti-annexin 5a antibody prior to permeabilization. Samples were washed well to remove any unbound antibodies and fixed a second time in 4% paraformaldehyde to cross-link any externally bound annexin 5a antibodies. Samples were then permeabilized with 0.5% Triton X-100 and counterstained with rhodamine-phalloidin to visualize the stereocilia. Annexin 5a was present on the surface of some supporting cells, however; there was little to no annexin 5a detected on the apical surface of the hair cells (Figure 3-4). These data indicate that annexin 5a in the stereocilia is present only on the internal, cytosolic face of the membrane. These data also demonstrate that annexin 5a staining observed in hair cell stereocilia is from endogenous proteins and not from a contaminating source such as serum components in the blocking buffer.

γ-actin localizes properly in Anxa5-null mice

Given the similarities between the localization of annexin 5a and γ-actin in the stereocilia and the proposed specific interaction of the two proteins, I hypothesized that annexin 5a may function to coordinate membrane:actin

Figure 3-4

Annexin 5a immunofluorchemistry of P7 organ of Corti without permeablization prior to incubation with primary anti-annexin 5a antibody (green). Samples were counterstained with rhodamine-phalloidin (red) to visualize the stereocilia and cell structure. Annexin 5a only (**A**) and merged image (**B**). Note that annexin 5a is not present in the stereocilia, but some external annexin 5a is visible on the surface of some supporting cells (arrows). Scale bar = 10 μm.

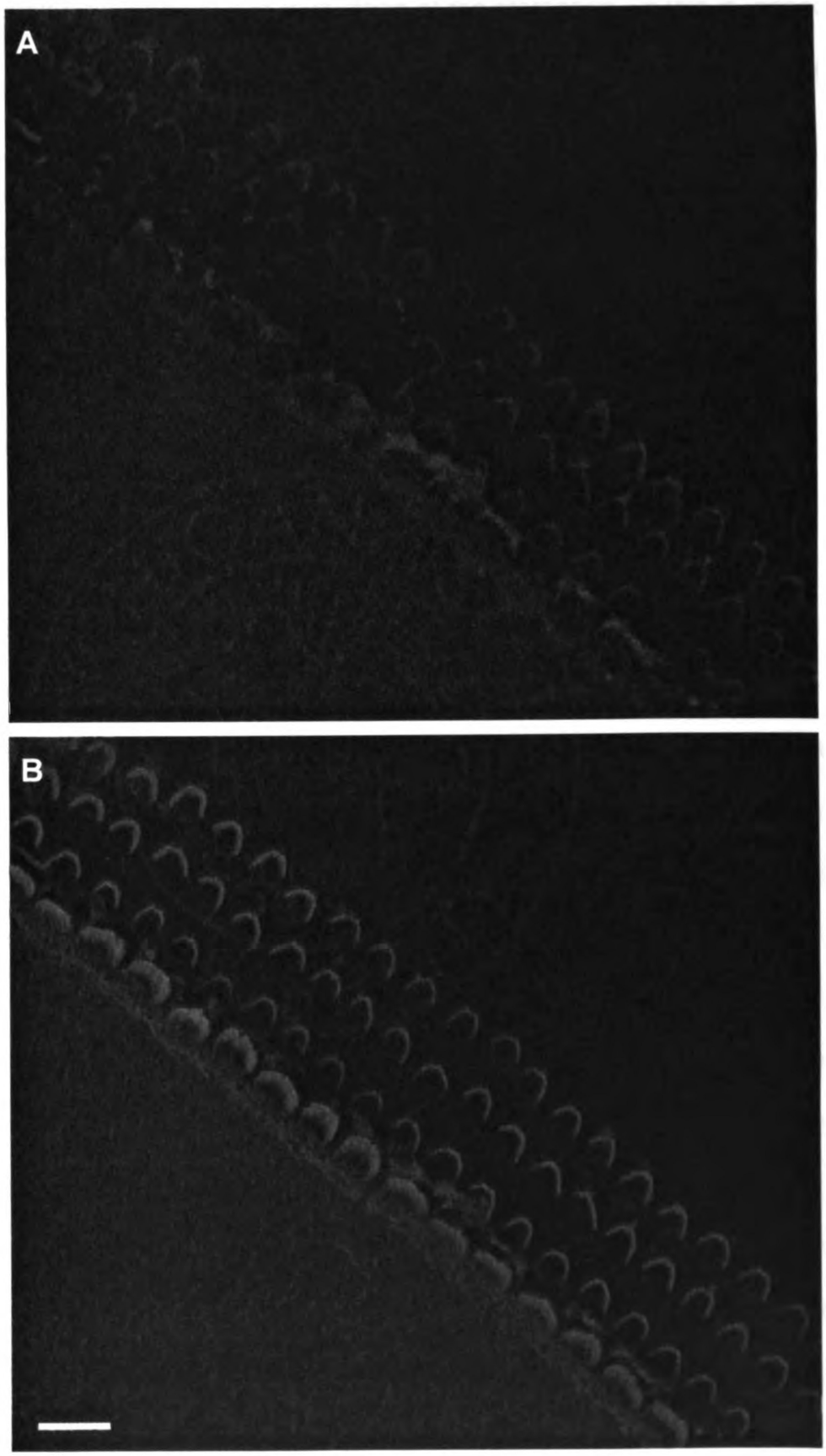
A
B

dynamics during development and maturation of the stereocilia. If this is indeed the case, I expected to see an absence of or improper localization of γ-actin within the stereocilia of *Anxa5* knock-out mice. To investigate this hypothesis, I stained whole mount organ of Corti samples with anti-γ-actin in P28 mice (Figure 3-5). No differences in localization of γ-actin to the periphery of the stereocilia in the IHCs were observed. Due to restrictions in resolution, it is difficult to discern the precise location of γ-actin in the OHCs, though there is no obvious change compared to wild-type controls.

Gaps in the filamentous actin core of vestibular hair cells have been described previously (Belyantseva et al., 2009). Monomeric γ-actin and a number of actin binding proteins required for filament assembly and dynamics were reported to co-localize with these gaps, consistent with the hypothesis that γ-actin is required for stereocilia repair. I identified similar gaps in the saccula of P28 wild-type and *Anxa5*-null mice and used immunofluorochemistry to determine if annexin 5a also co-localized to gaps. In addition, I used *Anxa5*-null mice to establish if annexin 5a is necessary for the delivery of γ-actin to these gaps. Figure 3-6 shows the presence of such gaps in the F-actin core of vestibular stereocilia; however, annexin 5a is not abundant in these gaps, though diffuse staining similar to the rest of length of the undisturbed stereocilia is present. In contrast γ-actin localization to these gaps is prominent in the *Anxa5*-null vestibular hair cells. These data suggest that annexin 5a may strictly interact with γ-actin at the membrane and is not required for localization, actin filament dynamics or repair.

Figure 3-5

γ-actin localization in P28 wild-type (**A, B**) and *Anxa5*-null mice (**C, D**). γ-actin (green) is present around the periphery of the filamentous actin core (red) labeled with rhodamine-phalloidin in merged images (**B, D**) . At this age, the intensity of γ-actin in the outer hair cells of both wild-type and *Anxa5*-null mice was variable. Scale bars = 5 μm.

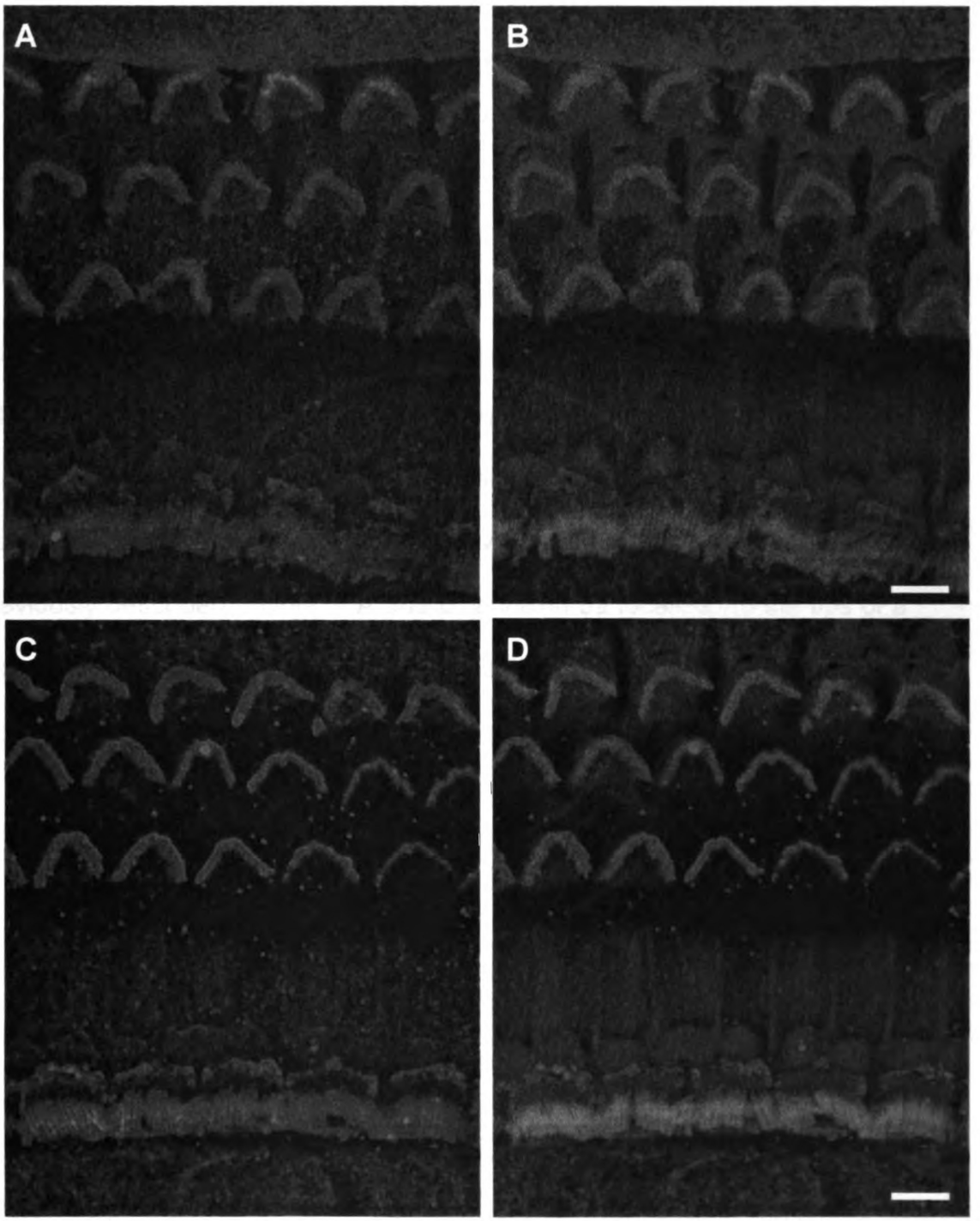
A
B
C
D

Figure 3-6

Gaps denoted by arrows in the F-actin core (red) of vestibular hair cell stereocilia were detected in both wild-type (**A, B**) and *Anxa5*-null (**C, D**) animals at P28. Annexin 5a (green) was not found to co-localize with the gaps (**B**) and in the absence of annexin 5 protein, γ-actin (green) was still able to co-localize (**D**), as was previously described. Note in **A** and **B**, annexin 5a localizes to the tips of a well developed bundle (arrow) whereas in neighboring cells with immature or degenerating bundles (asterisks) annexin 5a is found to occupy the entire bundle.

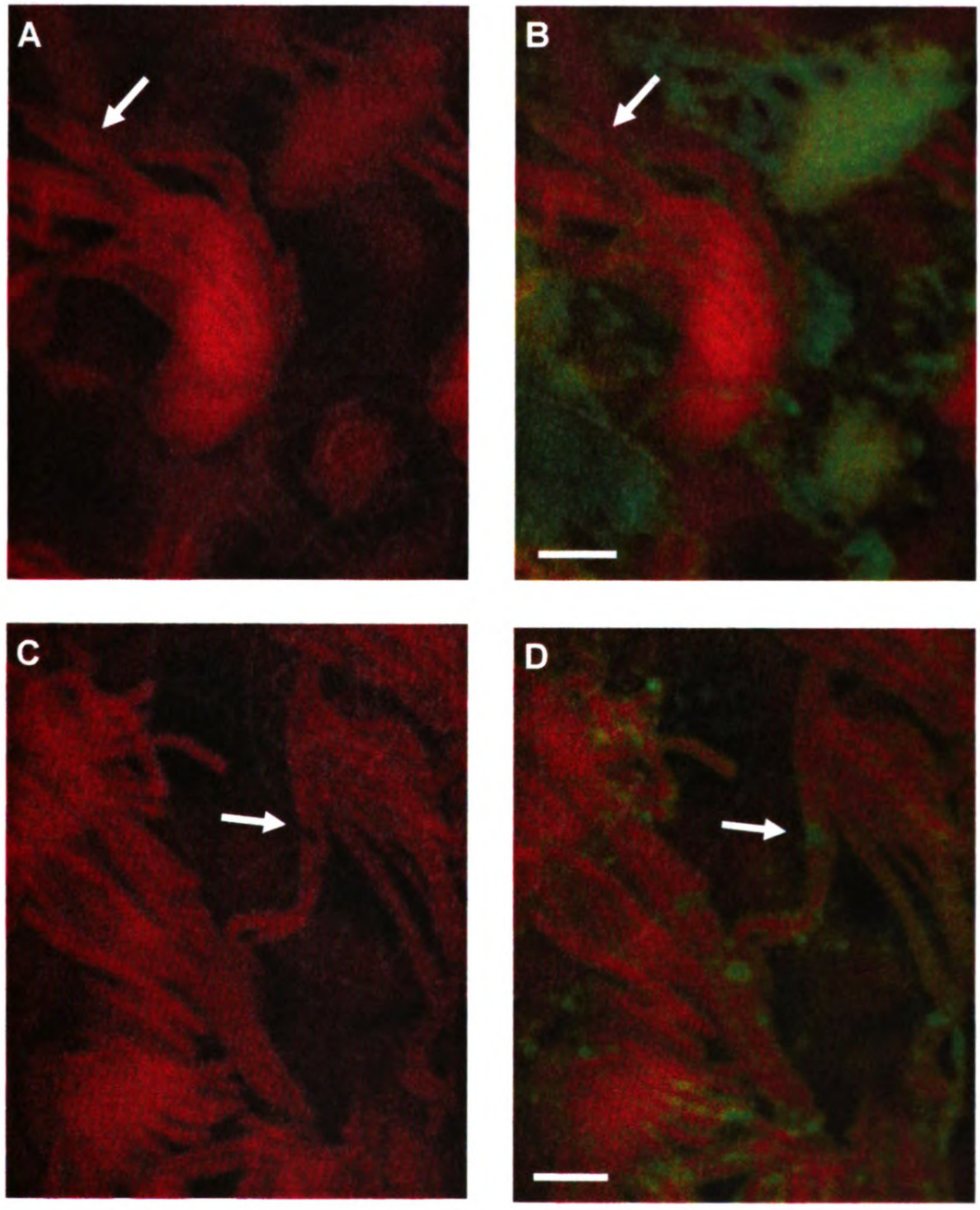
A
B
C
D

Annexin 5a knock-out mice do not have hearing deficits

Annexin 5a is both developmentally regulated and highly expressed in the mouse inner ear suggesting that lack of annexin 5a might result in hearing loss. Four month old mice were evaluated by auditory-evoked brainstem response (ABR) at 8, 16, and 32 kHz (n=3). All mice tested were within the normal range of hearing, having thresholds between 15 – 30 kHz. Therefore, no detectable difference in hearing exists between wild-type and *Anxa5*-null mice (data not shown).

GST-Pulldown shows annexin 5a is specific for γ-actin in whole cell lysates

To confirm the specificity of the interaction between annexin 5a and γ-actin, COS-1 cell lysates were used as an actin source. Recombinant GST-annexin 5a and GST proteins were expressed in Bl21.AI cells, bound to a glutathione sepharose column and then evaluated for purity using an SDS-PAGE and coomassie blue stain (Figure 3-7C). The columns were then incubated with COS-1 cell lysate with constant end-over-end rocking for 2 hours at 4°C. Previous reports demonstrate a calcium-dependent interaction, thus the Ca^{2+}-free binding buffer was supplemented with 0, 0.8 μM, 8.8 μM and 1 mM of free Ca^{2+} (Tzima *et al.*, 2000). Columns were washed to remove unbound proteins, and the GST or GST-annexin 5a complexes were eluted using reduced glutathione sepharose and probed for the presence of γ-actin or β-actin using isoform specific antibodies (Figure 3-7). As expected, results from the western blots show that only the γ- isoform of cytoplasmic actin was bound to GST-annexin 5a. However, contrary to

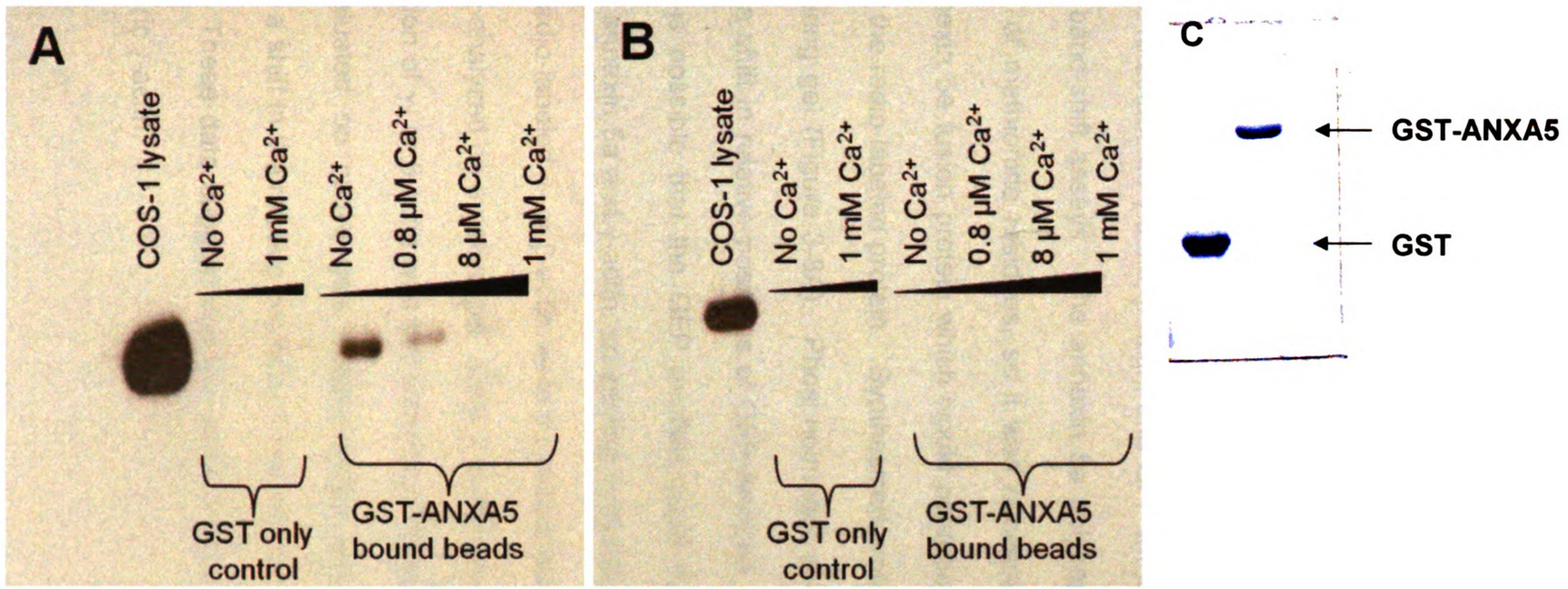

Figure 3-7

GST-pulldown using recombinant GST-ANXA5 and GST only control. COS-1 cell lysates were bound in the presence and absence of free Ca2+ in the binding buffer. Eluted fractions were analyzed using western blot. Post-transfer, membranes were probed with either anti-γ-actin (**A**) or anti-β-actin (**B**). Purified recombinant proteins were evaluated using SDS-PAGE and coomassie blue stain (**C**) .

previous reports, the interaction was enhanced at lower Ca^{2+} concentrations and in the absence of free Ca^{2+} in the binding buffer.

Pure Annexin5a does not interact with monomeric or filamentous γ-actin in vitro. Proteins that bind to actin are generally specific for either monomeric or filamentous actin. To determine if annexin 5a interacts with γ-actin monomers or filaments, radiolabeled γ-actin, β-actin, and GFP-annexin 5a were synthesized *in vitro* for band-shift assays. The annexin 5a polypeptide has an unusually low inclusion of methionine residues, so it was necessary to *in vitro* synthesize a GFP-annexin 5a fusion protein which would contribute sufficient methionines to visualize the radio-labeled protein. Synthesized proteins were size evaluated on a denaturing gel (Figure 3-8A). Phosphoimager analysis of dried gels did not indicate a shift in relative positions of GFP-Annexin 5a, γ-, or β-actin (Figure 3-8B). It is possible that the GFP peptide could interfere with the interaction between annexin 5a and γ-actin, so varying concentrations of unlabeled annexin 5a and radio-labeled γ- or β-actin were incubated at room temperature for 1 min and then analyzed on a native gel. Similar to the previous experiments, a shift in the position of γ- or β-actin was not observed. Protein:protein interactions were also evaluated on native gels supplemented with ATP, ADP, and/or Ca^{2+}, however a shift in the relative position of the proteins was not apparent (data not shown). These data suggest that the annexin 5a:γ-actin interaction is not with monomeric γ-actin.

Figure 3-8

Gel-shift assays to investigate the interaction between annexin 5a and monomeric γ- and β-actin. SDS-PAGE analysis of the *in vitro* synthesized radio-labeled proteins (**A**). Varying amounts of each protein as indicated above the gel (**B**) were gently mixed together and incubated for one minute at room temperature. Ten percent native gels were run at 4°C until the hemoglobin had moved 1/3 the distance of the gel. Gels were dried onto filter paper and proteins were visualized using a phorphorimager. The gel pictured in (**B**) was supplemented with 1 mM ATP and 1 mM $CaCl_2$.

A

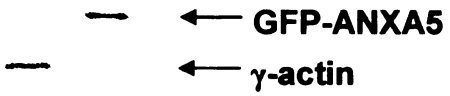
GFP-ANXA5
γ-actin

B

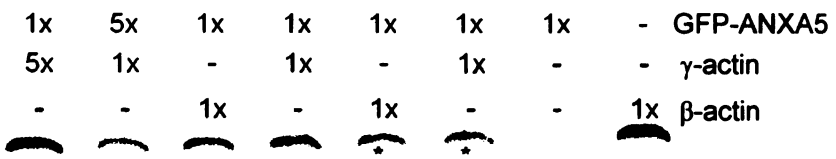
1x 5x 1x 1x 1x 1x 1x - GFP-ANXA5
5x 1x - 1x - 1x - - γ-actin
- - 1x - 1x - - 1x β-actin

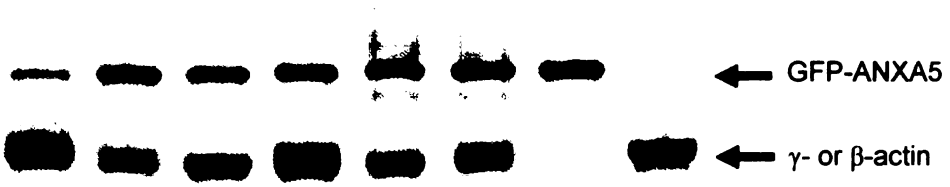
GFP-ANXA5
γ- or β-actin

Annexin 5a was tested for interaction with purified polymerized γ-actin followed by centrifugation to pellet actin filaments while leaving unpolymerized actin in the supernatant. Lacking the expertise for actin purification and co-sedimentation assays, I established a collaboration with Sarah Bergeron at the University of Iowa. The results of the co-sedimentation assay are her data. If annexin 5a interacts with filamentous γ-actin, the annexin 5a would co-sediment with the filamentous actin in the pellet. Figure 3-9 shows a coomassie blue-stained SDS-page gel of the pellet and supernatant. Annexin 5a remained in the supernatant and did not co-sediment with filamentous actin in either the presence or absence of Ca^{2+}. It appears that the specific interaction seen in cell lysates requires factors not present in more highly purified systems.

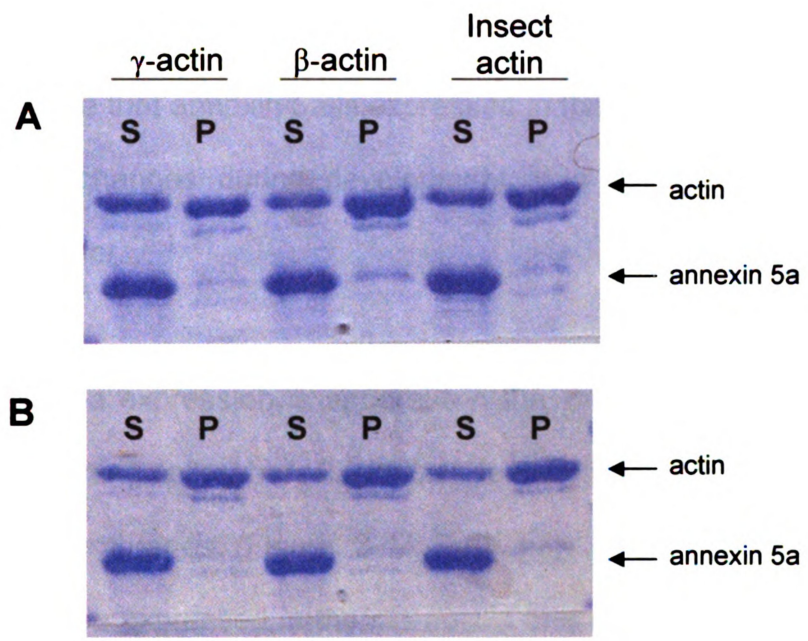

Figure 3-9

Co-sedimentation assay with γ-actin, β-actin, and insect actin. Actins were co-incubated with filamentous actin and then centrifuged to pellet filamentous actin. Annexin 5a remained in the supernatant (S) along with unpolymerized monomeric actin, whereas actin filaments were found in the pellet (P). Proteins were co-incubated in the presence (**A**) and absence (**B**) of 1 mM free Ca2+.

Discussion

I have completed a postnatal developmental localization profile for annexin 5a using immunohistochemistry. Organ of Corti and vestibular end organ tissues were imaged by confocal laser microscopy with a commercially available anti-annexin 5a antibody which I validated using *Anxa5*-null mouse tissue. These data demonstrate that annexin 5a is expressed in the inner ear at high levels and its localization changes during development in a cell-type and cell-structure dependent manner.

At P0 annexin 5a expression is apparent in the inner hair cells, vestibular hair cells, and supporting cells where it localizes to the stereocilia, cytoplasm, and cell and nuclear membranes (Figure 3-1A-D, Figure 3-3). By postnatal day 7, annexin 5a is also expressed in the stereocilia and cytoplasm of outer hair cells, but in contrast to inner hair cells, it is never prominent at the nuclear membrane in OHCs. In mature hair bundles, where annexin 5a is found at low levels throughout the stereocilia, it is concentrated at the tips above the phalloidin stained F-actin core. I conclude that expression of annexin 5a is developmentally regulated based on its localization to different cell structures during development of the organ of Corti and vestibular end organs. Annexin 5a may also play a role in maintenance of the stereocilia in terminally differentiated hair cells, given its persistent expression after development of the cochlea is complete.

Some aspects of the pattern of developmental expression and subcellular distribution of annexin 5a are reminiscent of γ-actin localization in developing hair cells. Belyantseva *et al* (2009) found that γ-actin expression is developmentally regulated; appearing first in the supporting cells, followed by the inner and then outer hair cells. In addition, the authors described unique localization to the periphery of inner hair cells stereocilia in mature hair cells and co-localization with gaps in the F-actin of vestibular hair cell stereocilia. It is possible that annexin 5a functions to localize γ-actin to the stereocilia during development, and then sequesters it to the periphery of the stereocilia until needed to repair breaks in the bundled F-actin core. If this is indeed the case, γ-actin would be predicted to mis-localize in the absence of annexin 5a. I used *Anxa5* knock-out mice to investigate this hypothesis, but found no differences in γ-actin localization in the inner hair cell stereocilia of null mice compared to wild-type. Likewise, γ-actin was still found in the F-actin gaps in the vestibular hair cell stereocilia of *Anxa5*-null mice. These data suggest that annexin 5a is not uniquely required γ-actin localization to hair cell stereocilia, nor is it likely to play a direct role in F-actin repair. Other annexins have been reported to bind actin, and three of these, annexins 2A, 4A, and 6A are expressed in the organ of Corti at relatively high levels according to both MPSS transcript data and hair bundle purification data (Peters et al., 2007; Shin et al., 2007). Therefore, it seems possible that other annexins are capable of compensating for the loss of annexin 5a.

Previous work in platelets showed that annexin 5a specifically interacts with the γ-isoform of actin (Tzima et al., 2000). This was done using GST-pulldown and co-sedimentation assays with repolymerized γ-actin from cell lysates – two preparations which do not account for or exclude other factors present in the cell that may facilitate the interaction between annexin 5a and γ-actin. I verified that GST-annexin 5a interacts specifically with γ-actin in a Cos-1 cell lysate. In contrast, when *in vitro* transcribed and translated (TnT) γ- and β-actin are used in a band-shift assay, an interaction between annexin 5a and γ-actin monomers is not observed. To address the question of whether annexin 5a interacts with actin filaments, we polymerized DNaseI-purified fractions of γ-actin produced using a baculovirus-based system and performed a co-sedimentation assay in the presence of 0 mM and 1mM free Ca^{2+}, but did not observe an interaction with F-actin.

Given the lack of interaction in 2 out of 3 *in vitro* assays described in this chapter, there is the potential that the interaction observed using a GST-pulldown is an artifact. It is also possible that the interaction of annexin 5a and γ-actin requires the presence of additional proteins that function as a complex. This would suggest that annexin 5a is not specific to γ-actin, but rather to an as yet unidentified protein. Another, and possibly more probable, scenario is one in which interaction with γ-actin occurs only when annexin 5a is bound to a phosphotidylserine membrane. As was previously demonstrated, annexin 5a associates with membranes in the presence of Ca^{2+} to coordinate architectural

changes in the cell via association with the cytoskeleton (Tzima *et al.*, 1999; Gerke *et al.*, 2005). In their GST-pulldown experiment, recombinant annexin 5a was incubated with washed platelet membranes. Similarly, the co-sedimentation assays involved re-polymerization of actin fractions from high speed centrifugation, a technique which may not necessarily exclude the presence of sections of membranes associated with lipid rafts that may have co-sedimented with F-actin in the preparation. In the GST-pulldown reported here, the recombinant proteins were incubated with whole cell lysate which also did not exclude cellular membranes. Neither the band-shift or co-sedimentation assay included membranes, and accordingly, an interaction was not observed in these assays. Future work including highly purified γ-actin and synthetic PS membranes or micelles, will be needed to address this hypothesis.

In summary, I describe the subcellular localization of annexin 5a in the inner ear of the post-natal mouse. Annexin 5a has been identified in multiple large-scale analyses of organ of Corti gene and protein expression. The information I provide in this chapter will be useful when considering protein:protein interactions within the hair cells of the inner ear.

References

Belyantseva, I. A., Perrin, B. J., Sonnemann, K. J., Zhu, M., Stepanyan, R., McGee, J., Frolenkov, G. I., Walsh, E. J., Friderici, K. H., Friedman, T. B., *et al.*, 2009. Gamma-actin is required for cytoskeletal maintenance but not development. Proc Natl Acad Sci U S A. 106, 9703-8.

Bergeron, S. E., Zhu, M., Thiem, S. M., Friderici, K. H., Rubenstein, P. A., 2010. Ion-dependent polymerization differences between mammalian beta- and gamma-nonmuscle actin isoforms. J Biol Chem. 285, 16087-95.

Brachvogel, B., Dikschas, J., Moch, H., Welzel, H., von der Mark, K., Hofmann, C., Poschl, E., 2003. Annexin A5 is not essential for skeletal development. Mol Cell Biol. 23, 2907-13.

Brisson, A., Mosser, G., Huber, R., 1991. Structure of soluble and membrane-bound human annexin V. J Mol Biol. 220, 199-203.

Concha, N. O., Head, J. F., Kaetzel, M. A., Dedman, J. R., Seaton, B. A., 1993. Rat annexin V crystal structure: Ca(2+)-induced conformational changes. Science. 261, 1321-4.

Furness, D. N., Katori, Y., Mahendrasingam, S., Hackney, C. M., 2005. Differential distribution of beta- and gamma-actin in guinea-pig cochlear sensory and supporting cells. Hear Res. 207, 22-34.

Gerke, V., Creutz, C. E., Moss, S. E., 2005. Annexins: linking Ca2+ signalling to membrane dynamics. Nat Rev Mol Cell Biol. 6, 449-61.

Gerke, V., Moss, S. E., 2002. Annexins: from structure to function. Physiol Rev. 82, 331-71.

Giambanco, I., Pula, G., Ceccarelli, P., Bianchi, R., Donato, R., 1991. Immunohistochemical localization of annexin V (CaBP33) in rat organs. J Histochem Cytochem. 39, 1189-98.

Gotow, T., Sakata, M., Funakoshi, T., Uchiyama, Y., 1996. Preferential localization of annexin V to the axon terminal. Neuroscience. 75, 507-21.

Hayes, M. J., Rescher, U., Gerke, V., Moss, S. E., 2004. Annexin-actin interactions. Traffic. 5, 571-6.

Hofer, D., Ness, W., Drenckhahn, D., 1997. Sorting of actin isoforms in chicken auditory hair cells. J Cell Sci. 110 (Pt 6), 765-70.

Huber, R., Berendes, R., Burger, A., Schneider, M., Karshikov, A., Luecke, H., Romisch, J., Paques, E., 1992. Crystal and molecular structure of human annexin V after refinement. Implications for structure, membrane binding and ion channel formation of the annexin family of proteins. J Mol Biol. 223, 683-704.

Huber, R., Romisch, J., Paques, E. P., 1990a. The crystal and molecular structure of human annexin V, an anticoagulant protein that binds to calcium and membranes. Embo J. 9, 3867-74.

Huber, R., Schneider, M., Mayr, I., Romisch, J., Paques, E. P., 1990b. The calcium binding sites in human annexin V by crystal structure analysis at 2.0 A resolution. Implications for membrane binding and calcium channel activity. FEBS Lett. 275, 15-21.

Jin, M., Smith, C., Hsieh, H. Y., Gibson, D. F., Tait, J. F., 2004. Essential role of B-helix calcium binding sites in annexin V-membrane binding. J Biol Chem. 279, 40351-7.

Kawaminami, M., Kawamoto, T., Tanabe, T., Yamaguchi, K., Mutoh, K., Kurusu, S., Hashimoto, I., 1998. Immunocytochemical localization of annexin 5, a calcium-dependent phospholipid-binding protein, in rat endocrine organs. Cell Tissue Res. 292, 85-9.

Kenis, H., van Genderen, H., Bennaghmouch, A., Rinia, H. A., Frederik, P., Narula, J., Hofstra, L., Reutelingsperger, C. P., 2004. Cell surface-expressed phosphatidylserine and annexin A5 open a novel portal of cell entry. J Biol Chem. 279, 52623-9.

Khaitlina, S. Y., 2001. Functional specificity of actin isoforms. Int Rev Cytol. 202, 35-98.

Luckcuck, T., Orchard, C. H., Harrison, S. M., Walker, J. H., 1995. Subcellular localization of annexins V and VI in isolated rat ventricular myocytes and porcine left ventricle. Biochem Soc Trans. 23, 28S.

Luckcuck, T., Trotter, P. J., Walker, J. H., 1997. Localization of annexin V in the adult and neonatal heart. Biochem Biophys Res Commun. 238, 622-8.

Markoff, A., Gerke, V., 2005. Expression and functions of annexins in the kidney. Am J Physiol Renal Physiol. 289, F949-56.

Matsuda, R., Kaneko, N., Horikawa, Y., Chiwaki, F., Shinozaki, M., Ieiri, T., Suzuki, T., Ogawa, N., 2001. Localization of annexin V in rat normal kidney and experimental glomerulonephritis. Res Exp Med (Berl). 200, 77-92.

Otey, C. A., Kalnoski, M. H., Lessard, J. L., Bulinski, J. C., 1986. Immunolocalization of the gamma isoform of nonmuscle actin in cultured cells. J Cell Biol. 102, 1726-37.

Peters, L. M., Belyantseva, I. A., Lagziel, A., Battey, J. F., Friedman, T. B., Morell, R. J., 2007. Signatures from tissue-specific MPSS libraries identify transcripts preferentially expressed in the mouse inner ear. Genomics. 89, 197-206.

Rosengarth, A., Luecke, H., 2003. A calcium-driven conformational switch of the N-terminal and core domains of annexin A1. J Mol Biol. 326, 1317-25.

Shin, J. B., Streijger, F., Beynon, A., Peters, T., Gadzala, L., McMillen, D., Bystrom, C., Van der Zee, C. E., Wallimann, T., Gillespie, P. G., 2007. Hair bundles are specialized for ATP delivery via creatine kinase. Neuron. 53, 371-86.

Trouve, P., Le Drevo, M. A., Kerbiriou, M., Friocourt, G., Fichou, Y., Gillet, D., Ferec, C., 2007. Annexin V is directly involved in cystic fibrosis transmembrane conductance regulator's chloride channel function. Biochim Biophys Acta. 1772, 1121-33.

Tzima, E., Trotter, P. J., Orchard, M. A., Walker, J. H., 1999. Annexin V binds to the actin-based cytoskeleton at the plasma membrane of activated platelets. Exp Cell Res. 251, 185-93.

Tzima, E., Trotter, P. J., Orchard, M. A., Walker, J. H., 2000. Annexin V relocates to the platelet cytoskeleton upon activation and binds to a specific isoform of actin. Eur J Biochem. 267, 4720-30.

Wang, L., Rahman, M. M., Iida, H., Inai, T., Kawabata, S., Iwanaga, S., Shibata, Y., 1995. Annexin V is localized in association with Z-line of rat cardiac myocytes. Cardiovasc Res. 30, 363-71.

Zhu, M., 2008. Examining the folding and stability of in vitro synthesized gamma-actin mutations. Cell and Molecular Biology. Ph.D. Dissertation.

CHAPTER 4

IDENTIFICATION AND CHARACTERIZATION OF A NOVEL GAMMA-ACTIN REGULATORY TRANSCRIPT

Abstract

Cytoplasmic actins are among the most ubiquitous and abundant proteins in the nucleated cell (Khaitlina, 2001). Despite wide-spread distribution, expression of these actins is differentially regulated in a tissue- and development-specific manner. In skeletal muscle containing tissues, cytoplasmic β- and γ-actin (*Actb, Actg1*) expression is down-regulated during differentiation of proliferating myoblasts into myotubes concurrent with the up-regulation of α-skeletal actin (*Acta1*). I identified a novel *Actg1* transcript, enriched in skeletal muscle, which produces an in-frame termination codon. Splicing to generate this alternative transcript is concurrent with previously described down-regulation of *Actg1* in C2C12 cells. A protein product corresponding to the use of this stop codon is not present. I therefore postulate that splicing to generate this alternative transcript is a means of post-transcriptionally down-regulating *Actg1* via the nonsense mediated decay pathway.

Introduction

Most vertebrates express six isoforms of actin: α-cardiac (*Actc*), α-skeletal (*Acta1*), α-aortic (*Acta2*), γ-enteric (*Actg2*), β-cytoplasmic (*Actb*), and γ-cytoplasmic (*Actg1*). The nucleotide coding sequence of the actins is remarkably well conserved among vertebrates, as is the amino acid sequence. In addition to the remarkable degree of conservation between species, there exists a high degree of homology between actin isoforms. Although much is known about their general function, tissue specific distribution and relative expression levels (Otey *et al.*, 1986; Otey *et al.*, 1987, 1988; Nakata *et al.*, 2001; Furness *et al.*, 2005; Belyantseva *et al.*, 2009), complete understanding of the functional specificity of the actin isoforms remains enigmatic.

In most cell types, the cytoplasmic actins are expressed at high levels. However, in mature muscle, α-skeletal actin is the predominant isoform and the cytoplasmic actins are present at comparatively low levels (Khaitlina, 2001). C2C12 mouse myoblast cell culture is widely used to understand the developmental regulation and expression of actin isoforms in muscle. In this system, myoblasts proliferate until induced to differentiate either via serum-starvation or addition of horse serum into the media. Differentiation of myoblasts involves exit from the cell cycle, fusion with neighboring cells, elongation, and movement of the nuclei to the periphery of the myotubes. Subsequent maturation is characterized by bundling of α-actin thin filaments to form myofibrils. In proliferating myoblasts, the two cytoplasmic actins, β and γ, are the

primary isoforms in the cell. During differentiation into myotubes, the cytoplasmic actins are down-regulated concurrent with the up-regulation of α-skeletal muscle actin which becomes the principal isoform. Down-regulation of *Actb* is controlled, in part, by a 40 nucleotide conserved element in the 3' UTR of the *Actb* transcript (DePonti-Zilli et al., 1988). In contrast, *Actg1* down-regulation is proposed to involve inhibition of splicing of intron 3 from the primary *Actg1* transcript to prevent the production of a mature RNA (Lloyd and Gunning, 2002). Evidence for this mechanism comes from experiments in which C2C12 cells were transfected with human *ACTG1* genomic DNA expression constructs. Deletions were generated in either the 3'UTR or intron 3 of the *ACTG1* expression constructs to determine if either of these conserved non-coding regions were necessary for down-regulation. Cells transfected with intron 3 deletion constructs constitutively express γ-actin during differentiation into myoblasts, whereas constructs containing intron 3 but lacking the 3'UTR appropriately down-regulated *Actg1* expression. These experiments by Lloyd and Gunning demonstrated that intron 3 is necessary for down-regulation, though this process is not fully understood.

A potentially relevant mechanism of post-transcriptional down-regulation is termed RUST - regulated unproductive splicing and translation (Lewis et al., 2003). RUST occurs by alternative splicing to include a regulatory exon which either contains or creates via frameshift, a premature termination codon (PTC). Introduction of a PTC results in subsequent degradation of the mRNA via nonsense mediated decay (NMD). Recent evidence suggests that as many as

4% of transcripts produced include alternatively spliced exons with PTCs, though there is some debate as to whether this splicing is functional or an artifact of highly active splicing factors in cells and therefore should be considered "noisy" (McGlincy and Smith, 2008). To help resolve this debate, Zhang *et al* outlined criteria to evaluate the potential for functional value of an alternative exon. Briefly, alternative transcripts should be considered the result of noisy splicing if 1) they have a low inclusion rate, 2) do not maintain the proper reading frame, 3) belong to a gene family in which a lot of alternative splicing occurs and 4) create a premature termination codon which is not evolutionarily conserved (Zhang et al., 2009).

I identified an alternatively spliced exon in *Actg1* transcripts from mouse skeletal muscle cDNA. This alternative transcript includes a novel 45 bp exon (exon 3a) located in the middle of *Actg1* intron 3 that introduces a PTC. A similar alternative γ-actin transcript is found in skeletal muscle from multiple other mammals. In mouse, splicing to include this exon is regulated in a tissue and development specific manner. Here I demonstrate that exon 3a is sufficient for post-transcriptional down-regulation of *Actg1*.

Materials and Methods

Bioinformatics

Sequence ascertainment and analysis was performed using UCSC Genome Browser/BLAT (http://www.genome.ucsc.edu/), Ensembl! (http://www.ensembl.org), Sequencher 6.0 (Gene Codes Corp.), and Clustal X2 (http://www.clustal.org).

Animals and Tissue Preparation

All animals were housed and euthanized according to IACUC and NIH guidelines. Tissue samples were harvested from 2 month old C57Bl/6J mice, snap frozen on dry ice and stored at -80°C. Prior to use for RNA or protein isolation, samples were further sectioned into ~50 mg pieces. Cat and dog skeletal muscle samples were courtesy of Dr. John Fyfe.

Cell Culture

All cell culture media and supplements were purchased from Invitrogen (Carlsbad, CA) unless noted otherwise. C2C12 myoblast cells were purchased from ATCC (Manassas, VA; CRL-1772) and propagated in DMEM containing 10% heat-inactivated fetal bovine serum and 2mM L-glutamine. Differentiation of the myoblasts into myotubes was achieved with the addition of DMEM containing 10% horse serum to 70% confluent myoblasts. Thirty-six hours post differentiation, 2% horse serum and 10 μM Ara-C (Sigma, St. Louis, MO) were

added to the differentiation medium to maintain myotube differentiation and inhibit the proliferation of myoblasts. Cells were maintained at 37°C in 5% CO_2.

RNA isolation and cDNA synthesis

Total RNA isolation from tissue and cell culture samples was achieved using standard Trizol (Invitrogen, Carlsbad, CA) purification followed by DNaseI (Roche, Basel, Switzerland) treatment if necessary as determined by no-RT controls. Human skeletal muscle total RNA was purchased from Ambion (Austin, TX). cDNA was synthesized using SuperScriptIII (Invitrogen, Carlsbad, CA) reverse transcriptase according to manufacturer's instructions. Briefly, equal amounts of total RNA (values ranged from 750ng to 1µg, though was constant between samples used for the same experiment) were incubated with 10 mM dNTPs and 500 ng of Oligo $dT_{12\text{-}18}$ at 65°C for 5 minutes to reduce RNA secondary structure. A cocktail containing RNase inhibitor, 0.1M DTT, 5x buffer, and SuperScriptIII enzyme were added to each reaction and incubated at 55°C for 1 hour. Samples were heat inactivated at 75°C for 20 minutes and stored at -20°C until needed.

Nuclear and Cytoplasmic RNA Isolation

Myotube cultures were lysed briefly with 1% Triton X-100 in PBS. Cells were gently scraped from the plate and evaluated by brightfield microscopy for the presence of intact nuclei. Samples were then centrifuged at 1,000xg for 5 minutes to pellet nuclei. The cytosol-containing supernatant was once again

examined under the microscope for the presence of nuclei prior to the addition of Trizol LS. The nuclei-containing pellets were resuspended in Trizol. RNA purification of both the cytosolic and nuclear fractions was done according to manufactures' instructions. Total RNA was quantitated using a Nanodrop and cDNA synthesis was executed as described above.

PCR Amplification

Actg1 cDNA was amplified using species-specific primers located in exons 3 and 4 respectively. PCR conditions are described in detail in the appendix. For most reactions described in this chapter, 25-28 cycles were sufficient to amplify within the linear range. Products were evaluated on 3% agarose gels supplemented with 0.3 µg/mL ethidium bromide and visualized using BioRad GelDoc System (Hercules, CA). When necessary, pixel intensity of the PCR products was quantitated using GelDoc software for semi-quantitative analysis.

Cycloheximide

To inhibit translation-dependent nonsense mediated decay, cells were treated with cycloheximide. Cycloheximide (Sigma, st. Louis, MO) was dissolved in 100% ethanol to a stock solution of 40 mg/mL and added to growth medium at a final concentration of 40 µg/mL. Cells were incubated in cycloheximide containing medium for 3 hours and immediately harvested in Trizol for RNA isolation and cDNA synthesis as described above.

Protein Isolation

Cells were harvested in Trizol (Invitrogen, Carlsbad, CA). After RNA purification, the phenol-containing organic phase was further processed for protein extraction using manufacturer's instructions. Briefly, 1.5 mL of isopropanol was added to precipitate the proteins, and samples were centrifuged at 12,000xg at 4°C. Protein pellets were washed three times in 0.3 M guanidine hydrochloride in 95% ethanol, followed by one final wash in 95% ethanol. Pellets were air-dried and re-dissolved in a solution containing 1% SDS and EDTA-free Complete Protease Inhibitor Cocktail (Roche, Basel, Switzerland). All samples were analyzed on a 10% Laemmli denaturing gel and visualized using Coomassie blue dye (appendix).

Western Blotting

Proteins were separated via SDS-PAGE on discontinuous 10% Laemmli gels (see appendix). Proteins were transferred in 10 mM Tris base, 100 mM glycine, 15% methanol (transfer buffer) at 4°C either overnight at a constant current of 5 mAmp or for 1.5 hours at a constant voltage of 110V onto polyvinylidene difluoride (PVDF) membranes (BioRad, Hercules, CA). Membranes were incubated in 5% non-fat milk in 0.025% Tween-20 in PBS pH 7.4 (blocking buffer) for either one hour at room temperature or overnight at 4°C. Rabbit polyclonal anti-γ-actin antiserum (Belyantseva *et al*, 2009; see Chapter 2 for description of antibody validation) was diluted 1:10,000 in blocking buffer. Membranes were incubated with primary antiserum for either 2 hours at room

temperature or overnight at 4°C. Goat polyclonal anti-rabbit IgG-HRP conjugated secondary antibody (Sigma, St. Louis, MO) was used at 1:3,000 in blocking buffer for one hour at room temperature. Proteins were detected using an ECL Detection Kit (GE Healthcare, Waukesha, WI) with Amersham Hyperfilm™ MP autoradiography film (GE healthcare, Waukesha, WI). The length of exposure was determined by signal intensity observed.

Expression Constructs

Human *ACTG1* was previously cloned into pcDNA3.1+ using BamHI and XhoI by Dr. Mei Zhu (pHs-FL). Intron 3 from human genomic DNA was cloned into pcDNA3.1-HsFL using endogenous XcmI sites in exon 3 and 4 of the coding DNA (pHs-I3). A splice site mutant (pHs-SSM) expression construct was generated using site directed mutagenesis to abolish the 3' acceptor site of exon 3a. Primers complimentary to a 31 bp segment containing the consensus splice site were designed with a single nucleotide substitution to change the canonical CAG|G acceptor sequence to a CGG|G. All clones were sequence validated.

Transfections and Mass Selection

C2C12 cells were transfected using Fugene 6 (Promega, Madison, WI) with a 3:2 ratio of µL of Fugene6:µg of plasmid. After 48 hours, 500 µg/mL of G418 (Invitrogen, Carlsbad, VA) was added to growth medium. Massive cell death was noted between days 3 and 4 of selection. Cells were subsequently maintained in

selective medium and passaged at least once prior to harvesting RNA and/or inducing differentiation.

Results

Identification of a novel Actg1 transcript

While investigating γ-actin expression in a knock-in mouse model, I identified a novel, alternatively spliced *Actg1* transcript. PCR amplification using primers designed to amplify mouse *Actg1* exon 3 to 4 (Figure 4-1A), but to not allow amplification of *Actb* and *Acta1* yielded an unexpected product from muscle cDNA. An amplicon of ~150 bp was observed in addition to the predicted amplicon of 102 bp (Figure 4-2, skeletal muscle). Sequencing of the 150 bp product revealed an alternatively spliced transcript that includes a novel 45 bp exon situated within intron 3 of the genomic DNA, which I term exon 3a (Figure 4-3B). In mouse, exon 3a is flanked by canonical splice acceptor and donor sites and inclusion introduces an in-frame termination codon. A search of the NCBI mouse EST database revealed transcripts which included exon 3a.

Exon 3a containing transcripts are enriched in muscle

To determine if this transcript was present in other tissues of the adult mouse, total RNA was isolated and cDNA prepared from ten different tissues including brain, kidney, intestine, testis, spleen, eye, diaphragm, heart, skeletal muscle (thigh), and lung. Only skeletal or cardiac muscle - leg muscle, diaphragm and heart - were positive for the presence of alternatively spliced transcripts, in addition to the normal *Actg1* transcript, which was the major product amplified (Figure 4-2). It should be noted that in addition to the PCR products

Figure 4-1

Comparison of the coding sequence of the three actin isoforms expressed in muscle: *Actg1*, *Actb*, and *Acta1* in mouse (A) and human (B). Primers to screen for inclusion of exon 3a in the *Actg1* transcript are depicted by shaded boxes. Primers were designed to span the exon 3-4 junction of *Actg1* using Primer 3 (http://frodo.wi.mit.edu). Primers were chosen such that the amplicons remained under 200 bp and maximized mismatches in at least one primer compared to the *Actb* and *Acta1* sequences so as to specifically amplify only *Actg1* transcripts. *Actg1*-specific amplification was verified using a HaeIII restriction digest (GGCC). Inclusion of exon 3a results in a 45 bp (mouse) or 41 bp (human) larger PCR amplicon. Asterisks indicate perfect homology between isoforms.

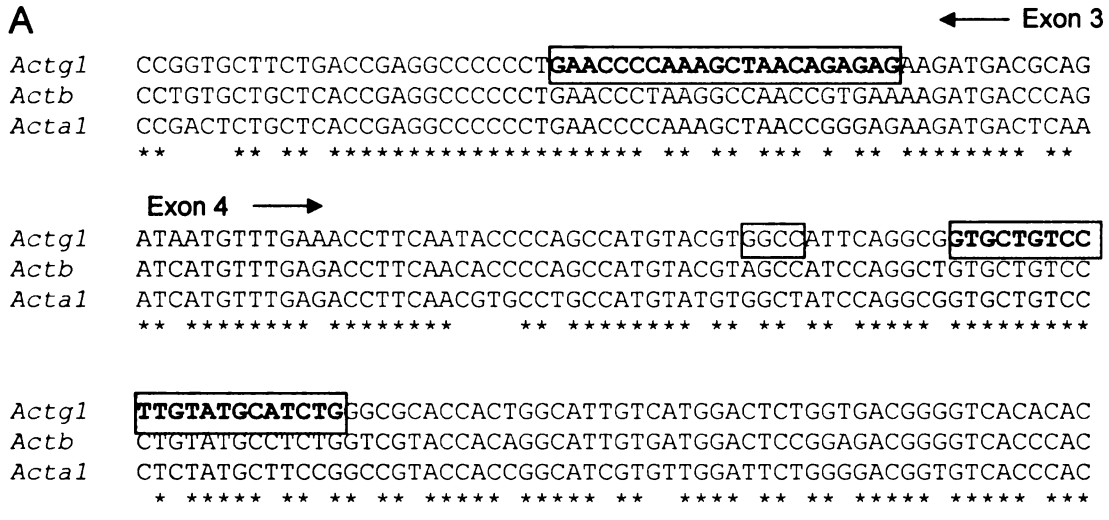
A
Exon 3
Actg1 CCGGTGCTTCTGACCGAGGCCCCCCTGAACCCCAAAGCTAACAGAGAGAAGATGACGCAG
Actb CCTGTGCTGCTCACCGAGGCCCCCCTGAACCCTAAGGCCAACCGTGAAAAGATGACCCAG
Acta1 CCGACTCTGCTCACCGAGGCCCCCCTGAACCCCAAAGCTAACCGGGAGAAGATGACTCAA
Exon 4
Actg1 ATAATGTTTGAAACCTTCAATACCCCAGCCATGTACGTGGCCATTCAGGCGGTGCTGTCC
Actb ATCATGTTTGAGACCTTCAACACCCCAGCCATGTACGTAGCCATCCAGGCTGTGCTGTCC
Acta1 ATCATGTTTGAGACCTTCAACGTGCCTGCCATGTATGTGGCTATCCAGGCGGTGCTGTCC
Actg1 TTGTATGCATCTGGGCGCACCACTGGCATTGTCATGGACTCTGGTGACGGGGTCACACAC
Actb CTGTATGCCTCTGGTCGTACCACAGGCATTGTGATGGACTCCGGAGACGGGGTCACCCAC
Acta1 CTCTATGCTTCCGGCCGTACCACCGGCATCGTGTTGGATTCTGGGGACGGTGTCACCCAC

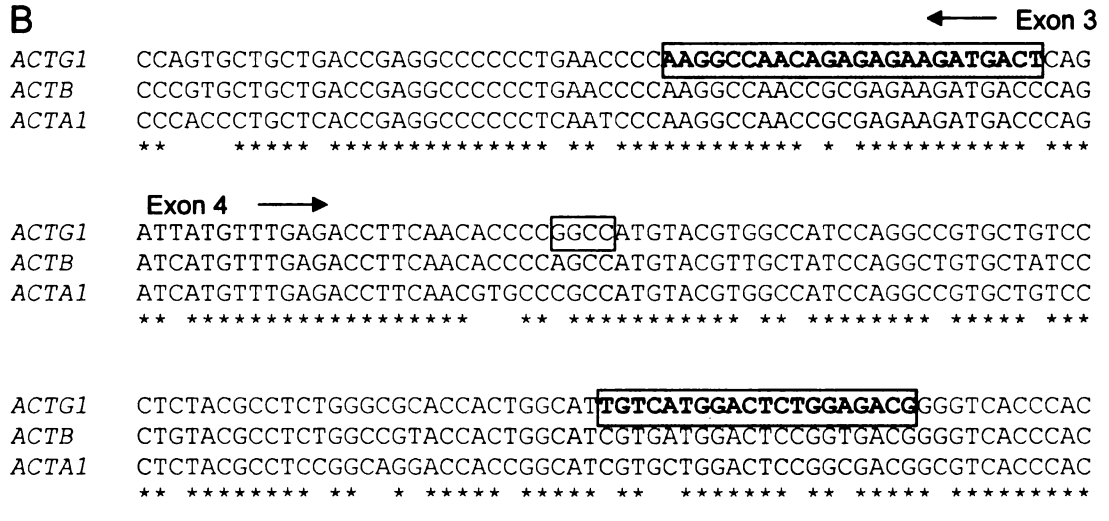
B
Exon 3
ACTG1 CCAGTGCTGCTGACCGAGGCCCCCCTGAACCCCAAGGCCAACAGAGAGAAGATGACTCAG
ACTB CCCGTGCTGCTGACCGAGGCCCCCCTGAACCCCAAGGCCAACCGCGAGAAGATGACCCAG
ACTA1 CCCACCCTGCTCACCGAGGCCCCCCTCAATCCCAAGGCCAACCGCGAGAAGATGACCCAG
Exon 4
ACTG1 ATTATGTTTGAGACCTTCAACACCCCGGCCATGTACGTGGCCATCCAGGCCGTGCTGTCC
ACTB ATCATGTTTGAGACCTTCAACACCCCAGCCATGTACGTTGCTATCCAGGCTGTGCTATCC
ACTA1 ATCATGTTTGAGACCTTCAACGTGCCCGCCATGTACGTGGCCATCCAGGCCGTGCTGTCC
ACTG1 CTCTACGCCTCTGGGCGCACCACTGGCATTGTCATGGACTCTGGAGACGGGGTCACCCAC
ACTB CTGTACGCCTCTGGCCGTACCACTGGCATCGTGATGGACTCCGGTGACGGGGTCACCCAC
ACTA1 CTCTACGCCTCCGGCAGGACCACCGGCATCGTGCTGGACTCCGGCGACGGCGTCACCCAC

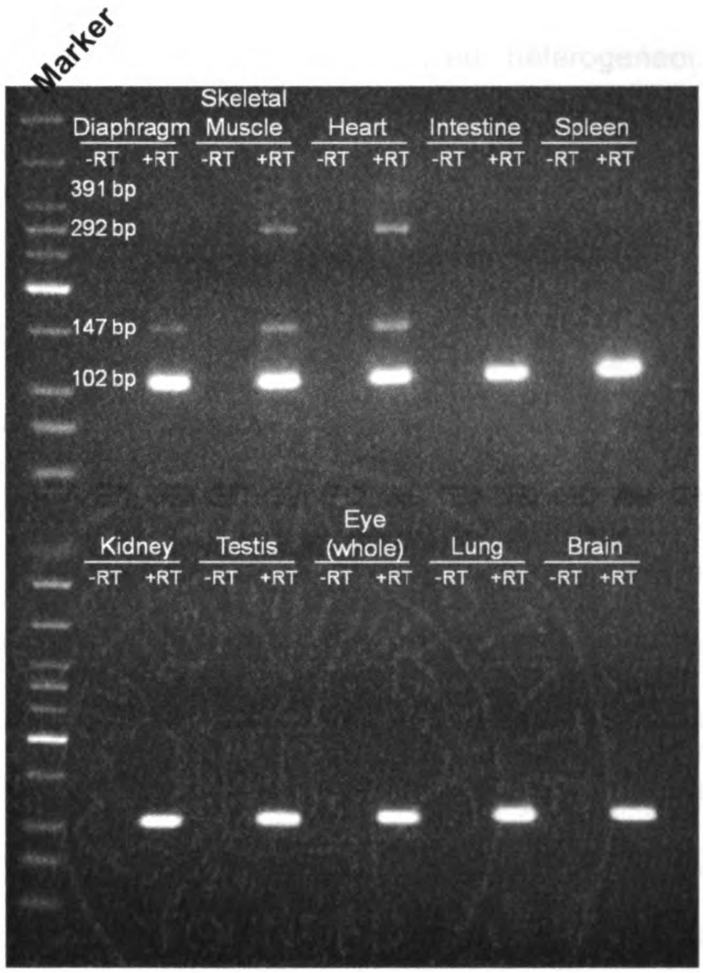

Figure 4-2

Tissue specific splicing to include exon 3a in the *Actg1* transcript. The larger PCR products at ~390 bp and ~290 bp are likely nuclear heterogenous RNA and intermediate spliceforms. The 147 bp product represents exon 3a-containing *Actg1* transcripts, while the 102 bp product represents normally spliced *Actg1* transcrips. Splicing to include exon 3a is limited to skeletal and cardiac muscle, and is not observed in the intestinal smooth muscle.

corresponding to the two alternatively spliced transcripts, I also observed larger amplicons that were not present in the no-RT controls. The sizes of these products are consistent with incompletely spliced, heterogeneous RNA in the nucleus.

Exon 3a is highly conserved among mammals

Evolutionary conservation of nucleotide sequence is typically indicative of functional significance. *In silico* analysis of *Actg1* intron 3 shows an unusually high degree of conservation among vertebrates, including the region containing the 45 bp alternatively spliced exon and flanking splice sites (Figure 4-3A,B). To determine if splicing of the *Actg1* transcript is an evolutionarily conserved event *in vivo*, I prepared cDNA from human, dog, and cat skeletal muscle total RNA. I designed species and isoform specific primers that are similar to the PCR assay described above (Figure 4-1B). Splicing to include exon 3a was observed in skeletal muscle cDNA from all species assayed. In dog skeletal muscle, the alternative transcript was present at nearly equal levels to the expected *Actg1* transcript (Figure 4-3C). All PCR products were sequenced to confirm the imputed exon 3a sequence generated by sequence alignment and shown in Figure 4-3B. Similar to the mouse, inclusion of exon 3a introduces an in-frame termination codon in cat, cow, dog, and rat. In humans and rhesus, exon 3a is 41 nt and unlike the mouse, cat, and dog, inclusion results in a frameshift of the *ACTG1* coding sequence creating a PTC in exon 4.

Figure 4-3

Exon 3a and sequence immediately 5' and 3' display a high degree of conservation between vertebrates, as shown by the UCSC genome browser vertebrate conservation track (**A**). Alignment of the nucleotide sequence of exon 3a in 7 mammals (**B**). Exon 3a is flanked by canonical splice sites in all species. The 50 bp region shown has 89% homology between species. For comparison, the 50 bp at the 3' and of exon 3 and 50 bp at the 5' end of exon 4 have 90% homology between species. Using species and isoform specific primers, I used RT-PCR to amplify across the exon 3-4 junction of *Actg1* in humans, cat, and dog skeletal muscle cDNA (**C**). Similar to the assay described in Figure 2, larger products are present corresponding to intermediate splice forms. The primary *Actg1* transcript corresponds to a ~100 bp product, whereas inclusion of exon 3a results in a larger, ~150 bp product, as visualized on a 3% agarose gel.

A

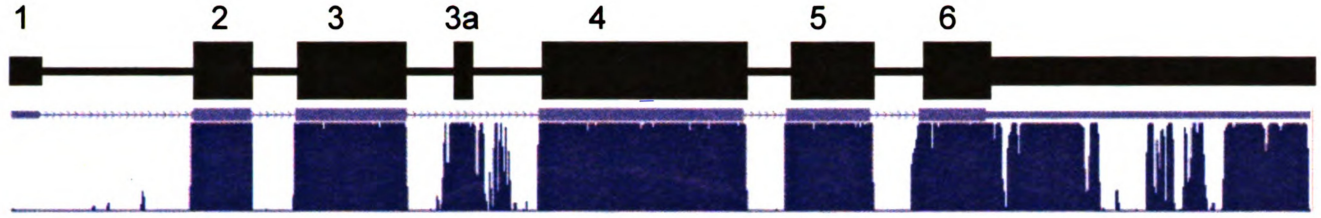

B

```
Human    CCAG:GCTCTGTTC:::CTCTCCCGGCATTTCCTCCCTGAAGCCTCCAGGTTTC
Rhesus   CCAG:GCTCTGTTC:::CTCTCCCGGCATTTCCTCCCTGAAGCCTCCAGGTTTC
Horse    CCAGGGTTCTGTTC:::CTCTCCTGGCATTTCCTCCCTGAAGTCTCAAGGTTTC
Cat      CCAGGGTTCTGTTC:::TTCTCCTGGCATTTCCTTCCTGAAGTCTCAAGGTTTC
Dog      CCAGGGTTCTGTTC:::CTCTCCTGGCATTTCCTTCCTGAAGTCTCAAGGTTTC
Rat      CCAGGGTTCTGTTCCTCCTCTCCTGGCATTTCCTCCCTGAAGCCTCCAGGTTTC
Mouse    CCAGGGTTCTGTTCCTCTTCTCCTGGCATTTCCTCCCTGAAGCCTCCAGGTTTC
         **** * *******     ***** ********** ******* *** *******
```

C

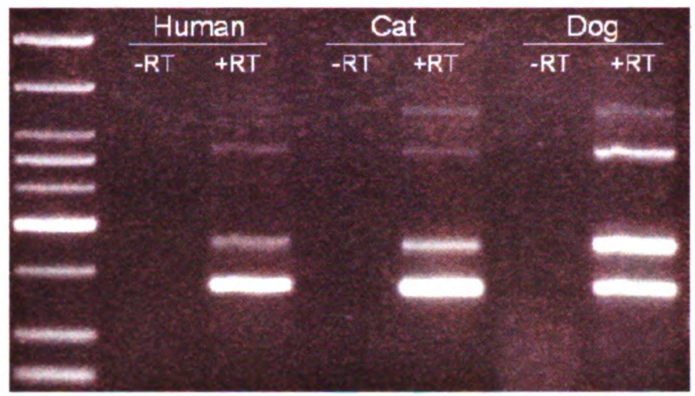

Developmental regulation of Actg1 alternative splicing

To investigate the function of the alternative *Actg1* transcript in muscle relevant tissue, I utilized a cell culture based model using the well-characterized C2C12 mouse myoblast cell line. C2C12 cells are well characterized and are frequently used to study transcriptional and proteome changes during the differentiation of myoblasts into myotubes (Kislinger *et al.*, 2005; Casadei *et al.*, 2009). Myoblasts were grown to ~70% confluence and then cultured in the presence of 10% horse serum for 36 hours to induce differentiation. Partially differentiated cell cultures were incubated further in 2% horse serum with 10 μM Ara-C to inhibit proliferation of undifferentiated myoblast cells (Figure 4-4A-C). Total RNA was harvested immediately prior to the addition of 10% horse serum and every 48 hours thereafter. Splicing of the transcript to include exon 3a corresponded with differentiation of myotubes (Figure 4-4D).

Cytoplasm contains RNA with exon 3a but no corresponding protein product

Although the PCR assay is capable of detecting intermediate splice variants, it is possible that the alternative transcript is the result of promiscuous splicing in the nucleus and not exported to the cytoplasm for translation. Total RNA was isolated from both cytoplasmic and nuclear fractions of mature myotube cultures. Using PCR, I found that the intermediate spliceforms remained in the nuclear fraction, whereas only the typical and alternatively spliced *Actg1* transcripts were present in the cytoplasmic fraction (Figure 4-5A,B).

Figure 4-4

Splicing to include exon 3a is a developmentally regulated event in skeletal muscle. C2C12 myoblasts (**A**) were grown to 70% confluence and induced to differentiate in DMEM + 10% horse serum. Partially differentiated cultures (**B**) containing both myoblasts and myotubes were observed by 2 days post-differentiation. After 36 hours, medium was replaced with DMEM + 2% horse serum and 10 μM Ara-C and cultured for an additional 4 days (**C**). RNA was harvested in Trizol and RT-PCR was used to assay for splicing to include exon 3a (**D**). As described in Figure 1, the primary *Actg1* transcript corresponds to a 102 bp product, whereas inclusion of exon 3a yields a 147 bp product.

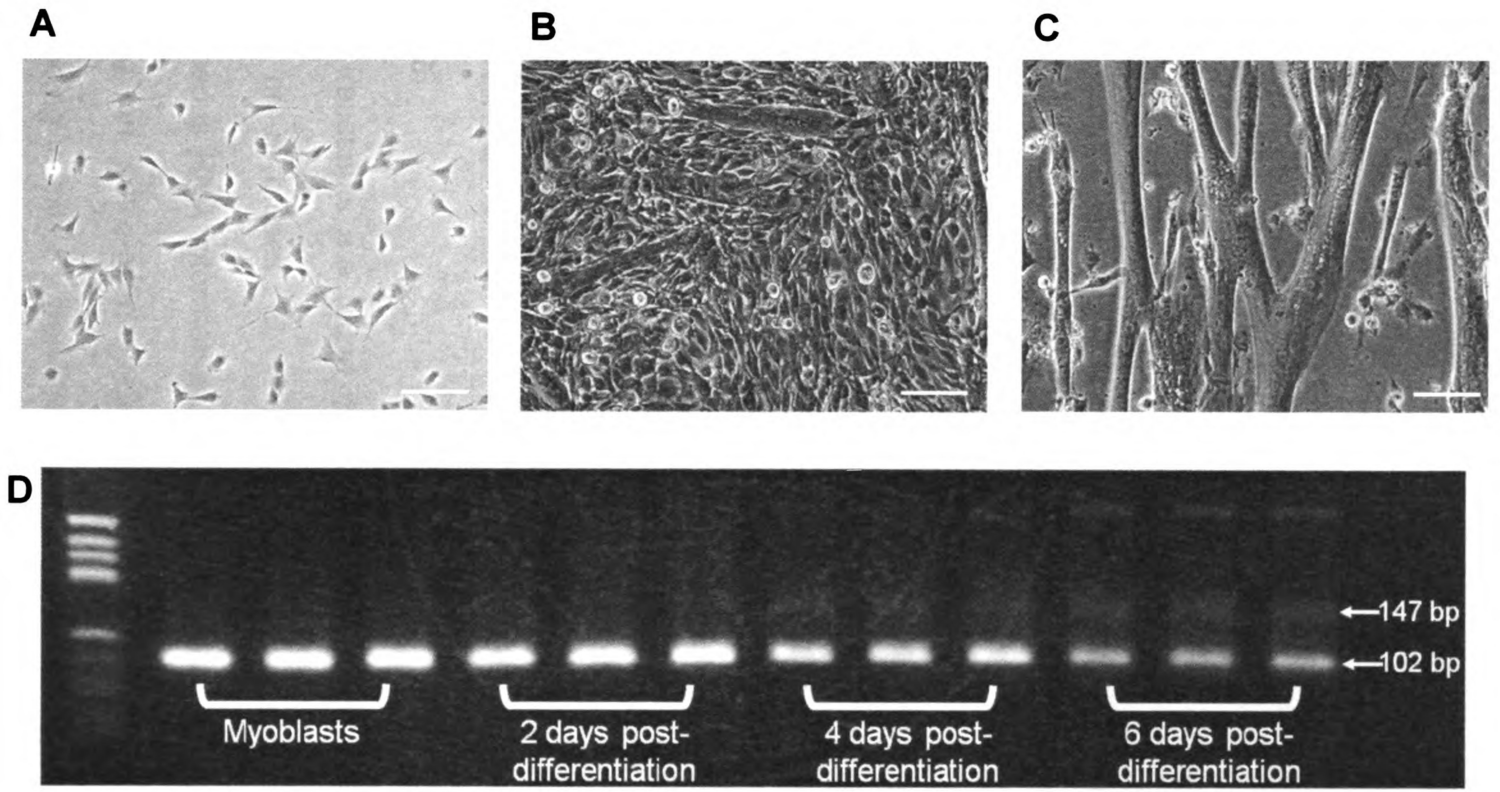
A
B
C
D
147 bp
102 bp
Myoblasts
2 days post-differentiation
4 days post-differentiation
6 days post-differentiation

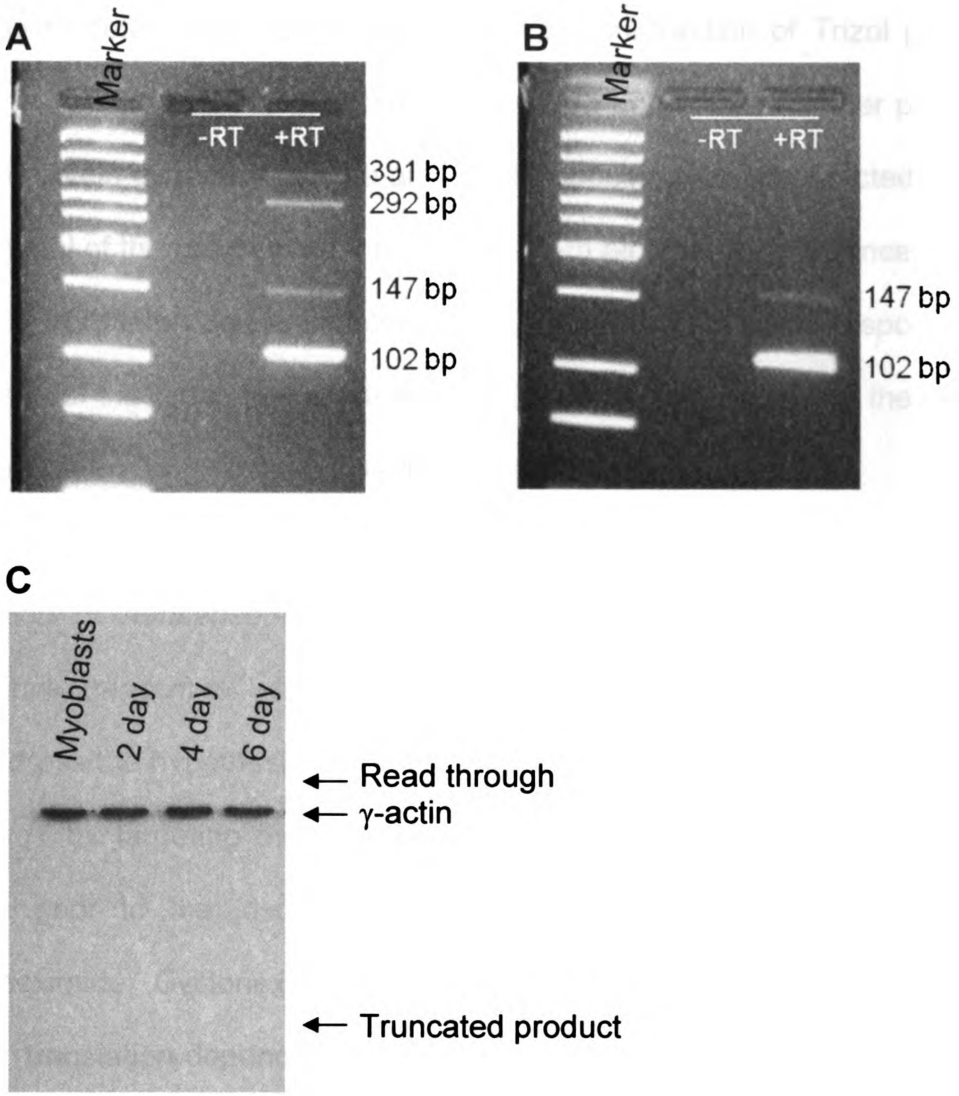

Figure 4-5

Exon 3a transcripts are found in the nuclear (**A**) and cytoplasmic (**B**) RNA fractions of myotubes (6 days post-differentiation). Partially spliced, heterogeneous RNA intermediates remained in the nuclear fraction. Western blot using an anti-γ-actin antibody demonstrates that a protein product corresponding to either a truncated product or read-through of the stop codon was not observed (**C**).

Given that the alternative transcript is exported to the cytoplasm, I used western blotting to detect a protein product. The phenol fraction of Trizol preparations used for the time-course experiment described above were further processed to obtain protein extracts. Using a anti-γ-actin specific antibody directed against the N-terminal of the polypeptide, I probed western blots for the presence of a protein product from exon 3a transcripts (Figure 4-5C). No peptide corresponding either to usage of the termination codon (~15 kDa) or a read-through of the termination codon in exon 3a (~45 kDa) was detected.

Inhibition of nonsense mediated decay results in an increase of exon 3a-containing transcripts

To address the hypothesis that exon 3a is regulatory and may repress translation of *Actg1* by targeting the transcript for NMD via introduction of a termination codon prior to the last exon of the typical transcript, I treated cells with cycloheximide. Cycloheximide targets the small ribosomal subunit and is used to inhibit translation-dependent NMD of PTC-containing transcripts. Cultures of proliferating myoblasts and mature myotubes were treated with either 40 µg/mL cycloheximide in ethanol or an ethanol-only control for three hours in otherwise standard growth conditions. Within the 3 hour treatment with cycloheximide, inhibition of NMD resulted in approximately 1.5x increase of exon 3a transcripts as measured by semi-quantitative analysis (Figure 4-6). These data indicate that exon 3a targets the transcript for translation-dependent NMD. Furthermore,

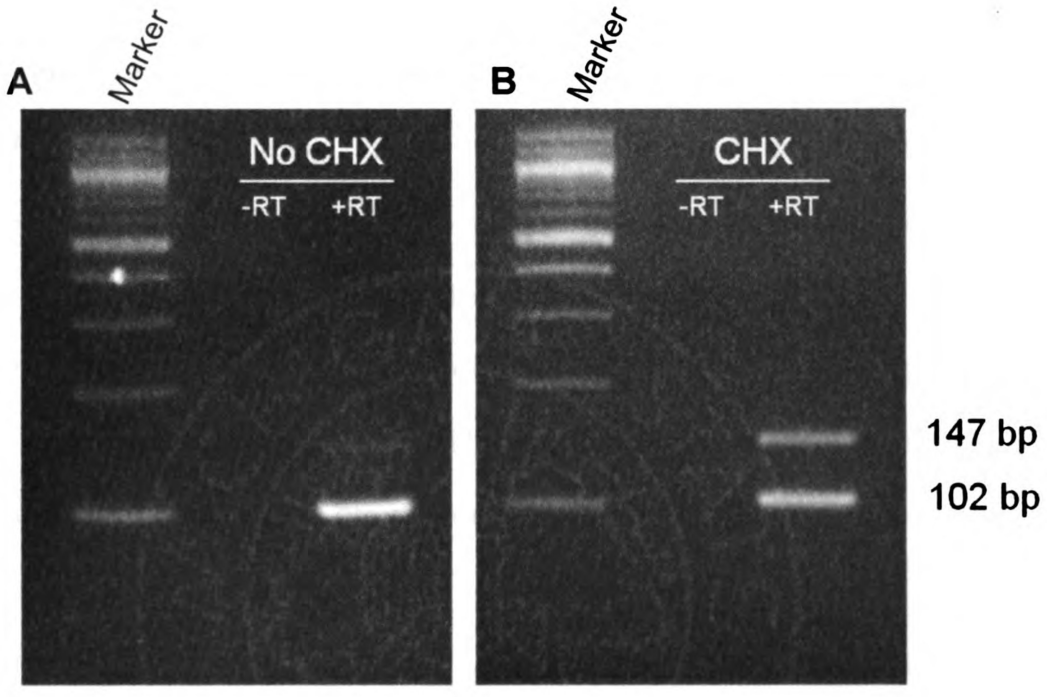

Figure 4-6

Cycloheximide (CHX) treatment of myotubes resulted in an increase in exon 3a transcripts. Semi-quantitative RT-PCR using primers described in Figure 1 was used to evaluate relative abundance in untreated (**A**) and cycloheximide treated (**B**) cells. Experiments were repeated in triplicate.

splicing to include exon 3a is a frequent event in mature myotubes, given the rapid increase in the relative abundance of the alternatively spliced product.

Cells expressing exogenous human ACTG1 regulate splicing to include exon 3a during development

It has been previously demonstrated that intron 3 is necessary to down-regulate *Actg1* (Lloyd and Gunning, 2002). I established a system to determine if the presence of intron 3 is sufficient to down-regulate *Actg1* via splicing to include exon 3a. To this end, I generated mass-selected C2C12 cell lines stably expressing either the coding region of human *ACTG1* with intron 3 genomic DNA (pHs-I3), or intron 3 with an A>G transition to mutate the splice-site (pHs-SSM). Both expression constructs are driven by a CMV promoter (Figure 4-7).

Using species specific primers, we were able to differentiate between endogenous mouse *Actg1* and exogenous human *ACTG1* transcripts. As expected, proliferating myoblasts spliced intron 3 from the mature human RNA transcript in cells expressing pHs-I3 and pHs-SSM. Both cell lines appeared normal as compared to wild-type myoblasts by phase-contrast microscopy. Differentiation was induced when cells were ~70% confluent by the addition of DMEM + 10% horse serum followed by 1 week in 2% horse-serum + 10 μM Ara-C. Both the pHs-I3 and pHs-SSM cells formed myotubes indistinguishable from wild-type. Analysis of RNA from pHs-I3 and pHs-SSM myotubes by RT-PCR shows splicing to include exon 3a in the *ACTG1* mRNA from pHs-I3, but not from

pHs-SSM (Figure 4-8A,B). Similar to endogenous exon 3a transcripts, the level of human exon 3a transcripts increased after a 3 hours treatment with cycloheximide (Figure 4-8C).

Figure 4-7

Diagrams of pHs-I3 (**A**) and pHs-SSM (**B**) . Both vectors contain the full length cDNA of human *ACTG1* under the control of a constitutive CMV promoter. The entire genomic intron 3 was cloned into XcmI sites located in exons 3 and 4. Mutagenic primers were used to mutate the 3' splice acceptor site as indicated.

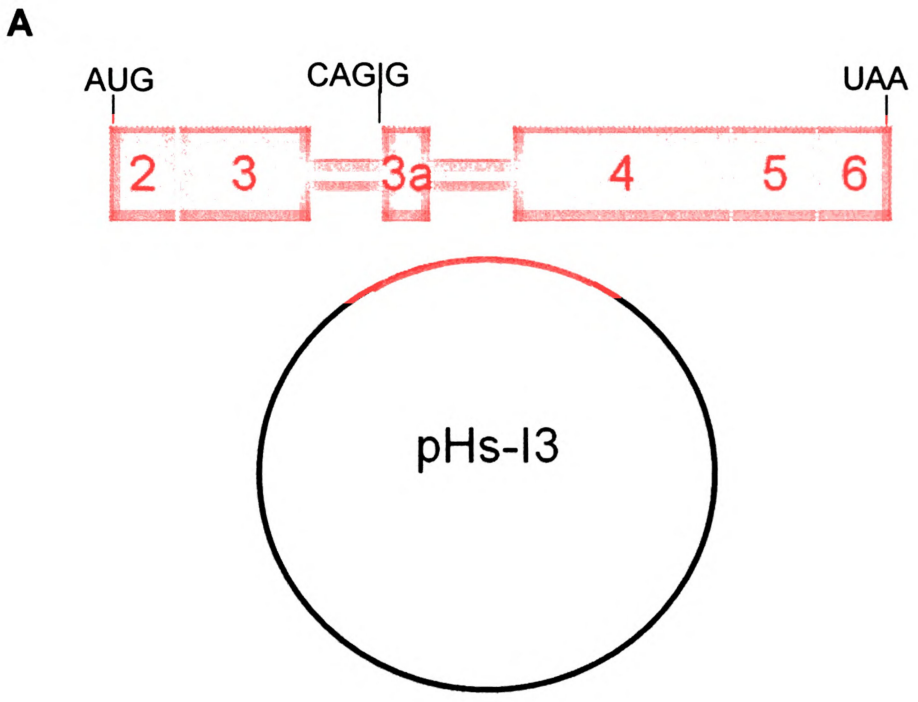
A
AUG
CAG|G
UAA
2
3
3a
4
5
6
pHs-I3

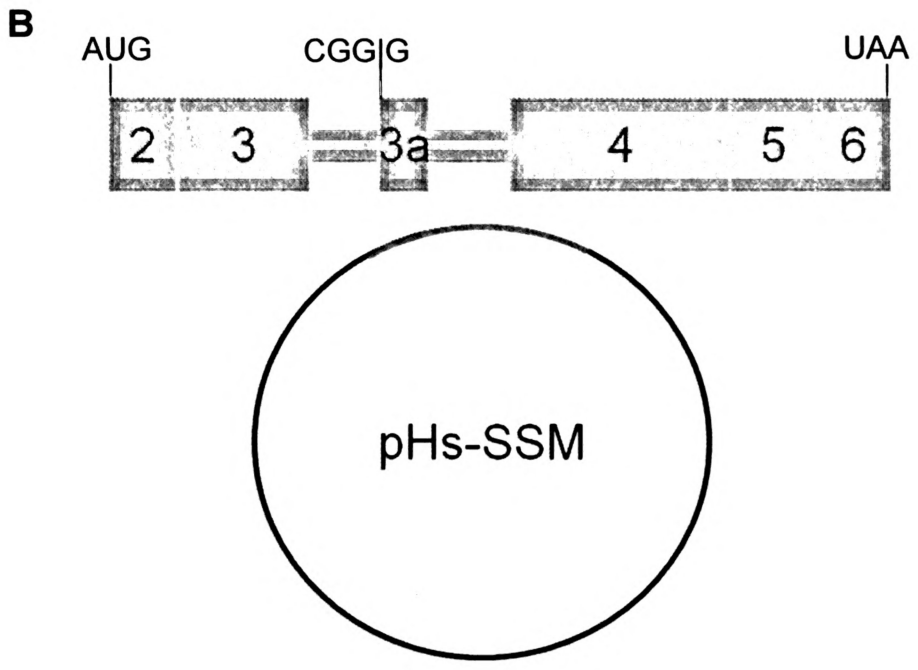
B
AUG
CGG|G
UAA
2
3
3a
4
5
6
pHs-SSM

Figure 4-8

C2C12 myotubes transfected with human ACTG1 constructs splice to include exon 3a only when a proper 3' splice acceptor site is present. Human ACTG1 is spliced to include exon 3a in cells stably expressing pHS-I3 (A), but not pHs-SSM (B). When treated with cycloheximide to inhibit translation-dependent nonsense mediated decay, an increase in exon 3a-containing transcripts from pHS-I3 was observed (C).

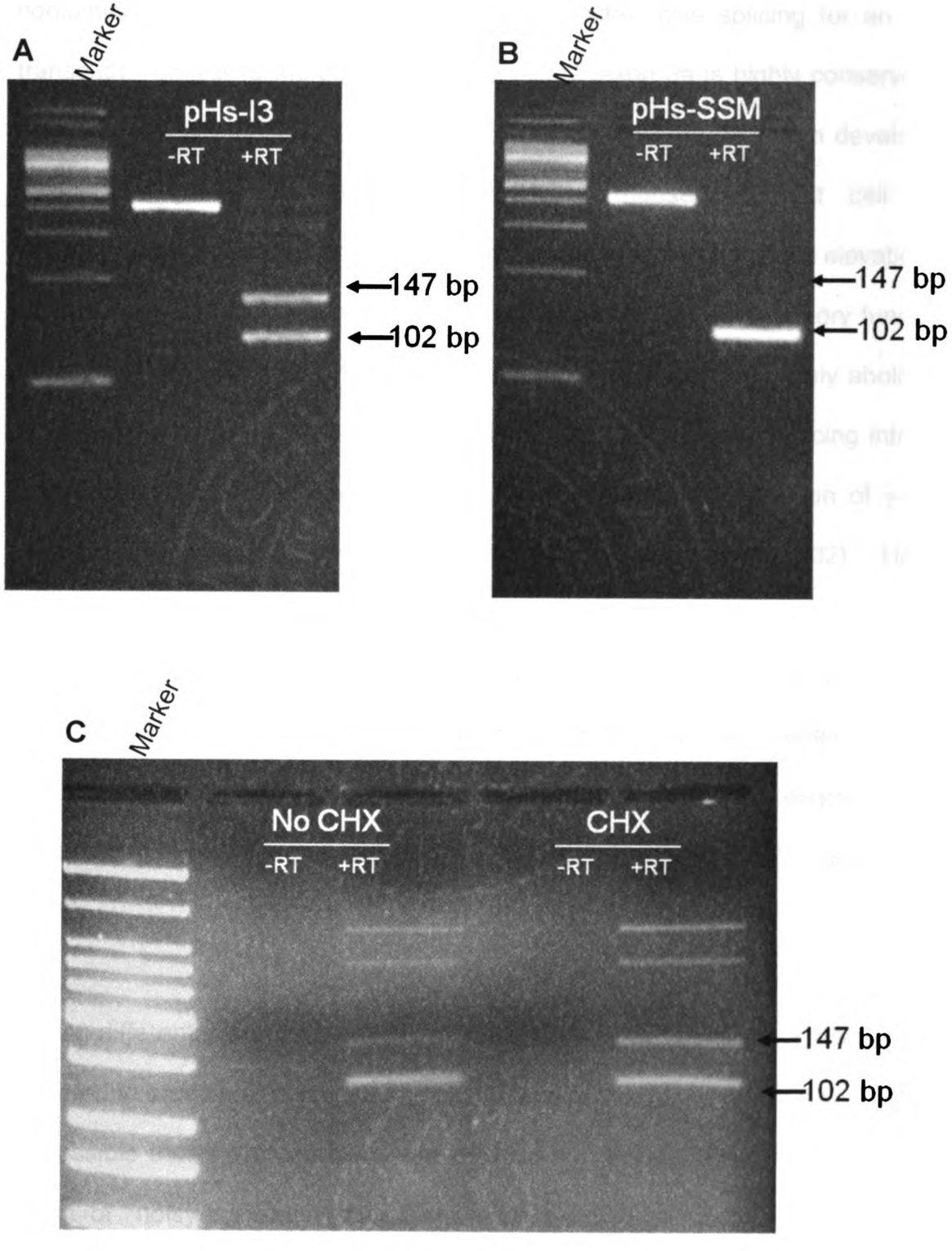
A
Marker
pHs-I3
-RT
+RT
147 bp
102 bp
B
Marker
pHs-SSM
-RT
+RT
147 bp
102 bp
C
Marker
No CHX
-RT
+RT
CHX
-RT
+RT
147 bp
102 bp

Discussion

In this study, I identified a novel *Actg1* splice variant enriched in skeletal muscle containing tissues. This is the first report of alternative splicing for an actin transcript. Similar to the coding exons of *Actg1,* exon 3a is highly conserved in vertebrates. I demonstrated that splicing is differentially regulated in developing muscle using the well-characterized C2C12 mouse myoblast cell line. Furthermore, inhibition of translation-dependent NMD results in an elevation in the level of exon 3a-containing transcripts, consistent with a regulatory function. Finally, a point mutation in the 3' acceptor site of exon 3a completely abolished splicing of exon 3a. Previous studies indicate that inhibition of splicing intron 3 from the primary *Actg1* RNA is responsible for the down-regulation of γ-actin during differentiation of myoblasts (Lloyd and Gunning, 1993, 2002). Here I demonstrate that this regulatory splicing incorporates an additional exon which is sufficient for down-regulation of *Actg1* via a mechanism not previously shown for an actin transcript. Based on this work, I hypothesize that γ-actin is down-regulated via alternative splicing to introduce a PTC and thus degrade *Actg1* transcripts via NMD, a process termed RUST (Green et al., 2003; Lewis et al., 2003).

During differentiation of myoblasts, multiple transcription and splicing factors are required to coordinate changes in expression required for differentiation. Thus, it is possible that the presence of the alternatively spliced *Actg1* transcript is the result of "noisy splicing". Large-scale analyses indicate that the majority of

alternatively spliced transcripts are likely generated in error because of their low abundance across multiple tissues and lack of correlation with expression differences in the genes examined (Pan *et al.*, 2006; McGlincy and Smith, 2008; Melamud and Moult, 2009). Using the guidelines established by Zhang and colleagues, I evaluated whether splicing to include exon 3a is spurious or functional splicing (Melamud and Moult, 2009; Zhang *et al.*, 2009). Our data indicate that splicing to include the alternatively spliced *Actg1* transcript does maintain the proper reading frame, except in humans. Gamma-actin does not belong to a gene family which is alternatively spliced, it does include an evolutionarily conserved termination codon, which is enriched in a tissue- and development-specific manner.

The premise of RUST seems inherently counter-intuitive as a regulatory mechanism, since the most efficient means of down-regulation would be to not transcribe the RNA at all. However, Soergel *et al* note that the production of large transcripts in any instance can be an inherently wasteful endeavor (Soergel *et al.*, 2006), as introns can constitute up to 95% of a primary RNA transcript (Lander *et al.*, 2001; Soergel *et al.*, 2006). It is possible that RUST serves as a mechanism to modulate expression of genes that are typically highly expressed and are essential in the cell. When a particular environmental or physiologic change dictates that only moderate levels of protein are required, it is necessary to down-regulate production without switching off transcription entirely. In such an instance, post-transcriptional degradation of a portion of excess transcripts

produced via NMD is more energy efficient than post-translational degradation of unnecessary proteins. This model is suitable for γ-actin in muscle, as it is expressed at high levels in proliferating myoblasts, but is also necessary at lower levels in differentiated myotubes and developed skeletal muscle.

Of interest, three regions of 13 nt, 32 nt, and 6 nt immediately adjacent to the 5' donor site of exon 3a are nearly perfectly conserved among vertebrates (Figure 4-9). These regions may contain recognition motifs for splicing factors such as muscleblind and muscleblind-like proteins that are necessary for coordinating gene expression changes between progenitor and differentiated muscle cells (Pascual *et al.*, 2006; Holt *et al.*, 2009).

Finally, I have established mass selected cell lines expressing exogenous human *ACTG1* with and without a functional splice site. If RUST is the mechanism by which γ-actin transcripts are degraded, I should observe an increase in splicing to include exon 3a from either the exogenous or endogenous γ-actin transcript in response to the amount of exogenous actin produced. A more quantitative approach, such as qRT-PCR will be necessary to investigate the intricacies of this mechanism.

In closing, this report documents the first identification and characterization of an alternatively spliced actin transcript. Subtle differences in sequence of exon 3a between primates and lower mammals further support the regulatory hypothesis.

In humans exon 3a is only 41 nucleotides and generates a PTC in exon 4 via a frameshift in contrast to mouse which is 45 nt and includes an in-frame PTC. This finding coincides with evolutionary importance of the PTC and not a translated product. Previous studies of RUST indicate that this type of regulation is not only conserved across species, but is typically found as a regulatory mechanism for members of the same gene family. It will therefore be useful to explore RUST as a regulatory mechanism for other actin isoforms.

Figure 4-9

Conservation of intron 3a. In addition to the high degree of conservation of the nucleotide coding sequence of exon 3a, the intronic region immediately 3' of the 5' splice donor site is well conserved. These sections of conserved sequence are good candidates for splicing enhancer or silencer motifs.

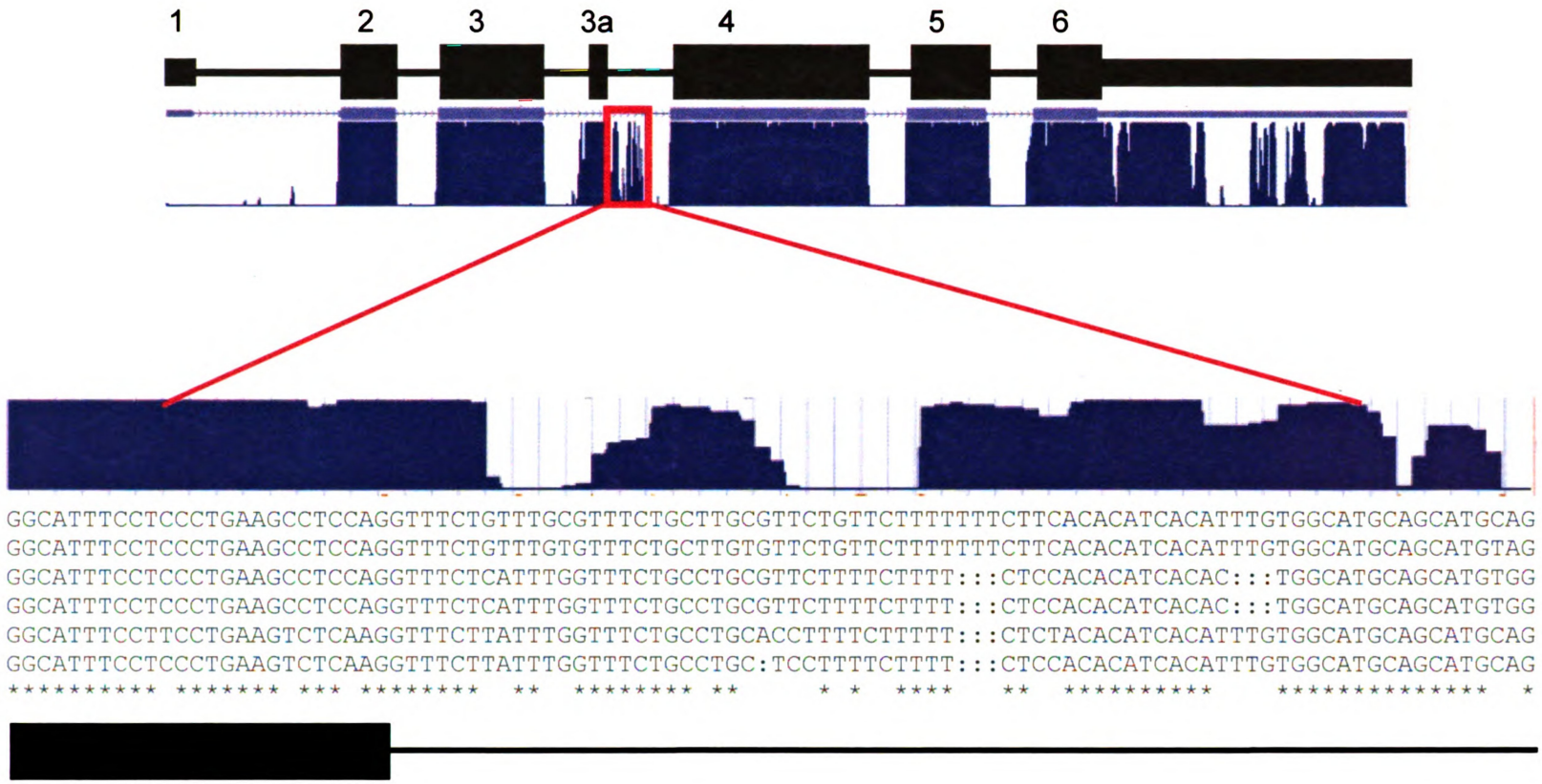
1
2
3
3a
4
5
6
GGCATTTCCTCCCTGAAGCCTCCAGGTTTCTGTTTGCGTTTCTGCTTGCGTTCTGTTCTTTTTTTCTTCACACATCACATTTGTGGCATGCAGCATGCAG Mouse
GGCATTTCCTCCCTGAAGCCTCCAGGTTTCTGTTTGTGTTTCTGCTTGTGTTCTGTTCTTTTTTTCTTCACACATCACATTTGTGGCATGCAGCATGTAG Rat
GGCATTTCCTCCCTGAAGCCTCCAGGTTTCTCATTTGGTTTCTGCCTGCGTTCTTTTCTTTT:::CTCCACACATCACAC:::TGGCATGCAGCATGTGG Human
GGCATTTCCTCCCTGAAGCCTCCAGGTTTCTCATTTGGTTTCTGCCTGCGTTCTTTTCTTTT:::CTCCACACATCACAC:::TGGCATGCAGCATGTGG Rhesus
GGCATTTCCTTCCTGAAGTCTCAAGGTTTCTTATTTGGTTTCTGCCTGCACCTTTTCTTTTT:::CTCTACACATCACATTTGTGGCATGCAGCATGCAG Dog
GGCATTTCCTCCCTGAAGTCTCAAGGTTTCTTATTTGGTTTCTGCCTGC:TCCTTTTCTTTT:::CTCCACACATCACATTTGTGGCATGCAGCATGCAG Horse
Exon 3a
Intron 3a

References

Belyantseva, I. A., Perrin, B. J., Sonnemann, K. J., Zhu, M., Stepanyan, R., McGee, J., Frolenkov, G. I., Walsh, E. J., Friderici, K. H., Friedman, T. B., *et al.*, 2009. Gamma-actin is required for cytoskeletal maintenance but not development. Proc Natl Acad Sci U S A. 106, 9703-8.

Casadei, L., Vallorani, L., Gioacchini, A. M., Guescini, M., Burattini, S., D'Emilio, A., Biagiotti, L., Falcieri, E., Stocchi, V., 2009. Proteomics-based investigation in C2C12 myoblast differentiation. Eur J Histochem. 53, 261-8.

DePonti-Zilli, L., Seiler-Tuyns, A., Paterson, B. M., 1988. A 40-base-pair sequence in the 3' end of the beta-actin gene regulates beta-actin mRNA transcription during myogenesis. Proc Natl Acad Sci U S A. 85, 1389-93.

Furness, D. N., Katori, Y., Mahendrasingam, S., Hackney, C. M., 2005. Differential distribution of beta- and gamma-actin in guinea-pig cochlear sensory and supporting cells. Hear Res. 207, 22-34.

Green, R. E., Lewis, B. P., Hillman, R. T., Blanchette, M., Lareau, L. F., Garnett, A. T., Rio, D. C., Brenner, S. E., 2003. Widespread predicted nonsense-mediated mRNA decay of alternatively-spliced transcripts of human normal and disease genes. Bioinformatics. 19 Suppl 1, i118-21.

Holt, I., Jacquemin, V., Fardaei, M., Sewry, C. A., Butler-Browne, G. S., Furling, D., Brook, J. D., Morris, G. E., 2009. Muscleblind-like proteins: similarities and differences in normal and myotonic dystrophy muscle. Am J Pathol. 174, 216-27.

Khaitlina, S. Y., 2001. Functional specificity of actin isoforms. Int Rev Cytol. 202, 35-98.

Kislinger, T., Gramolini, A. O., Pan, Y., Rahman, K., MacLennan, D. H., Emili, A., 2005. Proteome dynamics during C2C12 myoblast differentiation. Mol Cell Proteomics. 4, 887-901.

Lander, E. S., Linton, L. M., Birren, B., Nusbaum, C., Zody, M. C., Baldwin, J., Devon, K., Dewar, K., Doyle, M., FitzHugh, W., *et al.*, 2001. Initial sequencing and analysis of the human genome. Nature. 409, 860-921.

Lewis, B. P., Green, R. E., Brenner, S. E., 2003. Evidence for the widespread coupling of alternative splicing and nonsense-mediated mRNA decay in humans. Proc Natl Acad Sci U S A. 100, 189-92.

Lloyd, C., Gunning, P., 1993. Noncoding regions of the gamma-actin gene influence the impact of the gene on myoblast morphology. J Cell Biol. 121, 73-82.

Lloyd, C., Gunning, P., 2002. beta- and gamma-actin genes differ in their mechanisms of down-regulation during myogenesis. J Cell Biochem. 84, 335-42.

McGlincy, N. J., Smith, C. W., 2008. Alternative splicing resulting in nonsense-mediated mRNA decay: what is the meaning of nonsense? Trends Biochem Sci. 33, 385-93.

Melamud, E., Moult, J., 2009. Stochastic noise in splicing machinery. Nucleic Acids Res. 37, 4873-86.

Nakata, T., Nishina, Y., Yorifuji, H., 2001. Cytoplasmic gamma actin as a Z-disc protein. Biochem Biophys Res Commun. 286, 156-63.

Otey, C. A., Kalnoski, M. H., Bulinski, J. C., 1987. Identification and quantification of actin isoforms in vertebrate cells and tissues. J Cell Biochem. 34, 113-24.

Otey, C. A., Kalnoski, M. H., Bulinski, J. C., 1988. Immunolocalization of muscle and nonmuscle isoforms of actin in myogenic cells and adult skeletal muscle. Cell Motil Cytoskeleton. 9, 337-48.

Otey, C. A., Kalnoski, M. H., Lessard, J. L., Bulinski, J. C., 1986. Immunolocalization of the gamma isoform of nonmuscle actin in cultured cells. J Cell Biol. 102, 1726-37.

Pan, Q., Saltzman, A. L., Kim, Y. K., Misquitta, C., Shai, O., Maquat, L. E., Frey, B. J., Blencowe, B. J., 2006. Quantitative microarray profiling provides evidence against widespread coupling of alternative splicing with nonsense-mediated mRNA decay to control gene expression. Genes Dev. 20, 153-8.

Pascual, M., Vicente, M., Monferrer, L., Artero, R., 2006. The Muscleblind family of proteins: an emerging class of regulators of developmentally programmed alternative splicing. Differentiation. 74, 65-80.

Soergel, D. A. W., Lareau, L. F., Brenner, S. E., Regulation of Gene Expression by Coupling of Alternative Splicing and NMD. In: L. E. Maquat, (Ed.), Nonsense-Mediated mRNA Decay. Landes Bioscience, Austin, Tx, 2006.

Zhang, Z., Xin, D., Wang, P., Zhou, L., Hu, L., Kong, X., Hurst, L. D., 2009. Noisy splicing, more than expression regulation, explains why some exons are subject to nonsense-mediated mRNA decay. BMC Biol. 7, 23.

CHAPTER 5

CHARACTERIZATION OF A KNOCK-IN MOUSE MODEL FOR DFNA20 DEAFNESS.

Abstract

Ten dominant missense mutations in gamma-actin (*ACTG1*) have been reported as the cause of hearing loss in DFNA20 families. Although the mutations are located in different functional domains of gamma-actin, the end result is a progressive form of non-syndromic sensorineural hearing loss beginning in the high frequencies with an onset in the second to third decade of life. This shared phenotype is indicative of a common functional deficit in mutant gamma-actin protein function (Zhu *et al* 2003). To address questions regarding the effects of these mutations on the structure and function of the inner ear and whether these mutations cause hearing loss via a loss of function versus a dominant negative mode of action, we generated a knock-in mouse model for the p.P264L mutation.

Mice harboring the p.P264L substitution of ACTG1 in both the heterozygous and homozygous state are born at the expected Mendelian ratio, are viable, and do not have noticeable vestibular deficits. Mice homozygous for the p.P264L allele (normal level of expression) exhibit a high frequency loss by 4-5 weeks and nearly complete hearing loss by 6-7 weeks of age. In the organ of Corti, the hearing loss manifests by a loss of inner and outer hair cells with a base to apical progression. Morphologically, the outer hair cell loss is preceded by degeneration of the two shorter rows of stereocilia.

Compared to the previously characterized *Actg1*-null mice which have adult-onset progressive deafness, reduced viability and muscular myopathy

(Belyantseva *et al* 2009), the p.P264L mutation produces fewer pleiotropic effects and a profound deafness by 6-7 weeks of age. Taken together, our data suggest a dosage-dependent dominant negative mode of action for p.P264L.

Introduction

Mutations in γ-actin are the cause of nonsyndromic sensorineural hearing loss in DFNA20 families (van Wijk *et al.*, 2003; Zhu *et al.*, 2003; Rendtorff *et al.*, 2006; Liu *et al.*, 2008; de Heer *et al.*, 2009; Morin *et al.*, 2009). The ten missense mutations identified are not clustered in a single functional domain of the actin monomer, so there are few clues as to how these mutations affect the function of the protein. A number of *in vitro* and *in vivo* experiments have provided clues; however, there are several caveats and limitations to these assays. For example, experiments in yeast provided information about how the mutations affect important actin functions such as polymerization and depolymerization kinetics and nucleotide exchange rate (Bryan *et al.*, 2006; Bryan and Rubenstein, 2009; Morin *et al.*, 2009). However, yeast have only one actin, and the physiological conditions and requirements of a unicellular organism are quite different from that of the polarized epihelial hair cells in the organ of Corti in humans. To overcome this issue, studies to investigate mutant γ-actin function were also done using mammalian cell and explant cultures. CL4 intestinal epithelial cells, cells with planar polarity, co-transfected with espin and mutant γ-actins made significantly shorter microvilli, however no difference in the recovery after treatment with actin depolymerization agents was observed, indicating that the microvilli were capable of repair and/or regeneration (Korrapati Ph.D Dissertation, 2009). While quite similar to stereocilia, intestinal microvilli lack key structures and organization that are characteristic of auditory hair cell bundles. Organ of Corti explant cultures were biolistically transfected with GFP-tagged

mutant γ-actin plasmids, however no differences in incorporation of mutant actin into the stereocilia were observed compared to wild-type actin (Belyantseva, unpublished personal communication). Though these experiments addressed the structural limitations of the CL4 cells, limitations in the length of time that organ of Corti explants can remain in culture, in addition to the abundance of endogenous wild-type actin, complicate this method of analysis.

Our goal was to generate a knock-in mouse model to understand the pathophysiology of the p.P264L missense mutation. We chose this particular mutation because it causes the earliest onset and most rapidly progressing deafness in humans (Zhu *et al.*, 2003). A γ-actin knockout mouse model was previously generated and characterized (Belyantseva *et al.*, 2009). Similar to the phenotype observed in humans, knockout mice suffered from progressive hearing loss beginning in the high frequencies. However, unlike DFNA20 deafness, the hearing loss was accompanied by a muscular myopathy, reduction in total body size, and reduced viability. Knock-out mouse models do not appropriately address gain of function or dominant negative modes of action. Likewise, a transgenic mouse model which results in the over expression of the mutant allele in the context of full wild type expression, may also complicate the analysis of a missense mutation. By generating a knock-in mouse model, we can evaluate the effects of the mutant p.P264L allele expressed at physiologically relevant levels in relevant tissues and cell types, and at the appropriate times during development.

The knock-in targeting vector was designed and cloned in our laboratory by Dr. Mei Zhu (Figure 5-1). Chimeric mice were generated by the University of Michigan Transgenic Animal Model Core. Dr. Zhu verified the location and orientation of the transgene at the 5' and 3' ends by Southern blotting. Together we bred chimeras to wild-type C57Bl/6J mice and screened offspring for germline transmission of the mutant allele. At this point, Mei left the University and I took over the maintenance and characterization of this mouse model.

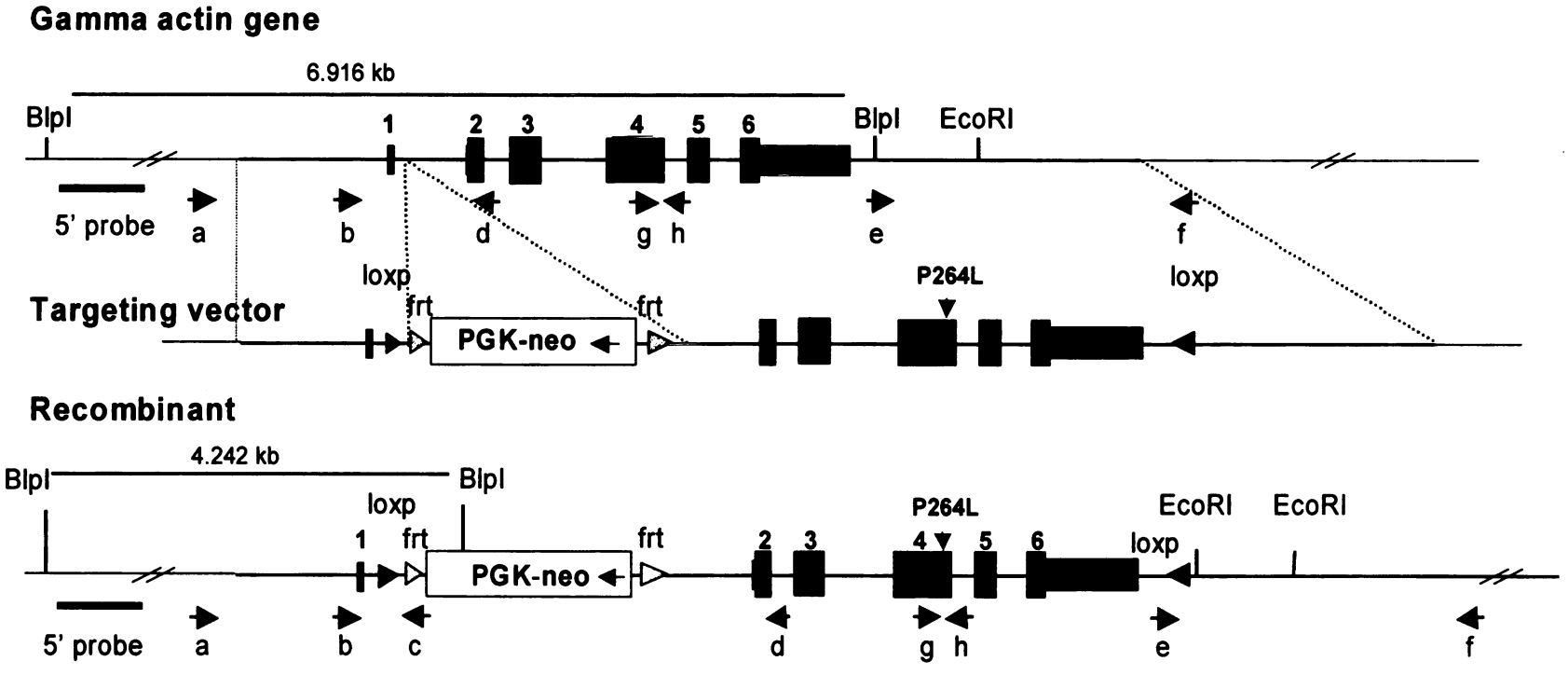

Figure 5-1

Schematic of the p.P264L targeting construct. There is a *neo* selection cassette within intron 1 of *Actg1*. The selection cassette is flanked by two frt sites to facilitate excision via Flpe recombinase mediated recombination. A C>T transition in exon 4 of *Actg1* cDNA creates a missense mutation found in one of the DFNA 20 families. The presence of this mutation generates a novel AluI restriction site, a feature which is exploited for genotyping by PCR and RFLP.

Materials and Methods

Animals

All animals used in this study were housed and euthanized according to IACUC and NIH approved guidelines. Tail snips <1 cm were collected at 14-21 days old. DNA was isolated using a high salt precipitation (see appendix. PCR and Taq polymerase (Promega, Madison, WI) were used for genotyping (see appendix). Primers situated within exon 4 and intron 4 of genomic DNA were used to amplify a 194 bp region which includes the mutation: $^{5'}$TGGCTACTGCTGCATCATCT$^{3'}$ and $^{5'}$GCCACTACATTCTGTGTGTT$^{3'}$. The p.P264L allele introduces a C>T transition, resulting in a novel AluI recognition site within the amplicon that allows for identification of wild-type, heterozygous, and homozygous mice. Primers flanking the *neo* cassette $^{5'}$CCCGCTTTTGGAAAGAT$^{3'}$ and $^{5'}$GGCCACTCCTCTCAACTAAC$^{3'}$ were used to screen for the removal of the selection cassette.

Generation of congenic mice

After germline transmission of the p.P264L (PL) allele was established, I backcrossed hetereozygouse males to wild-type C57Bl/6J females purchased from Jackson Labs. One backcross was to a transgenic *Flpe* recombinase female to remove the neo selection cassette. After removal of the neo cassette, and as soon as the animals had greater than 90% contribution from the C57Bl/6J background, I crossed +/PL by +/PL mice to generate PL/PL homozygotes. We continued to backcross to the C57Bl/6J background to obtain congenic mice.

Rotarod

Mice were first trained on the Rotarod with daily tests for one week. Accelerating Rotarod tests were done three times per week, with three trials each day using a accelerating protocol for a total of five weeks (Crawley, 2000). Briefly, the rod accelerated from 4 rpm to 40 rpm during each 5 minute test. Latency to fall off was recorded for each three tests. The longest latency for each day was determined and averaged for all mice within a single genotype across a single week.

Protein isolation

Brain samples from six week old mice were harvested immediately after sacrifice and snap frozen on dry ice. Samples not immediately used were transferred to -80°C for long-term storage. Approximately 50 mg of brain was homogenized in standard SDS-lysis buffer mammalian lysis/binding buffer composed of 100 mM KCl, 10 mM PIPES, 5 mM EGTA, 1% Triton X-100, pH7.4 with Complete protease inhibitors (Roche, Basel, Switzerland). Brains were homogenized using a rotor homogenizer for thirty seconds at full speed and centrifuged for 15 minutes at 13,000 x g in a microcentrifuge at 4°C to pellet insoluble material. The protein concentration of each sample was determined using a Bradford assay (BioRad, Hercules, CA) with BSA as a standard.

Western Blotting

Proteins were separated via SDS-PAGE on discontinuous 10% Laemmli gels (see appendix). Proteins were transferred in 10 mM Tris base, 100 mM glycine, 15% methanol (transfer buffer) at 4°C either overnight at a constant current of 5 mAmp or for 1.5 hours at a constant voltage of 110V onto polyvinylidene difluoride (PVDF) membranes (BioRad, Hercules, CA). Membranes were incubated in 5% non-fat milk in 0.025% Tween-20 in PBS pH 7.4 (blocking buffer) for either one hour at room temperature or overnight at 4°C. Rabbit polyclonal anti-γ-actin antiserum (Belyantseva *et al*, 2009; see chapters 1 and 2 for description of antibody validation) was diluted 1:10,000 in blocking buffer and rabbit polyclonal anti-β-tubulin antiserum (Abcam, Cambridge, MA; ab6046) was diluted 1:1000 in blocking buffer. Membranes were incubated with primary antiserum for either 2 hours at room temperature or overnight at 4°C. Goat polyclonal anti-rabbit IgG-HRP conjugated secondary antibody (Sigma, St. Louis, MO) was used at 1:3,000 in blocking buffer for one hour at room temperature. Proteins were detected using an ECL Detection Kit (GE Healthcare, Waukesha, WI) with Amersham Hyperfilm™ MP autoradiography film (GE healthcare, Waukesha, WI). The length of exposure was determined by signal intensity observed. Pixel intensity of each band was measured using BioRad's GelDoc software (Hercules, CA).

Immunofluorochemistry

Immunofluorochemisty was done as previously described (Belyantseva et al., 2009) with modifications. Cochleae were harvested and immediately perfused with 4% paraformaldehyde (Electron Microscopy Sciences, Hatfield, PA). The organ of Corti and vestibular end organs were microdissected in PBS pH 7.4. Samples were permeabilized with 0.5% Triton X-100 in PBS pH 7.4 and non-specific immunoreactivity was blocked in 5% BSA and 2% goat serum (Invitrogen, Carlsbad, CA) in PBS pH 7.4 (blocking buffer) for either one hour at room temperature or overnight at 4°C. Rabbit polyclonal anti-γ-actin (Otey *et al*, 1986, Belyantseva *et al*, 2009; see chapters 2 and 3 for description of antibody validation) was diluted 1:300 in blocking solution. Tissues were incubated with primary antiserum for either 2 hours at room temperature or overnight at 4°C. Polyclonal antiPolyclonal anti-rabbit IgG secondary antiserum conjugated to AlexaFluor 488 (Invitrogen, Carlsbad, CA; A11008) was used to label primary antibodies. Secondary antiserum was used at 1:500 in blocking buffer and incubated for 30 minutes at room temperature. Samples were counterstained with rhodamine-phalloidin (Invitrogen, Carlsbad, CA) at 1:200 in blocking buffer and DAPI (Invitrogen, Carlsbad, CA) at 1:10,000 in PBS pH7.4. Samples were imaged using Olympus Fluoview LMS (Center Valley, PA) and either a 60x or 100x objective lens. Aside from adjustments to brightness and contrast, no image manipulation was used.

Auditory-evoked Brainstem Response (ABR)

These procedures were performed by Karin Halsey at University of Michigan with their animal use agreement. Animals were anesthetized (ketamine 65 mg/kg, xylazine 3.5 mg/kg, and acepromazine 2mg/kg). Body temperature was maintained through the use of water circulating heating pads and heat lamps. Additional anesthetic (ketamine and xylazine) was administered if needed to maintain anesthesia depth sufficient to insure immobilization and relaxation. ABRs were recorded in an electrically and acoustically shielded chamber (Acoustic Systems, Austin, TX USA). Needle electrodes were placed at vertex (active) and the test ear (reference) and contralateral ear (ground) pinnae. Tucker Davis Technologies (TDT) System III hardware and SigGen/BioSig software (TDT, Alachua, FL USA) were used to present the stimulus and record responses. Tones were delivered through an EC1 driver (TDT, aluminum enclosure made in-house), with the speculum placed just inside the tragus. Stimulus presentation was 15 ms tone bursts, with 1 ms rise/fall times, presented 10 per second. Up to 1024 responses were averaged for each stimulus level. Responses were collected for stimulus levels in 10 dB steps at higher stimulus levels, with additional 5 dB steps near threshold. Thresholds were interpolated between the lowest stimulus level where a response was observed, and 5 dB lower, where no response was observed.

Scanning Electron Microscopy (SEM)

Samples were prepared for scanning electron microscopy as described previously (Belyantseva *et al.*, 2009) with minor modifications. Briefly, cochleae were dissected from the temporal bone of mice and immediately fixed by perfusion through the oval window with 2.5% glutaraldehyde in 0.1M sodium cacodylate pH7.3 supplemented with 1mM $CaCl_2$. After a 2 hour incubation at room temperature with vigorous shaking, samples were transferred to dilute 0.125% glutaraldehyde in cacodylate pH8.0 supplemented with 0.5mM $CaCl_2$ for storage until use. Immediately prior to microdissection, the samples were rinsed in 1xPBS three times. The boney capsule of the cochlear bulla was gently removed along with the stria vascularis, Reisner's membrane, and tectorial membrane to reveal the apical surface of the auditory hair cells. The first apical turn was also removed and mounted separately so as to reveal the second, basal turn. Samples were taken through a series of ethanol solutions (25%, 50%, 75%, 90%, 95%) with three final rinses in 100% ethanol.

Cochleae were further processed in a Balzers critical point dryer with four rounds of flushing for 5 minutes each and then mounted onto carbon coated stubs. A thin coating of osmium tetroxide was applied followed by a second coating with gold. Samples were stored in a vacuum until imaged. A JOEL 6400 scanning electron microscope was used to image cochleae. I found that a working distance of 16 mm and numerical aperture 4 provided the best depth of field and

resolution for this type of sample. Accelerating voltage was variable and selected based on intensity of the LaB_6 filament.

Results

The mutant P264L protein is expressed at normal levels, however, the neo cassette reduces expression

I determined the expression of the mutant p.P264L allele by western blot analysis. Frequently, the presence of a neo selection cassette reduces the total level of a mutant protein in cells due to promiscuous splicing of the transcript to include the neo cassette; therefore animals with and without the neo cassette were analyzed. Brain samples were homogenized using a rotor homogenizer in lysis buffer supplemented with protease inhibitors and centrifuged to pellet insoluble material. One milligram of total protein from each sample was used for western blotting with a previously validated γ-actin specific antibody. I quantitated the pixel intensity of each product using a BioRad Gel Doc system and normalized to the β-tubulin loading control. Figure 5-2A demonstrates that P264L γ-actin is as abundant in homozygous knock-in mice (PL/PL) as γ-actin in wild-type littermates (+/+). In contrast, the P264L protein produced in mice still harboring the neo selection cassette (PL-neo) show an 80% reduction compared to wild-type littermates (Figure 5-2B). The remainder of the data that I present in this chapter is from mice with the full expressing (PL) allele.

P264L heterozygotes and homozygotes are physically fit and fertile

DFNA20 families do not show clinical signs other than hearing loss. However, the previously characterized γ-actin knock-out mice are born at lower than expected ratios, are less viable, smaller, and show muscular myopathy when

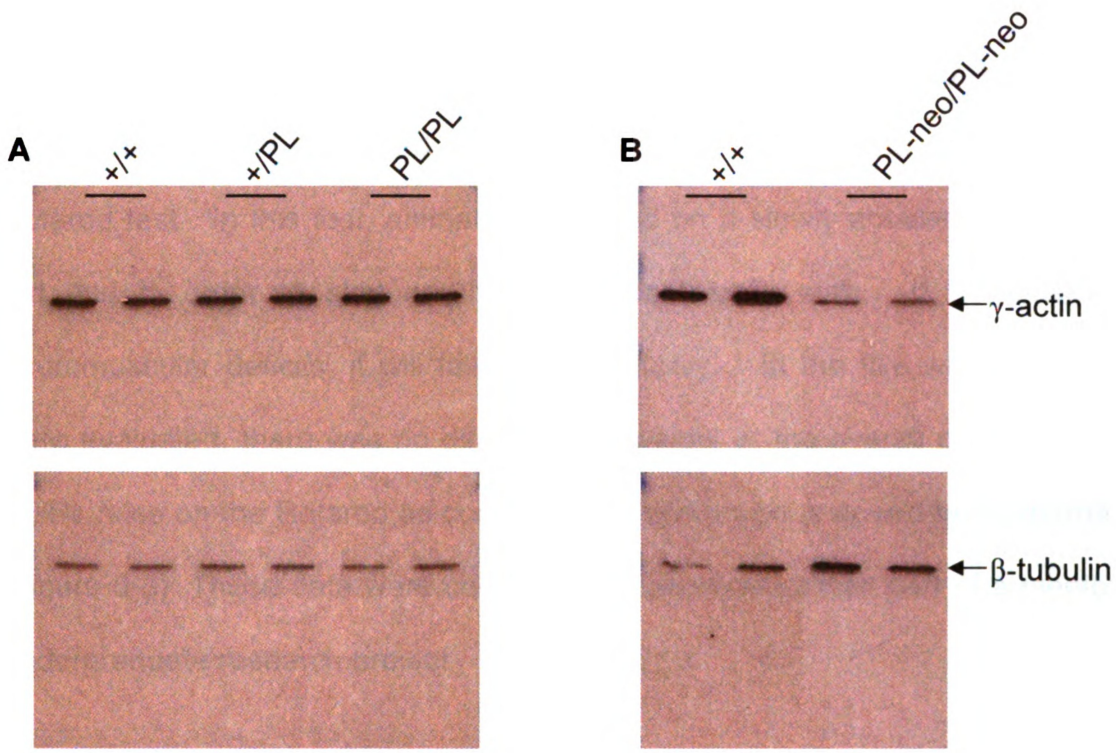

Figure 5-2

Western blots to determine expression of the recombinant p.P264L in the presence and absence of the *neo* cassette. The pixel intensity of each band was measured using Gel Doc software (BioRad). The quantity of γ-actin (top panel) was normalized to a β-tubulin loading control (bottom panel). The *neo* cassette reduces expression of the recombinant allele to 20% of normal. Excision of cassette restores wild-type levels of expression.

compared to wild-type and heterozygous littermates (Belyantseva *et al.*, 2009). In contrast, data from 10 matings of +/PL by +/PL mice indicate that these mice are born at the expected Mendelian ratio. To determine if the P264L protein causes reduced body size or muscular myopathy, we obtained weekly weight measurements and evaluated the neuromuscular health of the animals using a Rotarod test. In this test, animals are placed on a slowly accelerating spinning rod and in order to stay on they must continually walk. If a mouse has neuromuscular deficits, it will fall off prematurely. In the five weeks the mice were evaluated, there was no difference in weight or the overall performance of PL/PL mice on the Rotarod as compared to heterozygous or wild-type littermates (Figure 5-3). These data were collected by Lawrence Lee as part of a mentored undergraduate research project.

P264L homozygotes have an early onset, progressive hearing loss

Studying deafness in mice poses the difficulty of determining whether or not a mouse has heard a sound. The classic test is to snap or clap and observe the mouse for a whole body startle response. A more accurate method is auditory-evoked brainstem response (ABR) which allows for quantitative measurement of hearing in mice. An electrode is placed near the ear (subdermal) and the brainstem response to sound is measured. A typical response to sound is a six-peak waveform spaced at regular intervals. The intensity (dB SPL) at which a waveform is no longer detected determines the threshold of hearing in a mouse. We do not have the equipment or expertise for these experiments at Michigan

Figure 5-3

PL mice do not have muscular myopathy as determined by an accelerating Rotarod test (**A**), nor are they smaller than heterozygous or wild-type littermates (**B,C**). Mice were weighed immediately prior to the first Rotarod test of the day. Additional weight data were collected from mice used for ABR. n=4 except where noted with * when n=2.

A

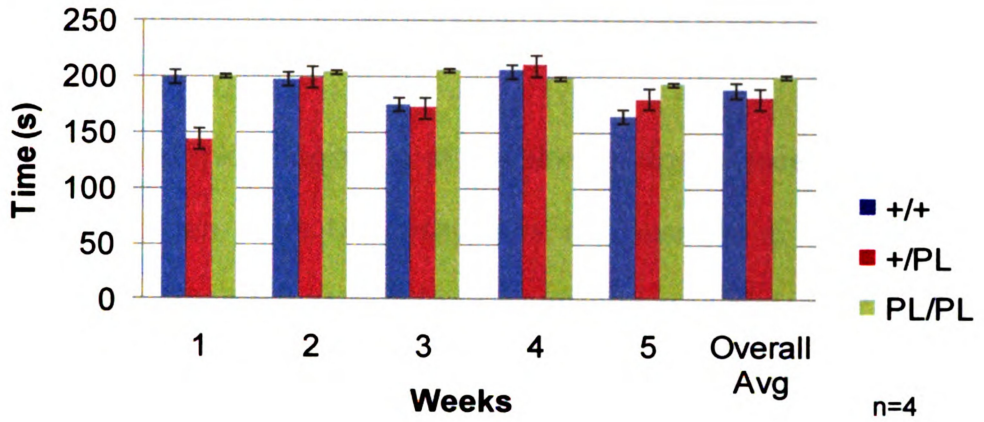
250
200
150
100
50
0
Time (s)
1
2
3
4
5
Overall Avg
Weeks
+/+
+/PL
PL/PL
n=4

B

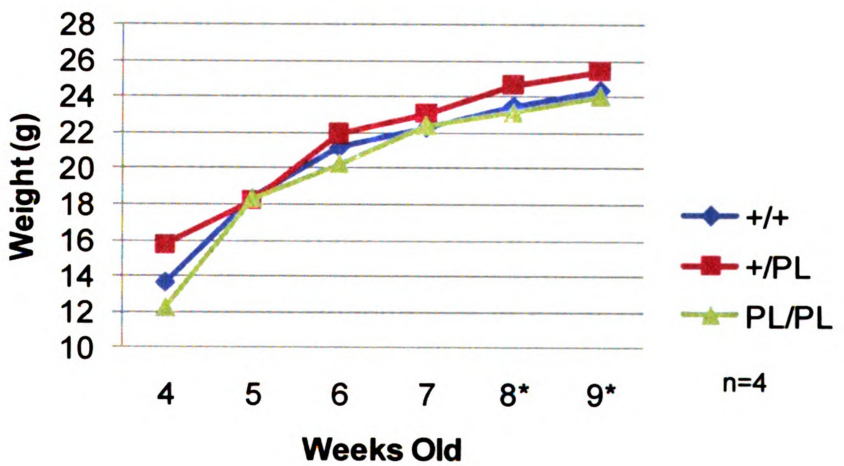
28
26
24
22
20
18
16
14
12
10
Weight (g)
4
5
6
7
8*
9*
Weeks Old
+/+
+/PL
PL/PL
n=4

C

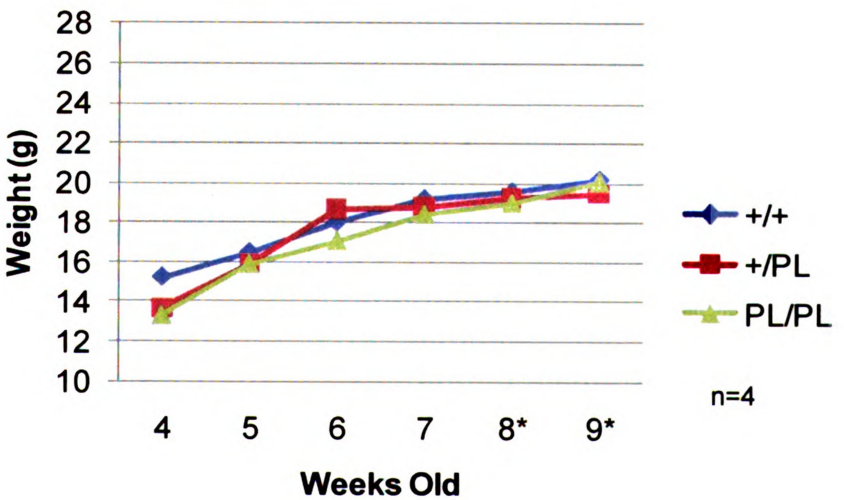
28
26
24
22
20
18
16
14
12
10
Weight (g)
4
5
6
7
8*
9*
Weeks Old
+/+
+/PL
PL/PL
n=4

State University, so I escorted mice to the University of Michigan where Karin Halsey, a technician in the Dolan laboratory, obtained these ABR data.

We chose to test mice beginning at 4 weeks of age. Once animals are taken outside of Michigan State University, it is not possible to house them in our facilities again. Therefore, I sacrificed all mice immediately after ABR because obtaining serial audiograms of the same animal was not possible. P264L homozygotes had a slight threshold shift in the 8-16 kHz range and a moderate shift at 32 kHz by 4-5 weeks of age (Figure 5-4). The most important range of hearing for mice is in the ultrasonic range of 40 kHz to 80 kHz, as these are the frequencies at which they communicate (Ehret, 2001). In mice, hearing is established around postnatal days 12-14 (P12-14) when innervation of the auditory hair cells is complete. Hearing loss at 4 weeks of age is an indication of early onset deafness. By 6-7 weeks of age, hearing loss was profound across all frequencies tested and a response was not observed within the limits of the test at 32 kHz (Figure 5-4). In contrast, 6-7 week old heterozygous and wild-type littermates were within the range of normal hearing at 8 and 16 kHz. The threshold shift at 32 kHz is likely due to the AHL (age related hearing loss) allele carried by C57Bl/6J mice. The high to low frequency progression of hearing loss in the PL homozygotes is similar to that observed in people with DFNA20 deafness.

Figure 5-4

Auditory-evoked Brainstem Response (ABR). Mice homozygous for the P264L (PL) mutation have early onset, rapidly progressing hearing loss. At 4-5 weeks of age, a moderate threshold shift is observed at 16 and 32 kHz. By 6-7 weeks of age, PL homozygotes have a profound hearing loss at 8 and 16 kHz and a complete loss at 32 kHz. It should be noted that hearing loss is also observed at 32 kHz in wild-type mice due to a mutation carried on the C57Bl/6J background. The range of normal hearing is indicated in yellow.

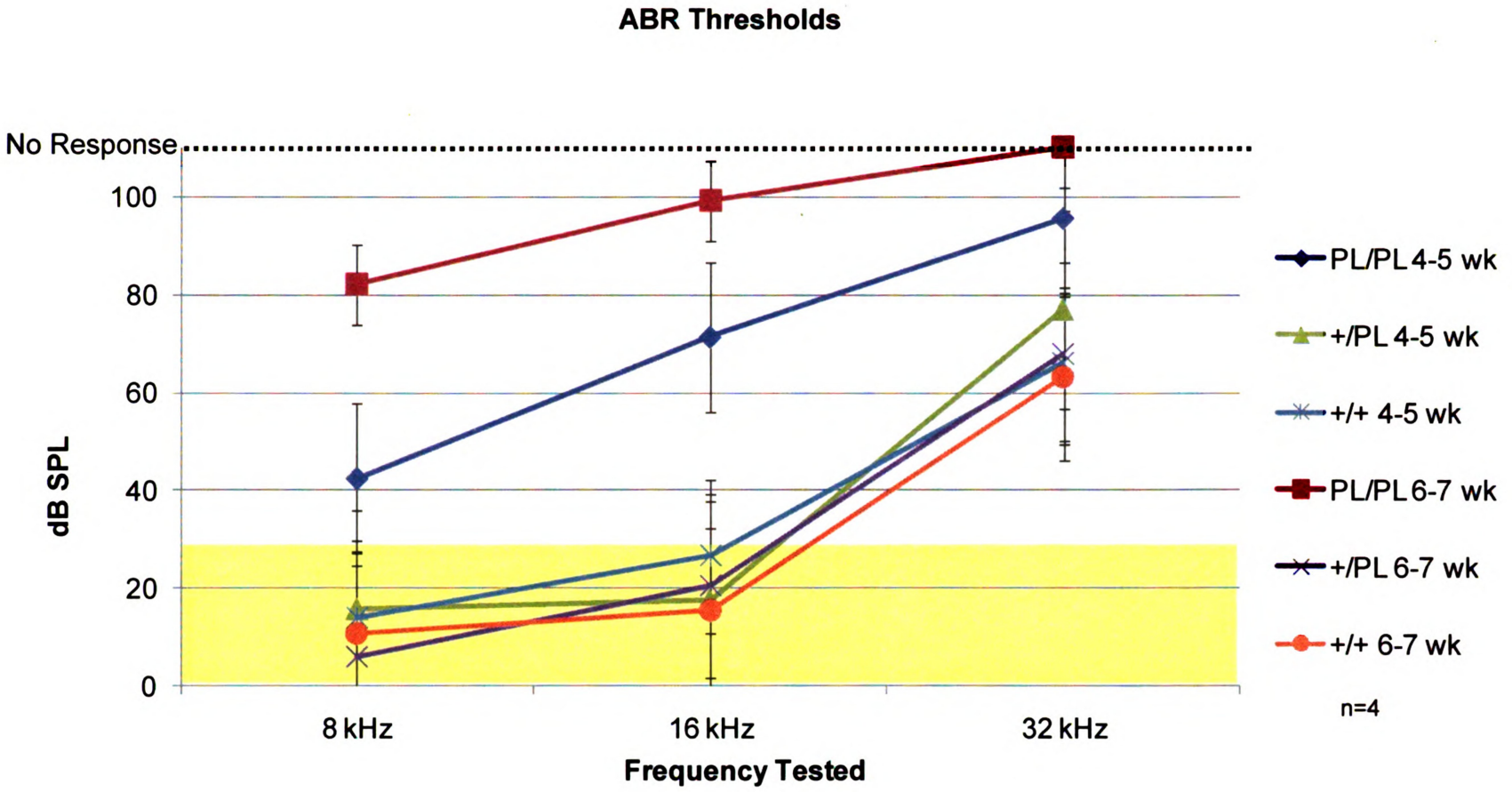
ABR Thresholds
No Response
100
80
60
40
20
0
dB SPL
8 kHz
16 kHz
32 kHz
Frequency Tested
PL/PL 4-5 wk
+/PL 4-5 wk
+/+ 4-5 wk
PL/PL 6-7 wk
+/PL 6-7 wk
+/+ 6-7 wk
n=4

Hearing loss in PL/PL mice is due to degeneration of stereocilia

Hearing loss in mice can manifest in a number of ways. In order to characterize the nature of the hearing loss in PL homozygotes, I examined the apical surface of the hair cells using scanning electron microscopy. Immediately after ABR, cochleae were fixed in glutaraldehyde supplemented with 1mM $CaCl_2$ via local perfusion through the oval window. Prior to imaging, samples were coated with a thin layer of osmium tetroxide to increase conduction of fine structures and then sputter coated with a second layer of gold to increase overall transduction. In order to expose all of the auditory hair cells in the cochlea, the first apical turn was mounted separately from the remainder of the cochlear bulla (Figure 5-5A). The apical turn contains hair cells that process sounds in the 4-8 kHz range (Meyer *et al.*, 2009). The remainder of the bulla processes sound from 8-64 kHz (Figure 5-5B).

Consistent with the ABR data, the least severe pathology was observed in the apical region of the cochlea. Figure 5-6 shows that the overall organization of the cochlea in mutant mice is similar to a wild-type littermate. Closer examination of the outer hair cells reveals that the two inner rows of stereocilia in the hair cell bundle of PL homozygotes are either degenerating or not properly formed (Figure 5-7). At this region of the cochlea the bundles are frequently slightly disarrayed, as can be seen in the same region from a wild-type littermate. This splaying, however, is distinct from the pattern of degeneration in mutant mice.

Figure 5-5

Low magnification scanning electron images of the apical turn (**A**), remainder of the cochlear bulla (**B**) and higher magnification image of inner and outer hair cells (**C**). I mounted the apical turn separately so as to expose more of the high frequency hair cells. The frequencies perceived by the apical portion of the cochlea range from 4 kHz at the far left to approximately 10 kHz to the right. The exposed hair cells of the intact cochlear bulla represent approximately 12 kHz to 32 kHz going clockwise from the 9 o'clock position. Scale bars = 200 nm.

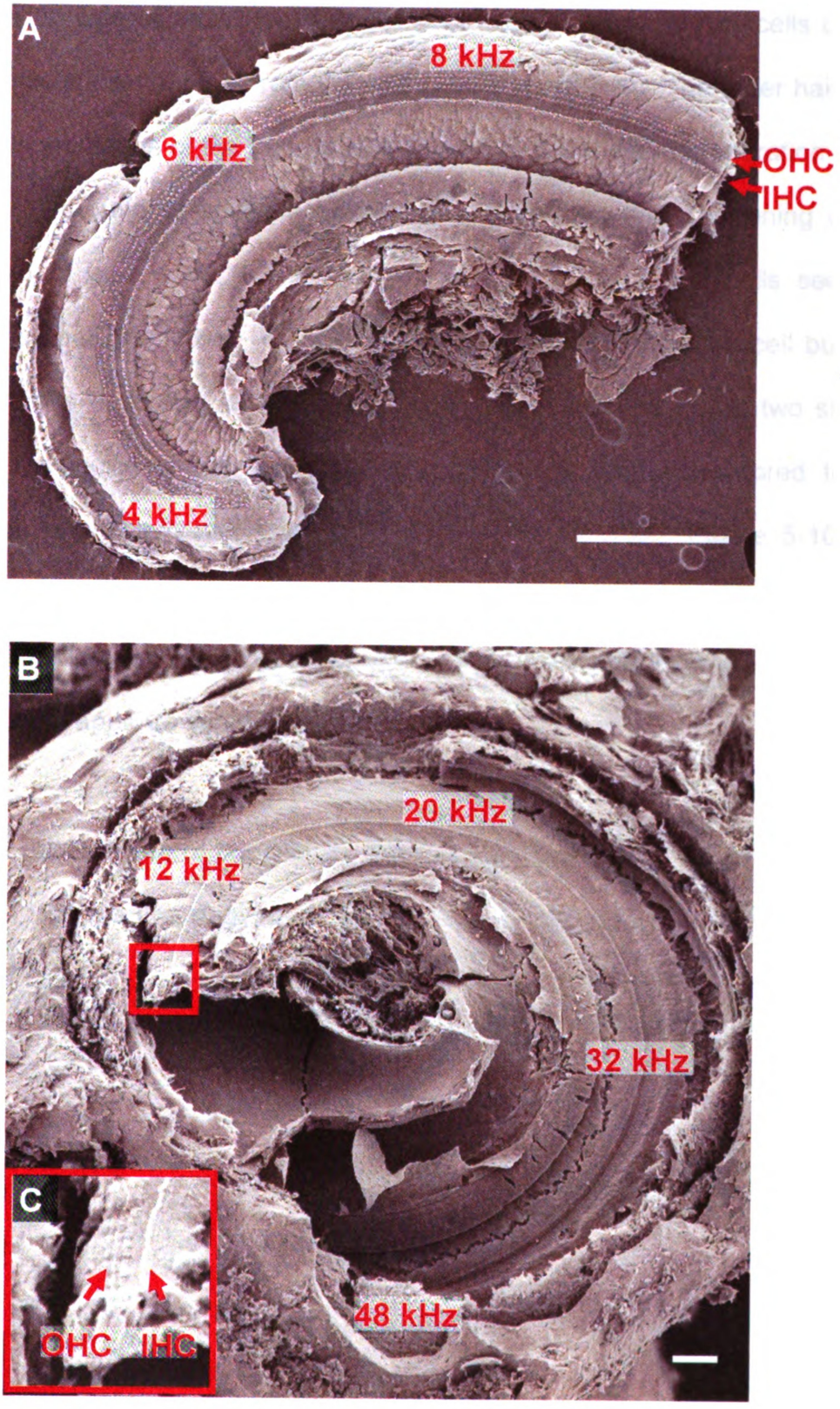
A
8 kHz
6 kHz
OHC
IHC
4 kHz
B
20 kHz
12 kHz
32 kHz
C
OHC
IHC
48 kHz

Moving down to the middle turn of the cochlea, a more severe pathology of degeneration was observed in PL mice. Both outer and inner hair cells of the mutant mice show changes from the wild type. (Figure 5-8). The outer hair cells display disorientation of the bundle as well as a more severe degeneration of the bundle with prominent splaying of the outer stereocilia and shortening of the inner rows of stereocilia (Figure 5-8). Although the inner hair cells seem to maintain proper orientation, a closer examination of the inner hair cell bundles reveals a loss of tenting and increased rounding at the tips of the two shorter rows of stereocilia where the basal end of the tip link is anchored to the membrane of the adjacent taller stereocililum (Figure 5-9). Figure 5-10 is a higher magnification image of two outer hair cells from a homozygous mutant mouse and wild-type. While the inner two rows of stereocilia have disassembled, the tallest row appears mostly intact.

The most basal region of the cochlea that I imaged was within the 32 kHz range. Figure 5-11 shows that degeneration of the hair bundle eventually results in loss of the hair cell.

Figure 5-6

Scanning electron micrographs of the organ of Corti in the 8 kHz range from a 6 week old wild-type (**A**) and PL homozygous (**B**) mouse. At this level of magnification, there is no difference in the overall organization of the hair cells.

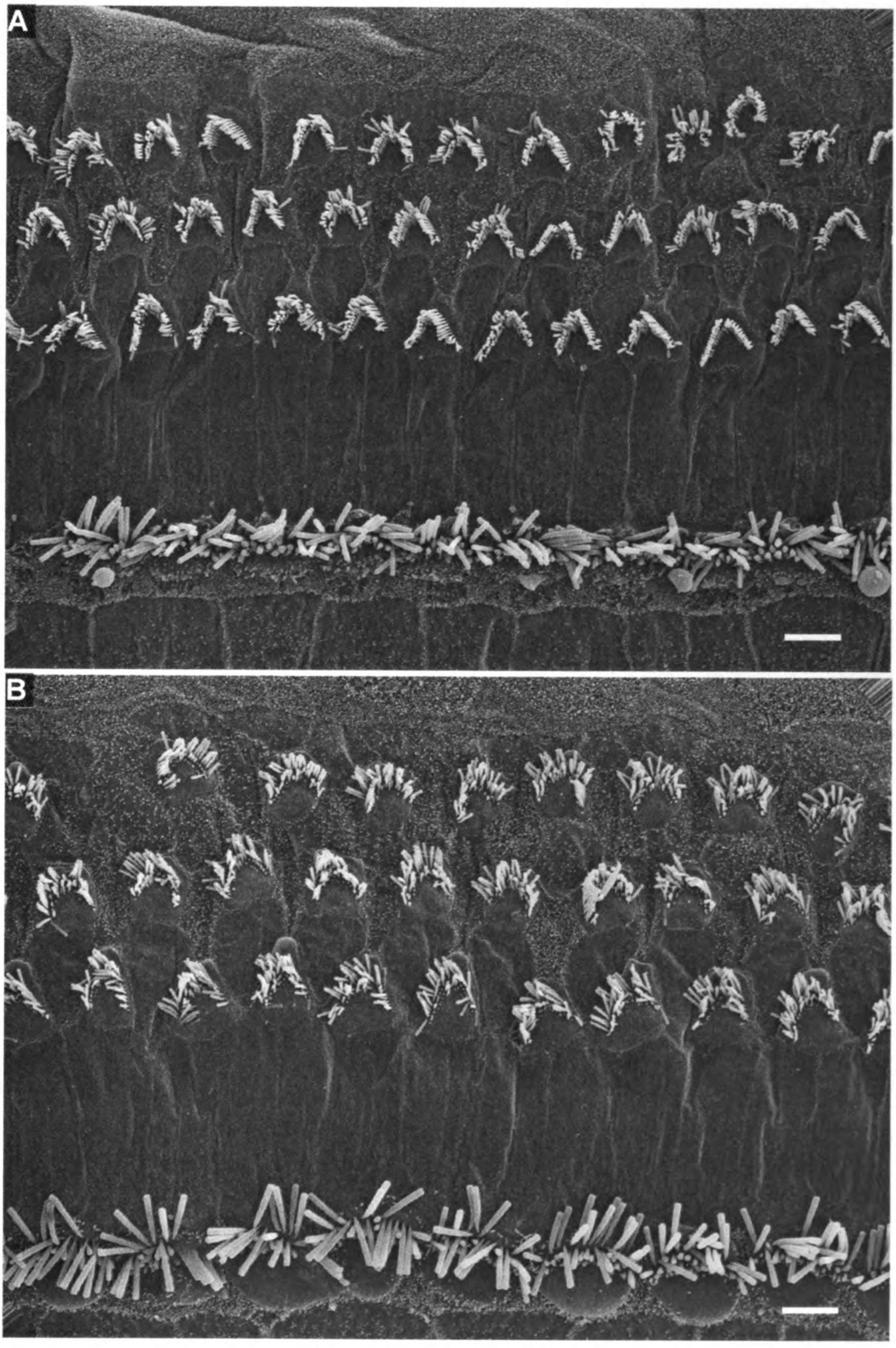
A
B

Figure 5-7

High magnification scanning electron micrographs of outer hair cell bundles in the 8 kHz range from a 6 week old wild-type (**A**) and PL homozygous (**B**) mouse. At this level of magnification, the degeneration of the two shortest rows of stereocilia is apparent in the PL homozygote. In this region of the cochlea, the outer hair cell bundles normally appear slightly disheveled; however, degeneration of stereocilia is not commonplace. Remarkably, the tallest row of stereocilia appears unaffected.

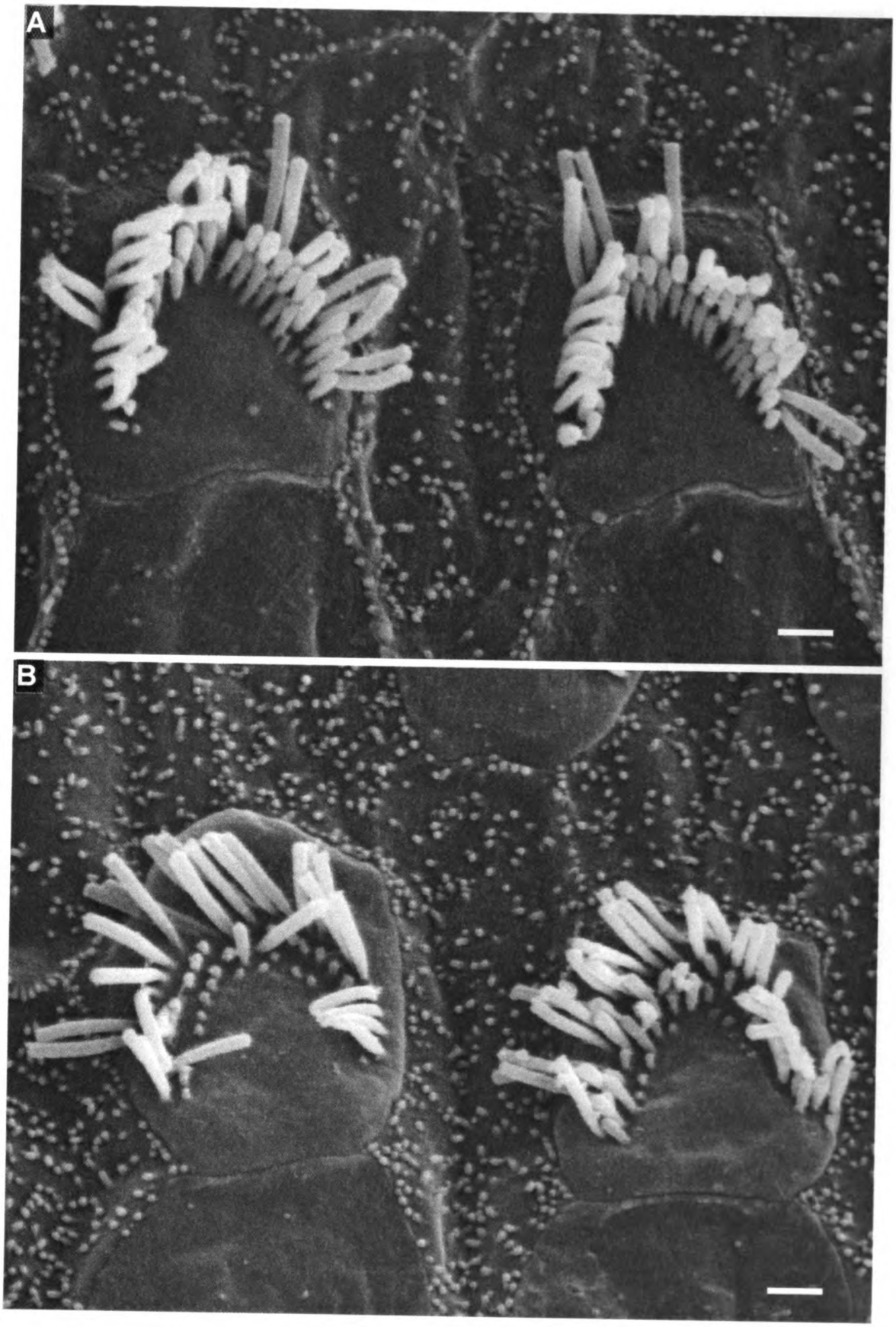
A
B

Figure 5-8

Scanning electron micrographs of the organ of Corti in the 16 kHz range from a 6 week old wild-type (**A**) and PL homozygous (**B**) mouse. At this level of magnification, improper orientation of the bundles (asterisks) and loss of the "v" shape of the outer hair cell bundle is apparent. No obvious differences are observed in the inner hair cells.

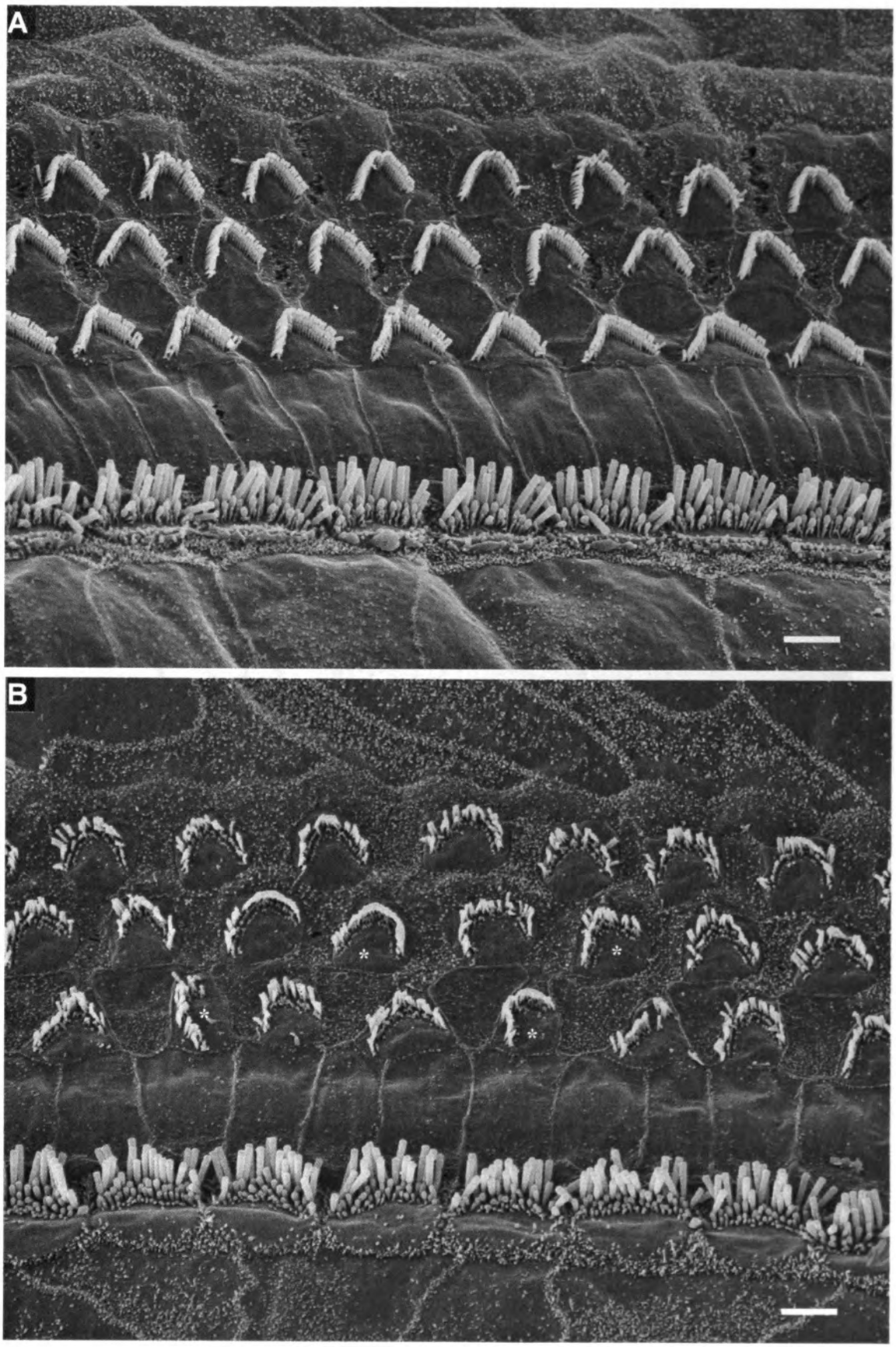
A
B

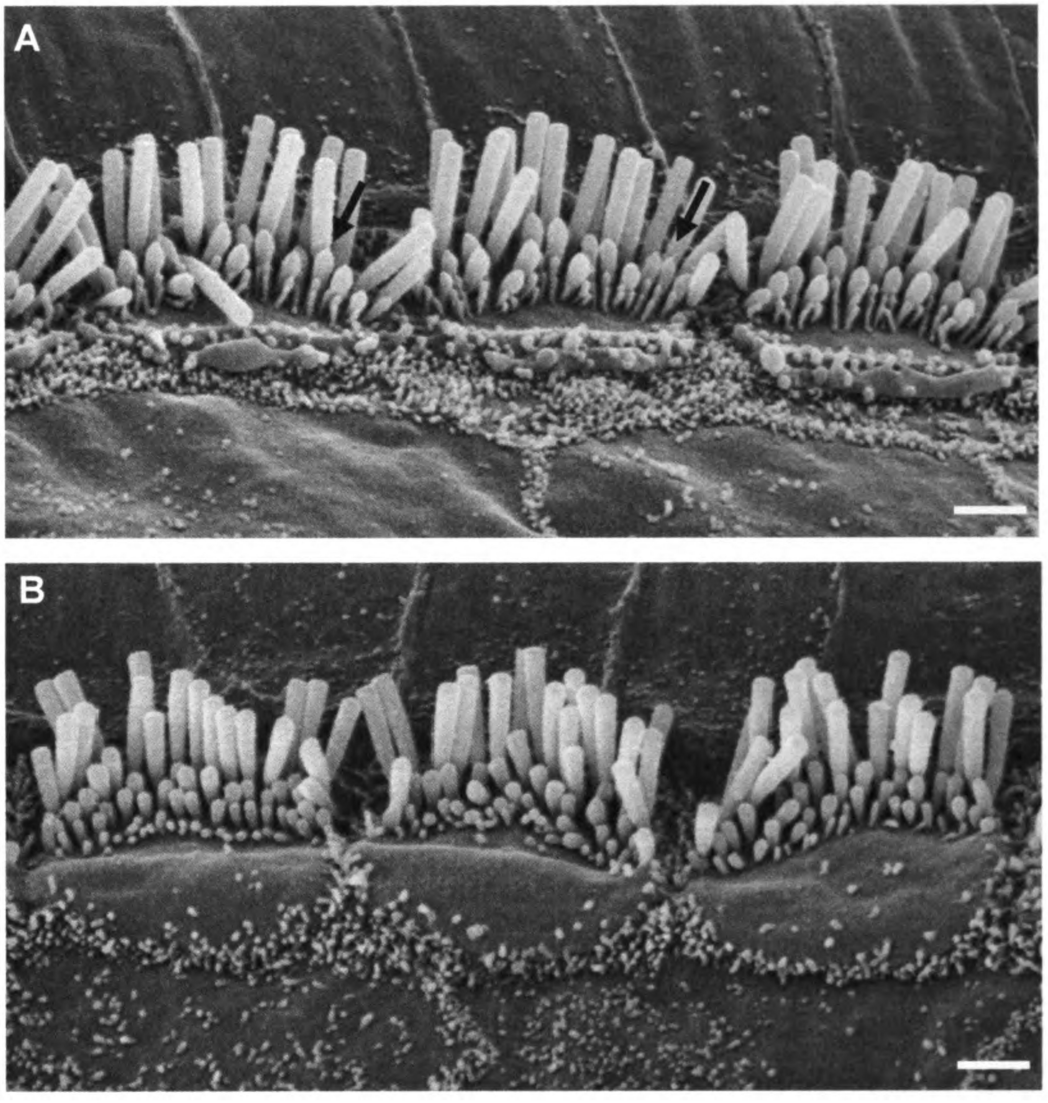

Figure 5-9

High magnification scanning electron micrographs of inner hair cell bundles in the 16 kHz range from a 6 week old wild-type (**A**) and PL homozygous (**B**) mouse. Tension from the tip links adjoining the shorter to taller stereocilia generates a "tented" appearance (arrows). The molecular machinery important for mechanotransduction is located in this structure. Marked loss of tenting and increased rounding of the tips of stereocilia is observed in PL homozygotes.

Figure 5-10

High magnification scanning electron micrographs of outer hair cell bundles in the 16 kHz range from a 6 week old wild-type (**A**) and PL homozygous (**B**) mouse. The characteristic "v" shape and staircase organization of outer hair cell stereocilia is apparent in wild-type but not mutant mice. At this level of magnification, disassembly of the two shortest rows of stereocilia is apparent in the PL homozygote, along with misorientation of the bundle and early signs of loss of the cell shape.

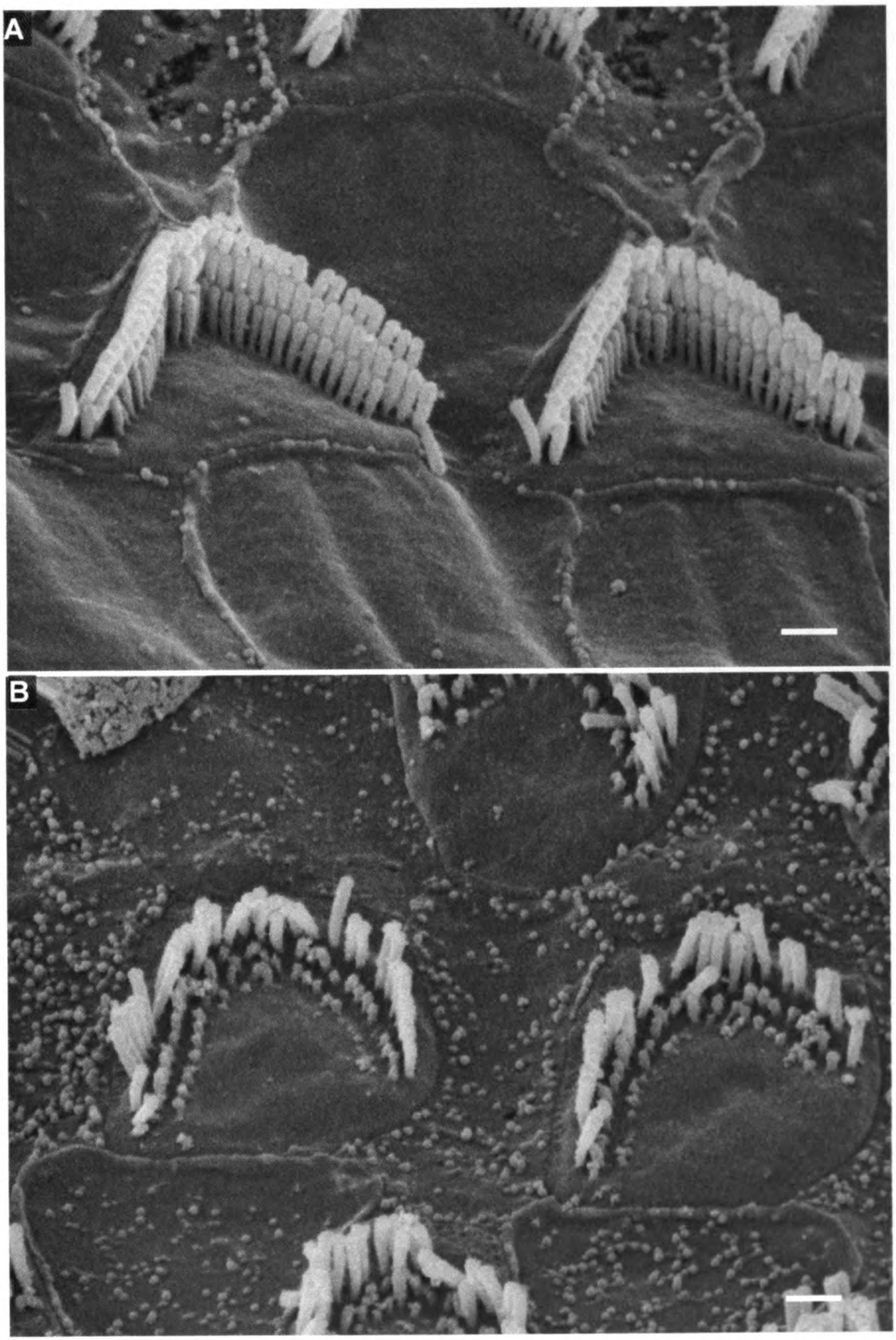
A
B

Figure 5-11

Scanning electron micrographs of the organ of Corti in the 32 kHz range from a 6 week old wild-type (**A**) and PL homozygous (**B**) mouse. In addition to degeneration of stereocilia and improper bundle orientation, loss of hair cells is observed in the mutant mouse.

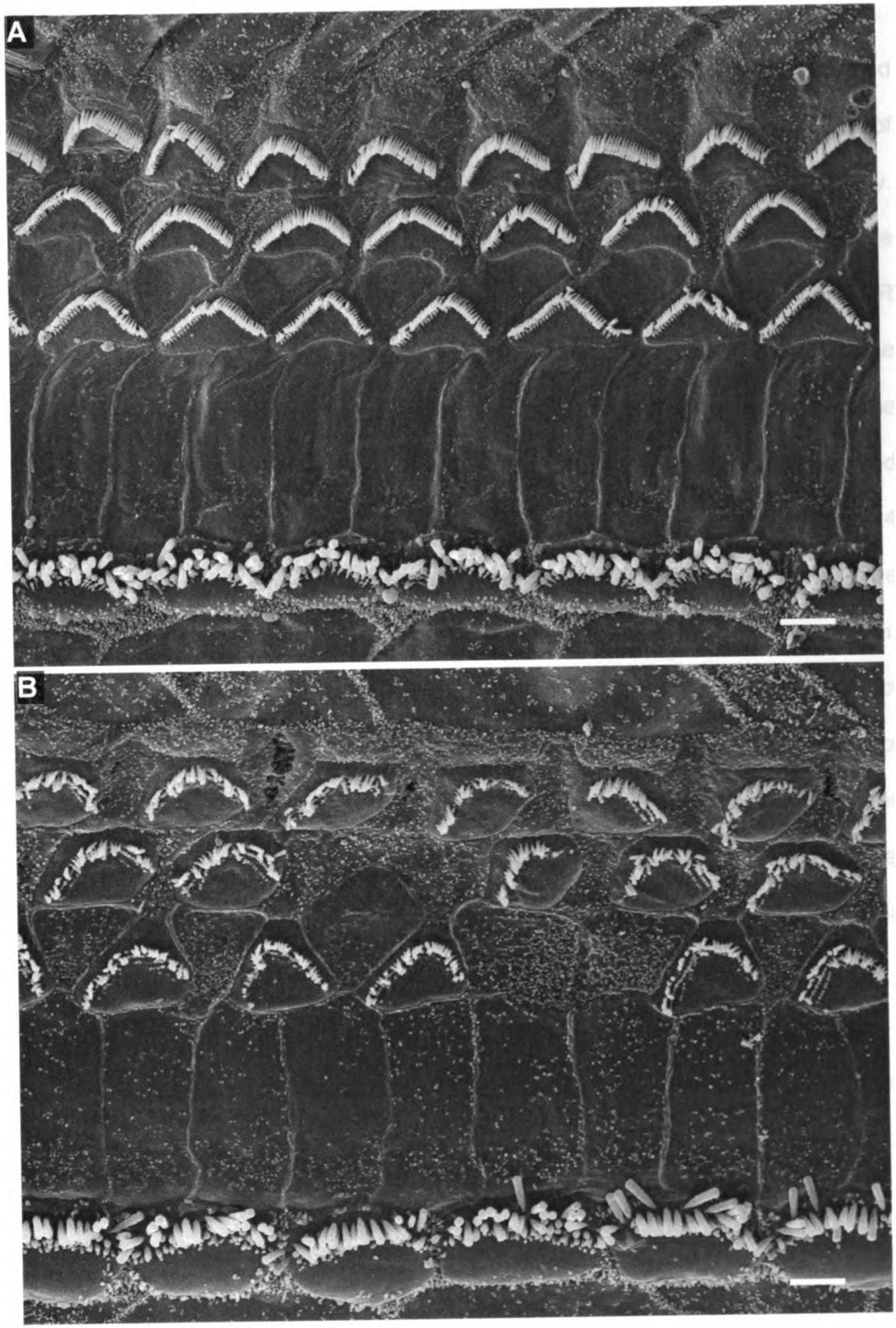
A
B

Mutant P264L γ-actin is properly localized to the stereocilia in homozygous mice

Given the hair cell phenotype, I hypothesized that γ-actin is not properly localized to or within the stereocilia of hair cells. To investigate this, I imaged the organ of Corti whole mounts using immunofluorochemisty with an anti-γ-actin antibody. Samples were counterstained with rhodamine-phalloidin and DAPI to visualize actin filaments and nuclei. Four week old animals were euthanized after ABR and immediately fixed in 4% paraformaldehyde via local perfusion through the oval window of the cochlea. After fine dissection to remove all supporting tissue and bone, the organ of Corti was dissociated from the modiolus and mounted onto slides in anti-fade reagent. Figure 5-12 is a representative image from a 4 week old mouse and shows that there is no difference in localization of wild-type versus P264L γ-actin. As expected, wild-type mice display a high concentration of γ-actin within the outer hair cell bundles (Figure 5-12A-C) and periphery of inner hair cell bundles (Figure 5-12D-F). Despite the improper orientation of several of the outer hair cell bundles in PL homozygotes, the mutant γ-actin is still present in the stereocilia (Figure 5-12G-L). The resolution of a confocal microscope is not sensitive enough to differentiate between rows of stereocilia within a single hair cell bundle.

One difference that I did observe was promiscuous actin filament formation in the body of the hair cell. One advantage of confocal imaging is the ability to visualize sections through a tissue. These sections can be compiled to create a maximum intensity projection or z-stack of cells and tissues. I implemented this technique

to track actin filaments through multiple focal planes (Figure 5-13). Even when over-exposed, these filaments were not observed in wild-type littermates.

Figure 5-12

Confocal microscopy of outer hair cell stereocilia (**A-C, G-I**) and inner hair cell stereocilia (**D-F, J-L**) labeled with anti-γ-actin in green (**A, D, G, J**) and counter-stained with rhodamine phalloidin in red to visualize filamentous actin (**C, F, I, L**). **B, E, H,** and **K** are merged images. Compared to wild-type (**A-F**), the mutant PL protein (**G-L**) localizes properly to the stereocilia in both inner and outer hair cells. Images are from P28 mice.

A
B
C
D
E
F
G
H
I
J
K
L

Figure 5-13

Maximum intensity projections of z-series taken at 5 μm intervals though the body of hair cells. Aberrant filaments are not observed in the outer hair cells from wild-type mice (**A**), but are abundant in PL homozygotes as indicated by arrows (**B**). This spurious filament formation is characteristic of unhealthy hair cells.

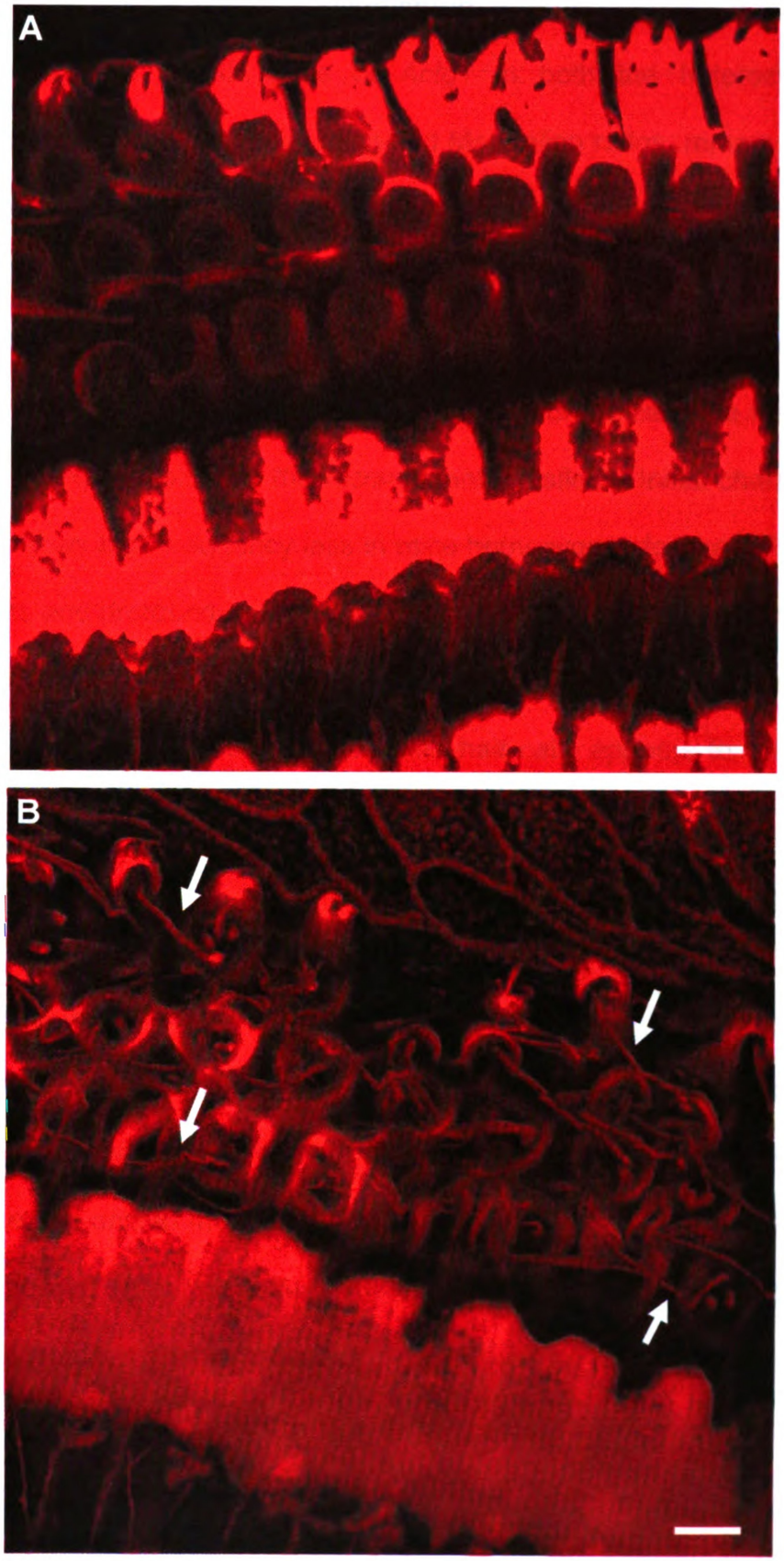
A
B

Discussion

Mice harboring the P264L allele of *Actg1* in both the heterozygous and homozygous state are born at the expected Mendelian ratios, remain viable, and do not have noticeable muscular myopathy. I evaluated the expression level of the knock-in allele using western blot and determined that the presence of the neo-selection cassette in intron 1 of the *Actg1* transcript results in reduced expression of the mutant protein, however, removal of the cassette restores wild-type levels of expression from the recombinant PL allele. Initial characterization of hearing shows high frequency loss in mice homozygous for the p.P264L allele at 4-5 weeks and profound deafness by 6-7 weeks. Hearing loss in homozygous mice corresponds with the lack of tenting in inner hair cells and resorption of stereocilia in outer hair cells. Loss of outer hair cells appears to be secondary and not the initial cause of deafness.

Compared to the previously characterized *Actg1*-null mice, which have reduced viability and muscular myopathy (Belyantseva *et al.*, 2009), mice with the P264L mutation have few or no pleiotropic effects but have a much earlier hearing loss. Additionally, the pattern of deterioration of the stereocilia is quite different between the two animal models. In the γ-actin knockout mouse, stereocilia loss was not specific to only the two shorter rows of the bundle; rather it was observed in patches (Belyantseva *et al.*, 2009). I believe that taken together, these data are more consistent with a dosage dependent dominant negative or gain of function mode of action for the missense mutation, in which the mutant

protein interferes with function of actin binding proteins or wild-type β-actin in the cell. If the P264L mutation causes a loss of function or haploinsufficiency, I expect that the phenotype of the knock-in mice would be more similar to γ-actin knockout mice.

C57Bl/6J mice are homozygous for a splice site mutation in exon 8 of cadherin 23 (CDH23) which results in age-related hearing loss (Johnson *et al.*, 2006) that is progressive and begins in the high frequencies. Fortunately, hearing loss observed in P264L knock-in mice occurs well before the onset of age-related hearing loss due to CDH23 mutations. However, given a dosage dependent model, I expect that +/PL, PL-neo/PL-neo, or PL/PL-neo mice will all have a later onset of hearing loss that is outside of the limits of what can be distinguished from the typical C57Bl/6J age-related hearing loss. To address this issue, I have begun to backcross to +/PL and +/PL-neo mice to the CBA/J background. CBA/J do not carry mutations associated with hearing loss and are used as the standard of normal hearing at Jackson Labs (2010).

Loss of tenting in the inner hair cells is a phenotype that is similar to what was recently reported by Shwander and colleagues (Schwander *et al.*, 2009). In the spontaneous *salsa* mutant harboring missense mutations in cadherin 23, the apical component of the tip link complex, a loss of tenting in inner hair cells is observed. Due to difficulties in obtaining upright and not splayed inner hair cell bundles, I have not yet been able to characterize the progression of this defect.

It will be useful in the future to use antibodies specific for the two tip link proteins, protocadherin 15 (Ahmed *et al.*, 2006) and cadherin 23 (Siemens *et al.*, 2004), to determine if these are properly localized in P264L mutant mice. Another possibility is to combine ultrahigh resolution scanning electron microscopy with backscatter electron analysis and immunogold labeling to determine if the tip link complex is properly formed.

The pattern of degeneration of the outer hair cell bundle of PL homozygotes is unlike any other phenotype previously described. Mutations in myosin 7a, a motor protein found along the lengths of the stereocilia, result in uniformly longer stereocilia (Self *et al.*, 1998). *Shaker-2* mice are deficient in myosin 15a, a motor protein localized to the tips of stereocilia, result in very short, stubby hair cell bundles (Anderson *et al.*, 2000). Similarly, mice with mutations in whirlin, the cargo of myosin 15a, also result in uniformly short hair cell bundles (Mogensen *et al.*, 2007; Mustapha *et al.*, 2007). Mutations in proteins that bundle actin filaments, such as espin and triobp, result in thin and floppy stereocilia (Zheng *et al.*, 2000; Kitajiri *et al.*, 2010). The pattern of degeneration that I observed in the P264L knock-in mice is the first to target specific rows of stereocilia and not the entire bundle.

The observations that I have made using SEM will help to guide future functional studies. Mechanotransduction, the process by which hair bundle deflections are converted into an electrical signal, occurs via the opening of mechanically gated

channels located in the tips of the two shorter rows of stereocilia (Beurg *et al.*, 2009). Therefore, much higher regional levels of calcium exist in the two shorter rows of stereocilia than the tallest. It is possible that the P264L missense mutation alters the ion requirements of a calcium- or potassium-dependent actin binding protein critical to proper stereocilia function.

The aberrant actin filament formation I observed inside the hair cells using confocal microscopy (Figure 5-13) is similar to cytocauds, thick bundled actin filaments that protrude out of the base of hair cells in the previously characterized *shaker-2* mouse (Beyer *et al.*, 2000). This phenotype may or may not be specific to mutations in actin or actin binding proteins, as cytocauds are also observed in old organ of Corti explant cultures from wild-type mice (Belyantseva, unpublished personal communication). Further characterization of the development of these peculiar structures may help us understand an aspect of actin dynamics in the hair cell.

One pertinent aspect of DFNA20 deafness that I have not addressed in this chapter is the lack of a vestibular phenotype. Gamma-actin is very abundant in vestibular hair cells, so one would expect that mutations which cause hearing loss would also result in a vestibular phenotype. In mice, vestibular disorders are frequently characterized by obsessive circling in cages, a behavior that I did not observe in P264L knock-in mice. Therefore, more sensitive methods of measuring vestibular dysfunction are necessary. Characterization of the

vestibular competence of these animals may provide information about the role of gamma actin in the vestibular hair cell.

In closing, the P264L mouse model provides useful information about the pathophysiology of this particular mutation, some of which may be applicable to the phenotype observed in humans. In addition, given the very specific pattern of degeneration of the stereocilia, this mouse model may be relevant to better understanding mechanotransduction and the molecular machinery involved.

References

Auditory-Evoked Brainstem Response (ABR) Thresholds. 2010. http://www.jax.org

Ahmed, Z. M., Goodyear, R., Riazuddin, S., Lagziel, A., Legan, P. K., Behra, M., Burgess, S. M., Lilley, K. S., Wilcox, E. R., Riazuddin, S., *et al.*, 2006. The tip-link antigen, a protein associated with the transduction complex of sensory hair cells, is protocadherin-15. Journal of Neuroscience. 26, 7022-7034.

Anderson, D. W., Probst, F. J., Belyantseva, I. A., Fridell, R. A., Beyer, L., Martin, D. M., Wu, D., Kachar, B., Friedman, T. B., Raphael, Y., *et al.*, 2000. The motor and tail regions of myosin XV are critical for normal structure and function of auditory and vestibular hair cells. Hum Mol Genet. 9, 1729-38.

Belyantseva, I. A., Perrin, B. J., Sonnemann, K. J., Zhu, M., Stepanyan, R., McGee, J., Frolenkov, G. I., Walsh, E. J., Friderici, K. H., Friedman, T. B., *et al.*, 2009. Gamma-actin is required for cytoskeletal maintenance but not development. Proc Natl Acad Sci U S A. 106, 9703-8.

Beurg, M., Fettiplace, R., Nam, J. H., Ricci, A. J., 2009. Localization of inner hair cell mechanotransducer channels using high-speed calcium imaging. Nat Neurosci. 12, 553-8.

Beyer, L. A., Odeh, H., Probst, F. J., Lambert, E. H., Dolan, D. F., Camper, S. A., Kohrman, D. C., Raphael, Y., 2000. Hair cells in the inner ear of the pirouette and shaker 2 mutant mice. J Neurocytol. 29, 227-40.

Bryan, K. E., Rubenstein, P. A., 2009. Allele-specific effects of human deafness gamma-actin mutations (DFNA20/26) on the actin/cofilin interaction. J Biol Chem. 284, 18260-9.

Bryan, K. E., Wen, K. K., Zhu, M., Rendtorff, N. D., Feldkamp, M., Tranebjaerg, L., Friderici, K. H., Rubenstein, P. A., 2006. Effects of human deafness gamma-actin mutations (DFNA20/26) on actin function. J Biol Chem. 281, 20129-39.

Crawley, J. N., 2000. What's wrong with my mouse? : behavioral phenotyping of transgenic and knockout mice. Wiley-Liss, New York.

de Heer, A. M., Huygen, P. L., Collin, R. W., Oostrik, J., Kremer, H., Cremers, C. W., 2009. Audiometric and vestibular features in a second Dutch DFNA20/26 family with a novel mutation in ACTG1. Ann Otol Rhinol Laryngol. 118, 382-90.

Ehret, G., 2001. [Adaptation of the mouse auditory system to perception of ultrasonic communication signals]. Zh Evol Biokhim Fiziol. 37, 431-6.

Johnson, K. R., Zheng, Q. Y., Noben-Trauth, K., 2006. Strain background effects and genetic modifiers of hearing in mice. Brain Res. 1091, 79-88.

Kitajiri, S., Sakamoto, T., Belyantseva, I. A., Goodyear, R. J., Stepanyan, R., Fujiwara, I., Bird, J. E., Riazuddin, S., Riazuddin, S., Ahmed, Z. M., *et al.*, 2010. Actin-

bundling protein TRIOBP forms resilient rootlets of hair cell stereocilia essential for hearing. Cell. 141, 786-98.

Korrapati, S., 2009. Functional analysis of cytoplasmic gamma-actin mutations causing non-syndromic, progressive autosomal dominant hearing loss. Genetics Program. PhD. Dissertation

Liu, P., Li, H., Ren, X., Mao, H., Zhu, Q., Zhu, Z., Yang, R., Yuan, W., Liu, J., Wang, Q., *et al.*, 2008. Novel ACTG1 mutation causing autosomal dominant non-syndromic hearing impairment in a Chinese family. J Genet Genomics. 35, 553-8.

Meyer, A. C., Frank, T., Khimich, D., Hoch, G., Riedel, D., Chapochnikov, N. M., Yarin, Y. M., Harke, B., Hell, S. W., Egner, A., *et al.*, 2009. Tuning of synapse number, structure and function in the cochlea. Nat Neurosci. 12, 444-53.

Mogensen, M. M., Rzadzinska, A., Steel, K. P., 2007. The deaf mouse mutant whirler suggests a role for whirlin in actin filament dynamics and stereocilia development. Cell Motil Cytoskeleton. 64, 496-508.

Morin, M., Bryan, K. E., Mayo-Merino, F., Goodyear, R., Mencia, A., Modamio-Hoybjor, S., del Castillo, I., Cabalka, J. M., Richardson, G., Moreno, F., *et al.*, 2009. In vivo and in vitro effects of two novel gamma-actin (ACTG1) mutations that cause DFNA20/26 hearing impairment. Hum Mol Genet. 18, 3075-89.

Mustapha, M., Beyer, L. A., Izumikawa, M., Swiderski, D. L., Dolan, D. F., Raphael, Y., Camper, S. A., 2007. Whirler mutant hair cells have less severe pathology than shaker 2 or double mutants. J Assoc Res Otolaryngol. 8, 329-37.

Rendtorff, N. D., Zhu, M., Fagerheim, T., Antal, T. L., Jones, M., Teslovich, T. M., Gillanders, E. M., Barmada, M., Teig, E., Trent, J. M., *et al.*, 2006. A novel missense mutation in ACTG1 causes dominant deafness in a Norwegian DFNA20/26 family, but ACTG1 mutations are not frequent among families with hereditary hearing impairment. Eur J Hum Genet. 14, 1097-105.

Schwander, M., Xiong, W., Tokita, J., Lelli, A., Elledge, H. M., Kazmierczak, P., Sczaniecka, A., Kolatkar, A., Wiltshire, T., Kuhn, P., *et al.*, 2009. A mouse model for nonsyndromic deafness (DFNB12) links hearing loss to defects in tip links of mechanosensory hair cells. Proc Natl Acad Sci U S A. 106, 5252-7.

Self, T., Mahony, M., Fleming, J., Walsh, J., Brown, S. D., Steel, K. P., 1998. Shaker-1 mutations reveal roles for myosin VIIA in both development and function of cochlear hair cells. Development. 125, 557-66.

Siemens, J., Lillo, C., Dumont, R. A., Reynolds, A., Williams, D. S., Gillespie, P. G., Muller, U., 2004. Cadherin 23 is a component of the tip link in hair-cell stereocilia. Nature. 428, 950-5.

van Wijk, E., Krieger, E., Kemperman, M. H., De Leenheer, E. M., Huygen, P. L., Cremers, C. W., Cremers, F. P., Kremer, H., 2003. A mutation in the gamma

actin 1 (ACTG1) gene causes autosomal dominant hearing loss (DFNA20/26). J Med Genet. 40, 879-84.

Zheng, L., Sekerkova, G., Vranich, K., Tilney, L. G., Mugnaini, E., Bartles, J. R., 2000. The deaf jerker mouse has a mutation in the gene encoding the espin actin-bundling proteins of hair cell stereocilia and lacks espins. Cell. 102, 377-85.

Zhu, M., Yang, T., Wei, S., DeWan, A. T., Morell, R. J., Elfenbein, J. L., Fisher, R. A., Leal, S. M., Smith, R. J., Friderici, K. H., 2003. Mutations in the gamma-actin gene (ACTG1) are associated with dominant progressive deafness (DFNA20/26). Am J Hum Genet. 73, 1082-91.

CHAPTER 6

CONCLUSIONS AND FUTURE DIRECTIONS

Conclusions and Future Directions

In this dissertation I describe three approaches to investigating the pathology of mutations in γ-actin and the identification of a new regulatory mechanism for γ-actin. First, I used a yeast 2-hybrid protocol to screen an inner ear library to identify novel inner ear actin binding proteins or isoforms. Given that there are over 100 actin binding proteins identified to date, we expected a robust screen. Though there were over 500 clones identified per screen, not surprisingly, the large majority were identified as either γ- or β-actin. Interestingly, the only other proteins identified as true positives in these two screens were cofilin 1, cofilin 2, cyclase associated protein 2, and ubiquitin E2i ligase. I anticipated that this screen would exclude proteins that interact only with filamentous actin; however, I did not expect so few actin monomer binding proteins. Directed yeast 2-hybrid experiments with the mutant actins and the six prey identified provides another experimental means for evaluating functional deficits of the mutations. This method of analysis may be particularly useful for investigating the interaction between DNFA20 mutations and cyclase associated protein (CAP). Data from band-shift assays done by Dr. Mei Zhu, a former graduate student, hint at a deficiency in this interaction; however, her attempts to investigate this directly were unsuccessful due to difficulties in expressing recombinant CAP proteins. The results of the yeast 2-hybrid screens demonstrate that CAP-prey expression is possible in yeast.

I also investigated the expression of annexin 5a, a γ-actin specific binding protein, in the inner ear. Annexin 5a is expressed at high levels in the cochlea, and its localization is very similar to γ-actin. There is some skepticism in the field as to whether this is truly a γ-actin specific interaction due to difficulties in detecting this interaction. In the methods I described in chapter three, purified annexins and actins were used and an interaction was not observed. Curiously, annexin 5a and γ-actin are both located in the periphery of the stereocilia and z-disc of muscle, regions that require unique linkage between membranes and actin filaments. The location of γ-actin is clearly not altered by lack of annexin 5a as demonstrated using the *Anxa5* knockout mouse. I hypothesize that this is likely due to functional redundancy between annexins, and that another annexin such as A2 substitutes for the function of annexin 5a. What my data does not address is whether the DFNA20 mutant proteins are capable of interacting with annexin 5a. Prior to generating the P264L knock-in mouse, testing this interaction would be nearly impossible. Our γ-actin antibody does not distinguish between wild-type and mutant actins, therefore, a pull-down with transfected cells would not answer this question. Furthermore, I was unable to detect an interaction using *in vitro* synthesized or purified actins, indicating that the interaction is dependent upon other factors not present in highly purified systems. This conundrum highlights the crux of difficulties in investigating the pathology of mutations in γ-actin. *In vitro* systems do not address the physiological requirements in the cell, let alone a tissue with planar and apical/basal polarity. On the other hand, cell and explant cultures transfected with mutant γ-actin

express a lot of endogenous γ-actin that may mask the effects of the mutant actins in cell culture. It may be interesting to repeat a GST-pulldown with annexin 5a and tissues from the P264L knock-in mouse.

The P264L knock-in mouse provides an excellent system to evaluate the pathophysiology of this missense mutation and to gain insight into the genetic mechanism by which it confers deafness. This mouse model appropriately recapitulates the human phenotype of progressive nonsyndromic deafness with normal vestibular function. Due to age-related hearing loss (AHL) mutations carried on the C57Bl/6J strain, it was impossible to study the effects of the P264L mutation in heterozygotes beyond three months of age. For this reason, we are currently working to create congenic P264L lines on the CBA/J strain. Using this "good hearing" background, we will be able to examine the long-term effects of deafness in heterozygotes

The pattern of degeneration that I observed in the PL mouse model is unique in that two rows of stereocilia within the bundle that degenerate first are those involved in mechanotransduction. We recently shipped mice to the University of Kentucky where Dr. Gregory Frolenkov, a hair cell physiologist, will investigate mechanotransduction in hair cells of these mutant mice. As mentioned previously, hearing is not established in mice until the cochlear hair cells are innervated around postnatal day 12. However, the maturation of the hair bundle is complete one week prior, and previous studies have shown that mechanotransduction currents can be measured in murine hair cells as early as

postnatal day 0. It will be interesting to see if the outer hair cells of P264L homozygous mice develop normally and are capable of early, pre-innervation mechanotransduction. Given the progression of hearing loss observed in these mice, I predict that postnatal hair cells will properly mechanotransduce.

Another unique feature of this mouse model is the lack of a vestibular phenotype. Similar to auditory hair cells, γ-actin is expressed at high levels in vestibular hair cells, so one would predict vestibular dysfunction. To address this, we established a collaboration with Dr. Sherri Jones of the University of North Carolina to measure the gravity response of P264L mice in a manner similar to that used in ABR testing. By this technique, subtle vestibular dysfunction has been observed in some mouse models of hearing loss in the absence of an overt phenotype.

One very rewarding aspect of my dissertation research was identifying the novel γ-actin transcript and having the opportunity to characterize its function. There are still many questions left to be answered which will require a more quantitative approach. First, I hypothesize that in response to the excess of *ACTG1* transcripts, endogenous transcripts, endogenous γ-actin will be down regulated. Second, the NCBI mouse EST database contains traces from alternatively spliced *Actg1* transcripts that were found in brain and testes. This may represent a low level of noisy splicing that is not tissue specific. Alternatively it may indicate that splicing to include exon 3a is a universal mechanism for down-

regulation of γ-actin. In either scenario, I believe that this project highlights the need for experimental validation of RUST.

APPENDICES

COMMONLY USED METHODS AND REAGENTS

A. PCR

Mastermix:

Component	Volume / 20 μL reaction	Final Concentration
5x GoTaq® reaction buffer (7.5 mM $MgCl_2$)	4 μL	1x 1.5 mM $MgCl_2$
25 mM dNTPs	0.16 μL	0.2 mM
10 μM forward primer	0.5 μL	0.25 μM
10 μM reverse primer	0.5 μL	0.25 μM
GoTaq® DNA polymerase 5u/μL	0.1 μL	0.5 units
Template DNA (10-100 ng/μL)	1 μL	0.5 - 5 ng
H_2O	13.74 μL	

*GoTaq® DNA polymerase and buffer are supplied by Promega©.

Cycling Conditions:

1. 95°C, 3 minutes
2. 95°C, 30 seconds
   59°C, 30 seconds
   72°C, 1 minute/1kb product
   ] 25-35 cycles
3. 72°C, 5 minutes

B. Polyacrylamide Gels (Reducing)

Stacking (3%)

Volume	Stock Solution
2.5 mL	0.5M Tris HCl / 4% sodium dodecyl sulfate (SDS) pH6.8
1.0 mL	40% Acrylamide/Bis 19:1
6.5 mL	ddH_2O
10 μL	Tetramethylethylenediamine (TEMED)
50 μL	10% ammonium persulfate
10 mL	**Final Volume**

Separating (10%)

Volume	Stock Solution
3.75 mL	1.5M Tris HCl / 4% sodium dodecyl sulfate (SDS) pH8.8
3.75 mL	40% Acrylamide/Bis 19:1
7.5 mL	ddH_2O
10 μL	Tetramethylethylenediamine (TEMED)
50 μL	10% ammonium persulfate
15 mL	**Final Volume**

C. Continuous Native Gels

Stacking (3%)

w/ $CaCl_2$	**w/out $CaCl_2$**	**Stock Solution**
1 mL	1 mL	200mM Tris HCl / 2.0M glycine (do not adjust pH)
2.5 mL	2.5 mL	40% Acrylamide/Bis 19:1
6.35 mL	6.37 mL	ddH_2O
20 µL	20 µL	100 mM adenosine 5'-triphosphate
20 µL	0 µL	100 mM $CaCl_2$
10 µL	10 µL	Tetramethylethylenediamine (TEMED)
50 µL	50 µL	10% ammonium persulfate
10 mL	**10 mL**	**Final Volume**